POLITECNICO DI TORINO

Corso di Laurea Magistrale in
Ingegneria Chimica e dei Processi Sostenibili

Tesi di Laurea Magistrale

Development of enzymatic processes for carbon dioxide and organic waste valorization: co-immobilization of FDH and GlyDH over hierarchical zeolites

Relatori
prof. Marco Piumetti
prof.ssa Debora Fino
prof.ssa Carminna Ottone
prof. Tonia Tommasi

Candidato
Ilaria Zonca

Ottobre 2021

Riassunto in italiano

L'attenzione nei confronti della problematica dell'elevata concentrazione di anidride carbonica in atmosfera è cresciuta negli ultimi anni in quanto punto focale del contrasto ai cambiamenti climatici. Il biossido di carbonio (CO_2) è infatti il prodotto gassoso di una grande varietà di processi naturali, tra cui la respirazione cellulare, i quali vengono spontaneamente controllati dall'efficiente sistema di termoregolazione terrestre, basato principalmente sulla fotosintesi. Lo sbilanciamento di questo sistema è imputabile alle emissioni antropogeniche, che, seppur rappresentino una minima percentuale di quelle totali, hanno portato alla drammatica situazione attuale, che vede una concentrazione di CO_2 in atmosfera che sfiora le 410 ppm. Una risoluzione radicale del problema dovrebbe prevedere, in linea teorica, l'annullamento della generazione di anidride carbonica alla sorgente, via attualmente non praticabile. Per questo, la ricerca degli ultimi decenni si sta concentrando su approcci di tipo "downstream" che mirino alla sua conversione in prodotti che siano meno dannosi e che abbiano maggior valore commerciale.

Un ulteriore ostacolo a questa strategia deriva dalla natura della molecola, che risulta essere particolarmente inerte per via dei doppi legami tra gli atomi di ossigeno e l'atomo di carbonio: per questo motivo, si rende necessario il ricorso alla catalisi. In particolare, i biocatalizzatori sono stati studiati negli anni con grande interesse essendo in grado di fornire una via maggiormente sostenibile per raggiungere lo stesso obiettivo di conversione, senza peraltro la necessità di impiegare temperature e pressioni molto elevate. L'imitazione di ciò che avviene in natura attraverso il ciclo fotosintetico, ma anche di altre vie metaboliche messe in atto a livello cellulare, è il trend che ha mosso lo sviluppo di due principali tipologie di biocatalizzatori: quelli costituiti da intere cellule, solitamente di batteri o funghi, e gli enzimi. I primi sono caratterizzati dai bassi costi operativi e di produzione, che avviene per via fermentativa, mentre gli enzimi richiedono procedure di espressione, estrazione e purificazione più onerose. Dall'altro lato, la selettività offerta da questi ultimi è incomparabile dal momento che consistono in singole proteine che catalizzano reazioni ben precise, mentre le cellule, per loro natura, mettono in atto vie metaboliche complesse che possono generare prodotti secondari indesiderati.

Questo lavoro di tesi si concentra sulla conversione enzimatica dell'anidride carbonica in prodotti a maggiore valore aggiunto; in quest'ottica è stata quindi effettuata una revisione preliminare della letteratura riguardante i principali enzimi utilizzati, sia su scala di laboratorio sia in impianti pilota, per tale scopo. Le classi di enzimi più comunemente coinvolte sono quelle delle ossidoreduttasi (EC 1) e delle liasi (EC 4). Queste ultime realizzano l'addizione di gruppi ai doppi legami tra carbonio e ossigeno e possono mediare, per esempio, l'interconversione tra anidride carbonica e bicarbonato (HCO_3^-), rendendosi utili soprattutto per le azioni di cattura della CO_2, ma anche per la sua fissazione a glucosio (tramite l'enzima RuBisCo). Le ossidoreduttasi, invece, consentono il trasferimento di elettroni da un donatore ad un accettore, generalmente per mezzo di cofattori, tra cui nicotinammide adenina dinucleotide (NADH) e nicotinammide adenina dinucleotide fosfato (NADPH). L'atomo di carbonio della CO_2 ha numero di ossidazione +4, motivo per cui può agire da accettore di elettroni, venendo ridotto ad altre molecole organiche; tra queste, sono d'interesse l'acido formico (in cui il carbonio ha numero di ossidazione +2), il metanolo (-2) e il metano (-4).

La via enzimatica principale per la produzione di metanolo (CH_3OH), inizialmente studiata da *Obert e Dave* nel 1999 e che da allora capitalizza la letteratura scientifica, consiste in una cascata di tre deidrogenasi: formiato deidrogenasi (FDH), la quale riduce la CO_2 ad acido formico, formaldeide deidrogenasi ($F_{ald}DH$), che riduce l'acido formico alla corrispondente aldeide, e infine alcol deidrogenasi (ADH), che riduce ulteriormente la formaldeide a metanolo. Ciascuna delle tre reazioni della serie consuma una mole di coenzima NADH, come mediatore di elettroni, per mole di anidride carbonica consumata. Nell'ambito di questa tesi verrà analizzato il primo step della cascata, la riduzione dell'anidride carbonica ad acido formico da parte dell'enzima formiato deidrogenasi, di tipo commerciale, estratto da *Candida boidinii*.

Dal punto di vista pratico, l'implementazione di tale processo è ostacolata da molteplici problematiche intrinsecamente legate ai biocatalizzatori, tra cui emerge la produttività generalmente insufficiente a sostenere gli elevati costi di produzione. A limitare ulteriormente le performance degli enzimi si aggiungono fenomeni di inibizione da prodotto, la cui concentrazione in aumento durante la reazione tende inoltre a spostare l'equilibrio verso i reagenti, l'esaurimento del cofattore e le difficoltà legate al mass transfer delle molecole coinvolte. D'altra parte, non è da trascurare la questione del recupero dell'enzima al termine del suo utilizzo, che in forma solubile risulterebbe difficile da separare dai prodotti e richiederebbe ulteriori operazioni di purificazione. Possibili strategie per promuoverne la fattibilità consistono pertanto nell'immobilizzare gli enzimi su supporti adeguati, in modo da renderne più facile il recupero mediante filtrazione, nonché creare un ambiente ottimale nelle vicinanze del sito attico, e nel rigenerare il cofattore per consentire l'avanzamento in continuo della reazione.

In letteratura sono stati studiati numerosi metodi per la riconversione della forma ossidata del cofattore (NAD^+) nella sua forma ridotta (NADH). Da una parte, consistendo in un trasferimento di elettroni, risultano particolarmente promettenti metodi di tipo elettrochimico o fotochimico; d'altro canto, l'utilizzo in tandem di un ulteriore ossidoreduttasi, che rigeneri il NADH utilizzando NAD_+ conducendo una reazione di ossidazione, può essere un approccio conveniente per la valorizzazione simultanea di altre sostanze di scarto. In questa tesi si è scelto di utilizzare l'enzima glicerolo deidrogenasi (GlyDH) da *Geobacillus stearothermophilus* al fine di produrre diidrossiacetone (DHA) ossidando glicerolo, scarto della produzione di biodiesel, contestualmente alla rigenerazione di una mole di NADH. In Figura 1, corrispondente alla Figura 3.8 nel testo, è riportato uno schema della reazione a catena, da cui è inoltre possibile osservare qualitativamente la differenza di diametro dei due enzimi, che può essere stimata a partire dal peso molecolare tramite l'Equazione 3.1, e risulta pari a 5.73 nm per FDH e 9.00 nm per GlyDH.

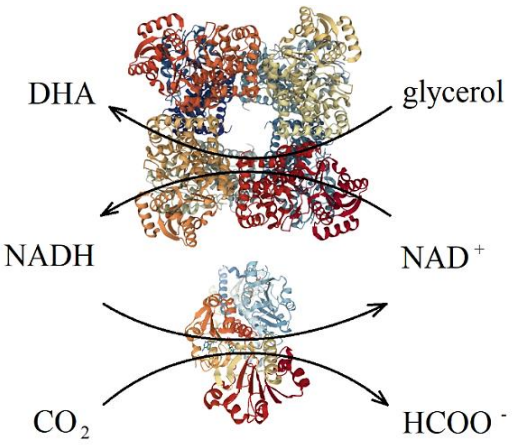

Figura 1 Schema di reazione a catena: conversione di CO2 ad acido formico da parte di FDH e rigenerazione del NADH da parte di GlyDH.

I due enzimi coinvolti, FDH e GlyDH, sono infatti caratterizzati da proprietà catalitiche (attività, stabilità termica e condizioni ottimali) e dimensioni differenti. Questo può risultare in un'ulteriore limitazione alla loro azione sinergica e quindi alla produttività globale del processo. Per far fronte all'esigenza di lavorare in condizioni che risultino ottimali per entrambi i catalizzatori, si è pensato di sviluppare supporti innovativi che potessero soddisfare un compromesso tra prestazioni convenienti, costi contenuti e sostenibilità ambientale. I supporti porosi inorganici sono particolarmente interessanti per la loro resistenza agli agenti fisici e per l'area superficiale molto elevata che offrono. Tra questi, le zeoliti sono costituite da tetraedri di forma generica XO_4, dove la X indica un atomo di alluminio oppure di silicio. Le zeoliti naturali come la clinoptilolite hanno il vantaggio di essere economiche e abbondanti in natura, ma hanno una struttura che può essere soggetta a maggior variabilità rispetto alle zeoliti di sintesi, come la ZSM-5. Nella struttura delle zeoliti naturali possono inoltre essere presenti eteroatomi, principalmente cationi, che ne possono modificare le proprietà. Generalmente questi materiali non vengono scelti per applicazioni biochimiche, essendo microporosi, ossia con diametro dei pori inferiore ai 2 nm, e quindi incompatibili ad ospitare enzimi come FDH e GlyDH che hanno diametro medio tra i 5.7 e i 9 nm. Per questo motivo, in questa tesi, un campione di clinoptilolite (B-Clino) e uno di ZSM-5 (B-ZSM5) sono state sottoposte a un processo di gerarchizzazione al fine di generare dei canali mesoporosi secondari all'interno della struttura microporosa primaria. La strategia adottata è quella della desilicazione alcalina con NaOH. Come raccomandato in letteratura, il rapporto Si/Al della B-Clino (tra 4.0 e 5.3) è stato innalzato preventivamente mediante attacchi acidi con HCl, al fine di evitare un'eccessiva perdita di cristallinità; questo passaggio non è stato invece necessario per la B-ZSM-5, che aveva già un rapporto Si/Al più elevato, pari a 25. Al fine di valutare l'eventuale effetto dei cationi presenti nel framework della clinoptilolite (prevalentemente K, Ca, Fe e Mg), sono stati realizzati due differenti campioni a partire dal materiale base: uno sottoposto a lavaggio con acqua ultrapura prima degli attacchi acidi (H-Clino) e uno sottoposto a scambio ionico con NaCl (H-Na-Clino). Per quanto riguarda la zeolite sintetica, non contenendo eteroatomi in quantità apprezzabili, è stato ottenuto un unico campione gerarchico (H-ZSM5).

Tutti i materiali sono stati esaminati attraverso le comuni prove di caratterizzazione superficiale e di bulk, tra cui: fisisorbimento di azoto (BET), XRD e microscopia elettronica FE-SEM e HR-TEM. Da esse è emerso un notevole incremento di area superficiale, fino al 600% per la clinoptilolite (fino a 300 m^2/g) e del 20% per la ZSM-5 (600 m^2/g), nonché l'evidenza di una distribuzione porosimetrica di tipo multimodale (riportata in Figura 2, corrispondente alle Figure 4.3 e 4.4 del testo), con picchi tra 20 e 80 nm. La cristallinità, rilevata dall'analisi XRD, è stata in buona parte mantenuta, così come la morfologia generale delle due zeoliti: lamellare per la clinoptilolite, granulare per la ZSM-5.

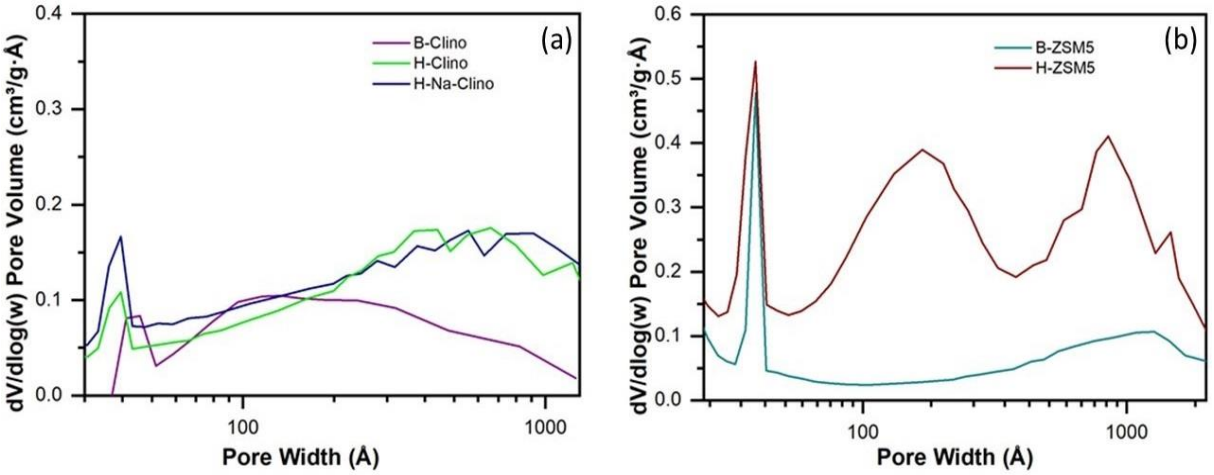

Figura 2 Distribuzioni porosimetriche per i campioni di clinoptilolite (a) e ZSM-5 (b).

Tra le molteplici tecniche di immobilizzazione, è stata selezionata quella che prevede l'instaurazione di legami covalenti tra gruppi funzionali presenti sul supporto e sull'enzima. In particolare, il supporto è stato funzionalizzato con gruppi amminici e aldeidici (gliossile), ponendolo a contatto con i reagenti GPTMS e APTES, rispettivamente. Il reagente APTES ha prodotto direttamente i gruppi amminici, mentre GPTMS ha prodotto inizialmente gruppi epossidici, che sono stati poi sottoposti a idrolisi con H_2SO_4 e infine a ossidazione con $NaIO_4$ per dare luogo ai gruppi aldeidici desiderati. Le moli di questi ultimi sono state quantificate per retro-titolazione degli ioni IO_4^- soluzione al termine del processo, rispetto a quelli iniziali. Tutti i materiali hanno dato risultati simili, intorno a 300 μmol/g. L'immobilizzazione covalente è stata condotta, come da letteratura, in due step successivi: il primo a pH neutro per generare le interazioni deboli tra i gruppi amminici del supporto e le ammine terminali dei residui di lisina dell'enzima; il secondo step a pH 10 ha invece favorito la deprotonazione di queste ultime, con formazione di legami covalenti imminici (basi di Schiff) con i gruppi aldeidici; nell'ultima parte del processo tali legami doppi sono stati ridotti con $NaBH_4$ a legami singoli, al fine di contenere eventuali modificazioni della struttura del sito attivo dell'enzima, spesso riscontrate in questo tipo di immobilizzazione. La resa, valutata mediante saggio di Bradford, è stata del 90-100% per il primo step a pH neutro. Invece, nel buffer alcalino sono stati riscontrati fenomeni di leaching, che hanno abbassato la resa di immobilizzazione al 60-80%.

Una misura quantitativa della co-immobilizzazione dei due enzimi è risultata invece inattuabile, essendo il saggio di Bradford incapace di discriminare il tipo di proteina rimasta in soluzione. Si è preferito, invece, procedere a una verifica qualitativa della buona riuscita del processo, applicando l'innovativo metodo di osservazione al microscopio in fluorescenza. In un primo momento i due enzimi sono stati marcati con opportuni coloranti della famiglia delle rodamine: FDH con ATTO 488, riconducibile a segnali nel canale di emissione verde, e GlyDH con ATTO 550, con emissione nel canale rosso. L'immobilizzazione simultanea dei due enzimi colorati è stata effettuata in modo del tutto simile a quanto già riportato per gli enzimi singoli, ma in ambiente oscurato per evitare il danneggiamento delle molecole attive. Prima del test, sono state effettuate prove di emissione dei supporti funzionalizzati, da cui è emerso come sia i materiali gerarchici (H-Clino, H-Na-Clino e H-ZSM5), sia B-ZSM5, siano in grado di produrre forti segnali in diversi canali, tra cui quelli di interesse. Pertanto, essi sono risultati inadatti alla prova e la scelta del supporto è ricaduta inevitabilmente su B-Clino. Come si può osservare in Figura 3 (corrispondente a Figura 4.14a,b nel testo), entrambi i coloranti (e quindi entrambi gli enzimi) sono chiaramente distinguibili nei rispettivi canali.

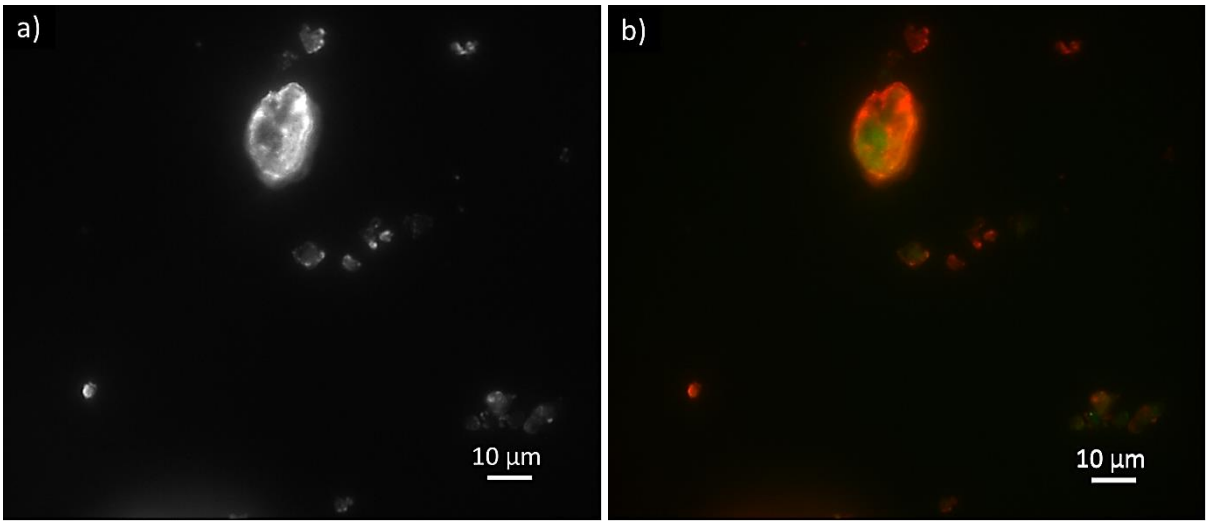

Figura 3 Immagini in fluorescenza: campo chiaro (a) e sovrapposizione di canali rosso e verde (b).

È inoltre possibile ricavare informazioni interessanti sul comportamento degli enzimi durante il processo di immobilizzazione, dal momento che essi risultano posizionati in modo fortemente disomogeneo sulla particella di supporto. Infatti, mentre il segnale verde emesso da FDH sembra essere distribuito in modo più uniforme anche nella parte centrale del granulo, quello rosso dato da GlyDH è localizzato in maggior quantità ai bordi. Questo può derivare dal fatto che FDH, di dimensioni minori, sia in grado di entrare in alcuni micropori, probabilmente modificando la sua forma, allungandosi e restringendosi, e dando quindi un segnale più omogeneo nella parte centrale; al contrario, GlyDH non riesce ad entrare nelle porosità, pertanto si immobilizza principalmente all'esterno, generando una sovrapposizione del segnale in fluorescenza che fa risultare il colore rosso più intenso sul contorno della particella.

L'attività enzimatica è stata determinata per via spettrofotometrica, valutando la velocità di produzione di NADH (con picco di assorbanza a 340 nm) derivante dalla corrispondente reazione di ossidazione. Per questo motivo, sono state studiate: la reazione inversa rispetto a quella di interesse per FDH, ovvero la conversione di formiato di sodio ($HCOO^-Na^+$) in CO_2, e la reazione diretta di interesse di GlyDH, ovvero l'ossidazione di glicerolo a DHA. L'attività dell'enzima supportato è stata quindi confrontata col valore iniziale dell'enzima solubile, tenendo conto della quantità di enzima immobilizzato, ottenendo infine l'attività residua R_{act} percentuale. Da questo punto di vista, H-Clino è risultato il supporto più performante, incrementando l'attività residua di FDH dal 10% (su B-Clino) fino a circa il 50%. Facendo un confronto con H-Na-Clino, che ha portato al 27% di attività residua, si può dire che, dal momento che le caratteristiche fisiche dei due materiali (area superficiale e porosità) sono simili, potrebbero avere avuto un ruolo chiave i cationi rimasti nella struttura di H-Clino, assenti invece in H-Na-Clino. Al contrario, inaspettatamente, H-ZSM5 ha portato a un peggioramento dell'attività residua di FDH, che è scesa dal 50% (di B-ZSM5) fino ad appena il 22%. Questo può essere indice della formazione di una struttura non propriamente gerarchica di H-ZSM5, bensì costituita da semplici mesopori e macropori di forma cilindrica, non connessi ai micropori originali, al contrario di H-Clino e H-Na-Clino. L'attività residua dell'enzima GlyDH, di dimensioni maggiori, non sembra invece aver risentito in alcun modo del differente supporto, rimanendo a un valore intorno al 35-40%. Questo comportamento può essere dovuto al fatto che, come suggerito dalle microscopie in fluorescenza, l'enzima si sia immobilizzato solo sulla superficie esterna, sia sui materiali base sia su quelli gerarchizzati.

Una serie di prove di attività sono state condotte, in modo analogo, con l'obiettivo di determinare le condizioni ottimali di pH e temperatura degli enzimi, liberi e immobilizzati, così come valutarne la stabilità termica nel tempo. Quest'ultima è stata valutata mantenendo il campione di biocatalizzatore alla temperatura di 50 °C per un certo periodo di tempo e misurandone l'attività residua a intervalli prestabiliti; le prove di pH ottimale sono state condotte alla temperatura costante di 30 °C, variando la soluzione tampone, mentre per le prove di temperatura ottimale si è proceduto a riscaldare la soluzione a pH costante pari a 7.5. Entrambi i test hanno dato risultati incoraggianti, avvalorando la scelta di tali materiali gerarchici, soprattutto per l'impiego concomitante dei due enzimi. Per quanto riguarda la stabilità, si è evidenziata una sostanziale variazione del modello di disattivazione termica: mentre l'attività degli enzimi liberi tende a diminuire in modo esponenziale annullandosi dopo un determinato periodo di tempo, quella degli enzimi immobilizzati su H-Clino ha esibito un valore asintotico di attività residua tra il 35 e il 40%. Avendo a che fare con due enzimi derivanti da microrganismi molto differenti, questo effetto è stato decisamente più evidente per FDH, rispetto a GlyDH, il cui gene appartiene a un batterio termofilo. L'immobilizzazione di FDH su H-Clino ha inoltre portato a un innalzamento della sua temperatura ottimale, che è passata da 50 °C a 60 °C. La differenza di pH ottimale dei due enzimi liberi consiste in un ulteriore limite per il loro impiego simultaneo: FDH mostra infatti il suo massimo di attività a pH 7.5, mentre GlyDH è più attivo a pH 10, a cui, tuttavia, si disattiva molto velocemente. In questo caso, l'immobilizzazione su B-Clino e H-Clino ha permesso lo spostamento del pH ottimale di GlyDH verso pH 8, simile a quello di FDH, e che non producesse fenomeni di disattivazione (Figura 4, corrispondente a Figura 4.9 nel testo).

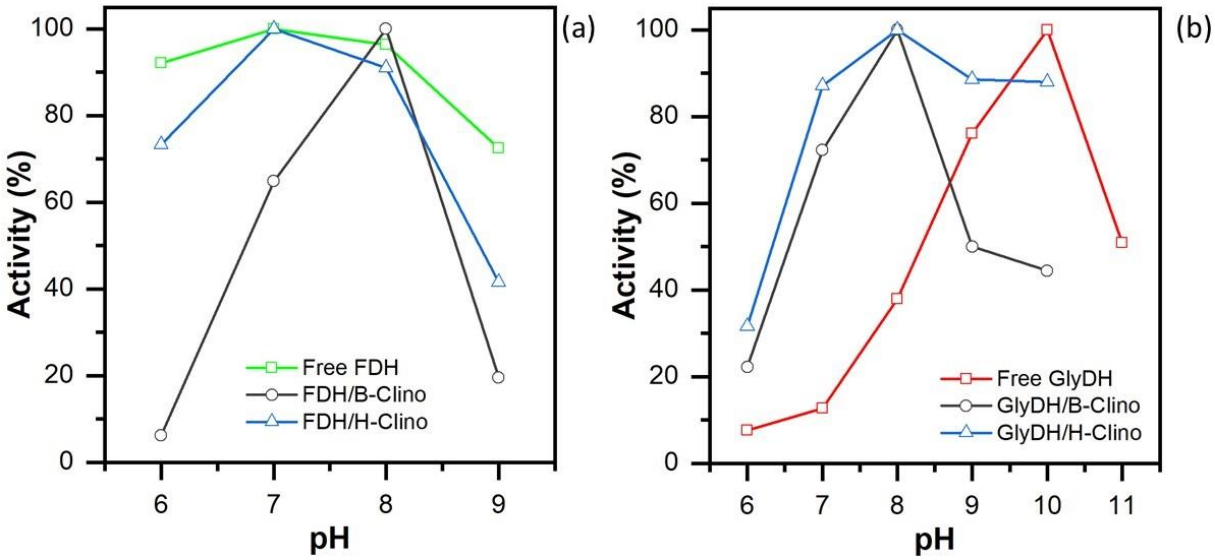

Figura 4 Risultati di pH ottimale per FDH (a) e GlyDH (b): enzima solubile (verde/rosso), enzima immobilizzato su B-Clino (grigio) e su H-Clino (blu).

Infine, è stata testata la reazione di riduzione della CO_2 ad acido formico, per semplicità in condizioni batch, con gorgogliamento di CO_2 in continuo. Il sistema è stato mantenuto alla temperatura di 30 °C, mentre il pH è passato, dopo 6 ore di reazione, dal valore iniziale di 7.5 al valore finale di 6.5 a causa della solubilizzazione dell'anidride carbonica nel buffer. Nel complesso sono state eseguite due prove di reazione distinte: la singola riduzione mediata da FDH su H-Clino e la reazione a catena tra FDH e GlyDH, sul medesimo supporto. Nel primo caso, alla soluzione tampone pH 7.5, in cui è stato sospeso il biocatalizzatore, è stato aggiunto il cofattore NADH in concentrazione 10 mM. In questo modo si è potuta constatare l'effettiva conversione ad acido formico, misurandone la concentrazione mediante cromatografia liquida (HPLC), che è risultata essere del 53% all'equilibrio. Nel secondo caso, invece, il NADH è stato sostituito da una uguale concentrazione di NAD^+ e di glicerolo, in modo da constatare l'effettiva azione di rigenerazione del cofattore mediata da GlyDH. Tuttavia, essendo quest'ultimo più lento (con un'attività specifica di 0.98 IU/g_{sup}) rispetto all'enzima principale (2.39 IU/g_{sup}), è stato necessario immobilizzarne una quantità quadrupla (4 mg di GlyDH e 2 mg di FDH per grammo di supporto) per ottenere una concentrazione di acido formico pari a 2.1 mM (Figura 5, corrispondente a Figura 4.18 nel testo). Tale risultato, oltre ad essere un'importante conferma del lavoro sinergico dei due enzimi, risulta essere indice di un ulteriore fenomeno riconducibile al supporto gerarchico. Quest'ultimo è legato a una forte diminuzione dell'inibizione da prodotto, di GlyDH nei confronti del diidrossiacetone, che per l'enzima in forma libera ha una concentrazione di inibizione massima intorno a 0.42 mM, come riportato in letteratura.

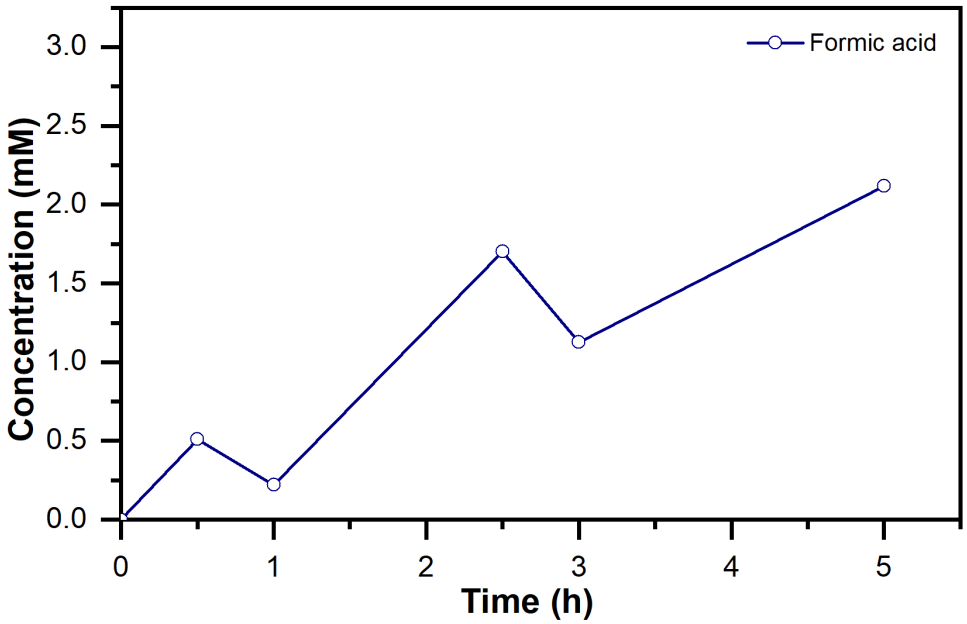

Figura 5 Reazione a catena di riduzione della CO_2 mediata da 2 mg di FDH e 8 mg di GlyDH per grammo di H-Clino (rapporto 1:4).

Queste osservazioni portano a dedurre le molteplici influenze delle zeoliti gerarchiche, sia sui singoli enzimi, sia sulla loro co-immobilizzazione. Esse si rivelano infatti dei potenti strumenti per aumentarne la stabilità e per armonizzarne le condizioni operative ottimali. Pertanto, questo lavoro di tesi pone le basi per la realizzazione di un sistema enzimatico efficiente e "autosufficiente" dal punto di vista operativo, nonché economicamente sostenibile.

Table of contents

1. Introduction

Carbon dioxide is the principal product of a large number of chemical reactions, not only related to anthropogenic activity, such as burning of carbon-rich fossil fuels or other industrial processes, but also owing to natural events. Among these, the largest share of CO_2 releases come from the one dissolved in oceans (42.84%), while the remainder results from respiration of living organisms, organic decomposition and volcanic eruptions [1]. Carbon dioxide contribute to the greenhouse effect, which in principle is a powerful earth thermoregulation phenomenon. Thus, nature has developed an equally efficient "control system" for CO_2 concentration, which is referred to as the "Global Carbon Cycle". Contrary to what one might think, carbon dioxide from human sources is a negligible amount compared to the one resulted from natural processes [1]. Even so, this is sufficient to unbalance that flawless mechanism, leading to a boost of global warming and the subsequent climate changes. Consequently, industrial development has given rise to an indiscriminate growth of carbon dioxide levels in the atmosphere, reaching the value of 409.50 ppm in August 2020, as reported by the National Oceanic and Atmospheric Administration [2]. In this regard, Figure 1.1 shows the trend of the monthly mean CO_2 detected by the Global Monitoring Laboratories since 2016.

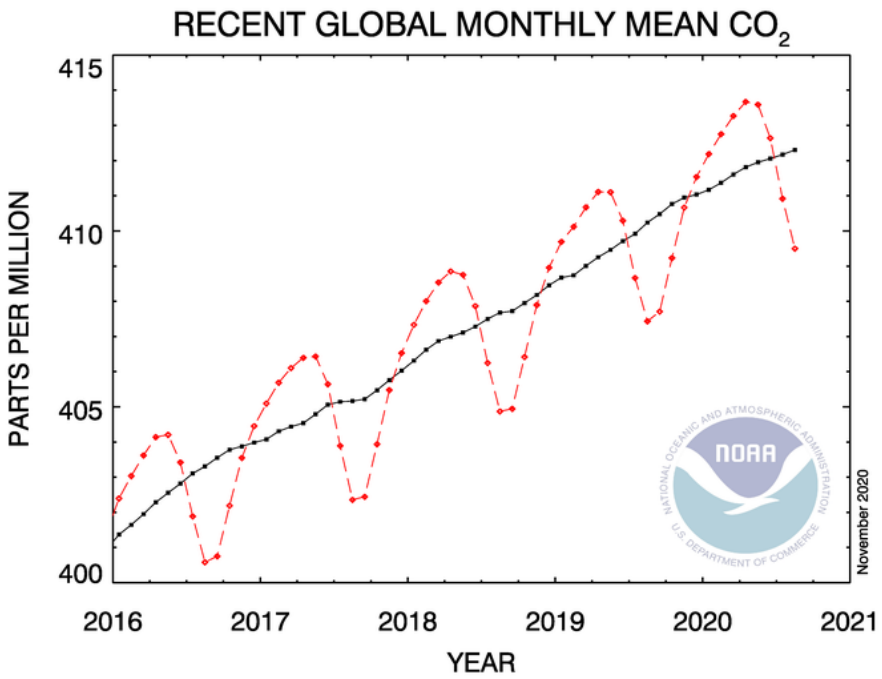

Figure 1.1 Carbon dioxide concentration trend in ppm (defined in dry air) between 2016 and 2020 on a global scale. Red curve represents the monthly mean value, while black line refers to the same values corrected with a moving average over seven adjacent seasonal cycles. From ref. [2]

The underlying cause is the pivotal role that characterizes fossil fuel exploitation in a great number of industrial and everyday activities, mainly combustion processes. Shortly after

the end of World War II, began what is called Anthropocene, that is the era of dramatic growing impact of human activity on biodiversity, species extinction and, on the whole, on planetary ecosystem. Although no precise time limits have been strictly defined, it is estimated to start from the first detonation of nuclear device in New Mexico (USA) in 1945 [3]. In the end, Anthropocene is dominated by a massive abuse of resources and consequent increase of greenhouse gases released in atmosphere. However, more generally, CO_2 emissions boost can be traced back to the industrial revolution, considering that pre-industrial level of carbon dioxide was around 270 ppm, while in 2015 it crossed the critical threshold of 400 ppm.

In these last decades, research attention was focused both on solutions aimed at minimizing the further production of carbon dioxide and on alternative ways to dispose of the exceeding amount of that already produced [4]. Upstream strategies comprise the exploitation of renewable energy sources rather than high-carbon fuels and the improving of energy efficiency, with a view to reducing the so-called "Carbon Footprint" of these processes. However, it has been shown that this can possibly reduce only 10-20% of the overall emissions [1]. Instead, downstream approach is focused on CCSU, namely carbon capture, storage and utilization processes, which are intended to catch CO_2 from atmospheric gaseous mixture, transport it to a storage facility and finally convert it into high-value products, drawing up a full-fledged "Artificial Carbon Cycle" [5].

Yet, carbon dioxide is extremely inert because of the double covalent bonds in its chemical structure, thereby some sort of catalytic system is required to achieve its conversion and valorisation. Although many different routes have been followed, notably thermo-catalytic, photocatalytic and electrocatalytic methods [5], all of these are dominated by a significant energy demand, in the form of high temperature and pressure conditions or either additional electric or solar energy. Moreover, in most cases, they lead to unprofitable levels of yield and selectivity with regard to products of interest.

1.1 Biochemical conversion of carbon dioxide: state of the art

According to what can be observed in the wide literature about this topic, a much cleaner and environmentally sustainable way to pursue this goal has been found in biological methods for CO_2 capture, including microbial and enzymatic processes.

Exploiting enzymes constitutes a promising technique, since they are able to convert carbonaceous substrates with an incomparable selectivity for a certain product [1]. Anyway, a distinction must be made between in-cell and pure enzymes. Indeed, other biocatalysts that share the same microbial cell can cause some modifications on the final product, nullifying, to all intents and purposes, enzymes' peculiar selectivity. Furthermore, complex metabolic pathways are difficultly predictable with a suitable level of accuracy, hence undesired reactions can occur with the formation of secondary metabolites [6]. On the other hand, pure enzymes result in higher costs compared to in-cells microbial application due to extraction and purification processes. In fact, depending on their specific metabolism, some microorganisms are able to produce extracellular or intracellular metabolites: these latter require further cell lysis and separation processes to get the protein of interest with an acceptable purification grade.

For this reason, enzymes have found broader application at large scale in food industry, processing a great deal of goods, or in pharmaceutical and fine chemicals fields, which are associated to higher value products, above €100 per kg [7]. Also, being proteins with different three-dimensional structures, enzymes can be often unstable under operating conditions of temperature or pH, whilst in-cells enzymes are in their optimal environment [4,6]. However, whole cells are affected in some ways by this difficulty as well due to the fact that they are living organisms requiring an accurate study of operating conditions and sometimes they may need to be immobilized too. As opposed to isolated enzymes, aerobic whole cells may necessitate also for additional oxygen supply or micronutrients (i.e. vitamins or minerals) to perform their vital functions, and this has to be taken into account during process design. Thereby, process development and immobilization solutions must be adopted in this way for both types of processes, in order to overcome this problem by recreating that kind of suitable environment [5].

Table 1.1 Comparison between advantages of in-cell and purified enzymes

In-cell enzymes	Cheaper process
	When extracellular production, no need for product purification
Purified enzymes	Incomparable selectivity
	No product modifications by other enzymes
	No metabolic side-products by unconcerned enzymatic pathways
	Non-living biocatalyst
	Easier process conditions regulation
	No need for aeration or micronutrients
	Easier immobilization
	Viable to tailor “artificial metabolic routes”

The shared purpose of biological processes is to simulate the complex cellular metabolic mechanism, which involves a considerable number of reactions, nearly all supported by a specific enzyme or an ensemble of multiple cooperating enzymes. In order to do this, six biosynthetic routes have been emulated, resulting mainly in redox reactions involving two classes of enzymes, namely oxidoreductases (EC class 1) and lyases (EC class 4), which employ CO_2 and bicarbonate (HCO_3^-) as carbon source [6]. In addition, some sort of “artificial” pathway, that are not present in nature, can be pursued by combining purified enzymes from different microorganisms, each of which has distinctive characteristics of thermal and chemical stability.

One important lyase has been reported to be carbonic anhydrase (CA, EC 4.2.1.1), which mediate the interconversion of these two compounds. A Zn^{2+} is coordinated to two cysteine and a histidine residue into the active site of the protein, and this is able to catalyse the hydration of carbon dioxide by nucleophilic attack (Figure 1.2). Besides, CA is of crucial interest in cells metabolism but has been discovered to be a key tool for carbon capture as well, since it accelerates the rate-determining desorption step [6].

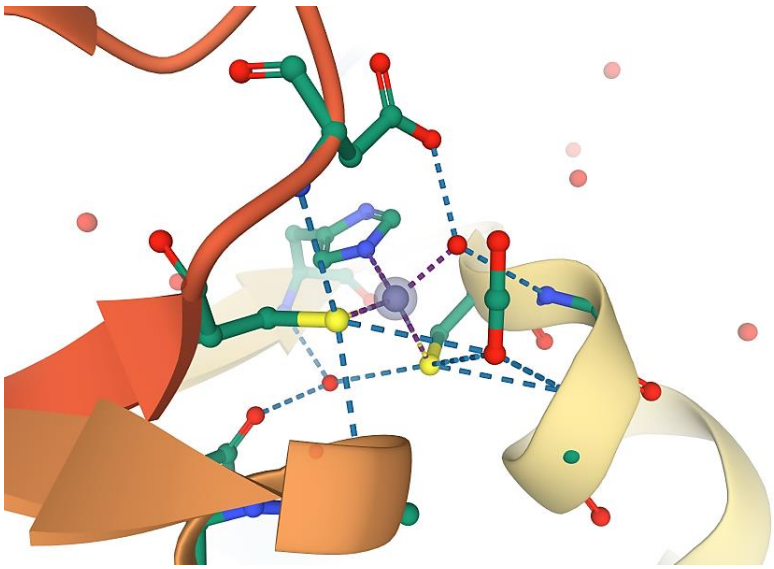

Figure 1.2 3D focus on β-carbonic anhydrase (EC 4.2.1.1) active sites, with the three amino acids (Cys40, His96, Cys99) and central Zn ion (in violet, highlighted) mediating the reaction between carbon dioxide and water, from PDB code: 5BQ1 [8]

Another significant enzyme belonging to the class of lyases is ribulose-1,5-bisphosphate carboxylase/oxygenase, often shortened as RuBisCo (EC 4.1.1.39), which is implicated in photosynthetic carbon fixation, i.e. Calvin cycle [5]. Despite it is known to be the most abundant enzyme in nature, notably in chloroplasts and in microalgae, due to its considerable relevance in biological processes, its application is restricted by low CO_2 fixation rates due to substrate competition with O_2. Actually, RuBisCo is far more selective towards oxygenation of ribulose-1,5-bisphosphate rather than carboxylation of the same substrate, and this means that very high concentration of CO_2 is needed to obtain glucose from this second reaction [1].

Instead, oxidoreductase enzymes promote mostly dehydrogenation reactions, allowing the production of valuable chemicals such as formic acid, carbon monoxide, methanol, methane and carbohydrates, with high stereo-specificity and selectivity. Thus, since oxidoreductases perform the reduction of carbon dioxide, they usually need a reduced cofactor to be oxidized by providing the number of electrons required by the specific reaction. For instance, both the reduction into CO by carbon monoxide dehydrogenase (CODH, EC 1.2.7.4), which is reported in Figure 1.3, and the reduction into formate by formate dehydrogenase (FDH EC 1.2.1.2) require the transfer of 2 electrons per mole, whilst 8 electrons are necessary to produce a mole of methane using a redesigned nitrogenase. Actually, this latter in his native form is able to

reduce nitrogen to ammonia with the shift of 6 electrons, therefore a remodelling of its active site by metal substitution would be needed to achieve the production of formate [6]. Hence, one of the central issues related to this kind of enzymatic reactions is the regeneration of cofactors, usually NADH, often resulting in a supplementary energy demand.

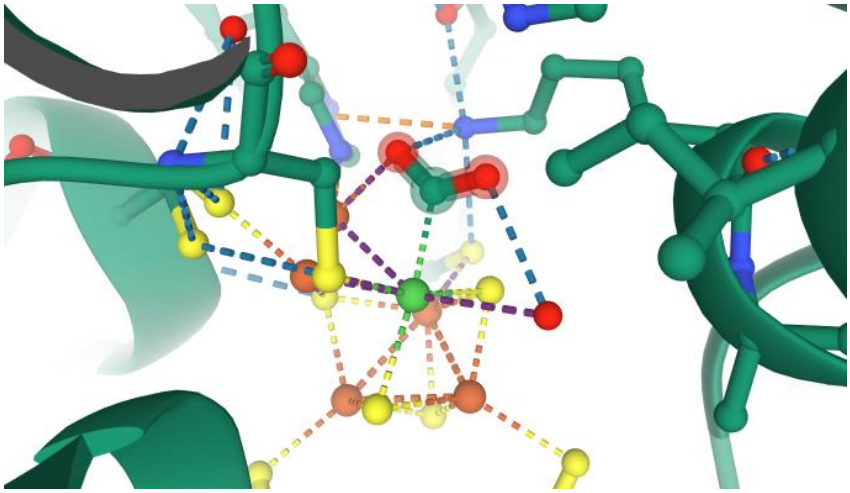

Figure 1.3 3D focus on carbon monoxide dehydrogenase (EC 1.2.7.4) active sites, with central Fe(3)Ni(1)S(4) cluster (Fe ions are in orange, nickel ion is in light green, sulphur is in yellow) bonding CO_2 (highlighted) and water (single red bead), from PDB code: 3B52 [9]

As already mentioned, high costs are related to enzymatic reactions due to the process of extraction from cells and purification of protein matter, thus recirculation of enzymes shall be implemented. Immobilization is one of the approaches that allow to achieve this outcome, alongside with the stabilization of the protein, that prevents it from losing its tertiary/quaternary structure because of some adverse operative conditions. Several methods have been examined, some of them involving more sustainable and effective materials than others [7].

This thesis work is focused on the investigation, development and possible future implementation of biological processes for the conversion of carbon dioxide into methanol, paying particular attention to solutions for enzyme immobilization and cofactor regeneration issues.

2. Enzymatic conversion of carbon dioxide into methanol

Methanol (CH_3OH) is the lowest-carbon alcohol, hence it is a fundamental building block chemical employed as a precursor for a large number of industrial processes, not only as a reagent but notably as a solvent or a denaturant. In particular, many organic compounds such as formaldehyde, acetic acid, phenolic resins and dimethyl ether (DME) can be produced starting from methanol as feedstock [10]. Since '70s oil crisis, methanol has been studied as a promising fuel due to its significant ease of storage as a liquid and transportation, introducing the concept of "Methanol Economy". By this, direct methanol fuel cells (DMFC) have been developed, despite their application is limited to small devices, such as mobile phones and laptop at most.

Beyond well-established methanol synthesis from syngas (i.e. carbon monoxide and hydrogen mixture), other routes can be pursued including CO_2 conversion [10]. Obviously, this leads to double benefit of atmospheric carbon dioxide mitigation and valuable product manufacture. Thermo-catalysis has been successfully developed for carbon dioxide hydrogenation into methanol (CH_3OH) over metals or oxides, such as copper based catalysts, but this often implies severe operative conditions, with temperature up to 200-300°C and pressure that can reach over 50-100 atm, as an order of magnitude [11]. Likewise, both gaseous hydrogen production, either by steam reforming or water electrolysis, and storage are challenging for harsh conditions in terms of extreme temperatures and high compression ratios. Thus, although it is able to get high productivity even at larger scale, this method is affected by a strong requirement of thermal and electrical energy, rendering it environmentally unsustainable [11]. Enhancement of renewable energy sources, among which solar and wind are the most feasible and economical, sets the stage for exploiting also electrochemical methods. Photochemical ways have been developed as well to carry on the complete reaction, designing a kind of artificial photosynthesis. However, they are constrained by significant variability over time [4,10]. As a potential alternative, biocatalysis has been recommended, besides research has been boosted in order to make it feasible and possibly competitive with other technologies. The main advantage of this latter is definitely their unparalleled selectivity towards methanol.

2.1 Multi-enzyme cascade

Multi-enzyme cascade is the most common enzymatic approach to reduce carbon dioxide to methanol as a final product [6]. During the last years of the past century many researchers started to investigate enzymatic ways, focusing mainly on reductive ones. For the first time, 1994, Yoneyama *et al.* [12] proposed a novel electrochemical hybrid path involving two enzymes in series, namely formate dehydrogenase (FDH, EC 1.2.1.2) and methanol dehydrogenase (MDH, EC 1.1.99.8) to produce methanol through halfway formation of formic acid. This entails the use of a mediator, i.e. methyl viologen (MV) or pyrroloquinoline quinone (PQQ), to transfer the needed electrons from an electrocatalytic auxiliary system.

Afterwards, this strategy has been modified by replacing methanol dehydrogenase with other two oxidoreductases. This ends up with an enzymatic cascade constituted by formate dehydrogenase (FDH), formaldehyde dehydrogenase ($F_{ald}DH$, EC 1.2.1.46) and alcohol dehydrogenase (ADH, EC 1.1.1.1), passing through the reduction of CO_2 to formic acid HCOOH, then to formaldehyde H_2CO and finally to methanol CH_3OH (Figure 2.1). Indeed, dehydrogenases are supposed to carry forward this series of reaction reversely, but the presence of large excess of cofactor nicotinamide adenine dinucleotide (NADH) as electron donor is capable of shifting the equilibrium in order to catalyse this path [13]. In particular, these three enzymes make sure to let the reaction cascade proceed this way with the support of three moles of NADH [6].

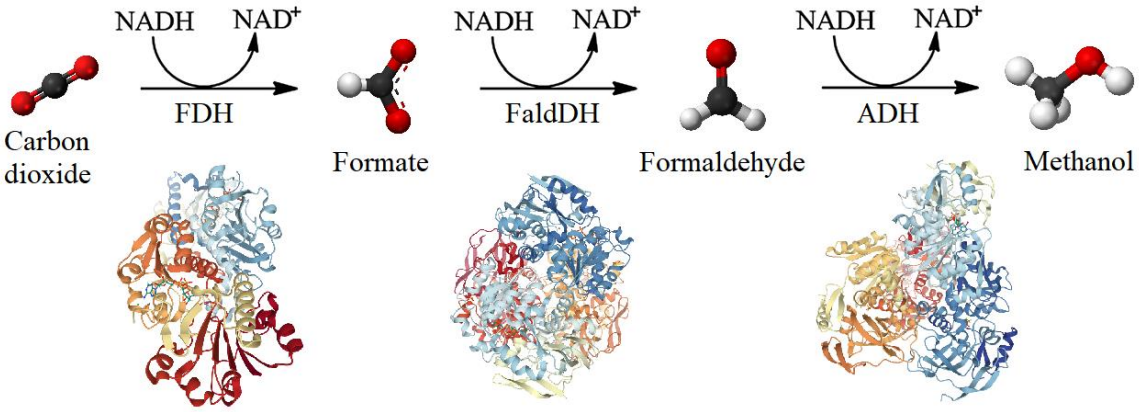

Figure 2.1 Dehydrogenases cascade reaction route: FDH is from PDB code: 5DN9 [14], $F_{ald}DH$ is from PDB code: 1KOL [15], while ADH is from PDB code: 4W6Z [16].

Similar enzymatic cascade is of interest in the context of whole biorefinery processes also for the hydrogenation of carboxylic acids yielding their corresponding alcohols. As part of "SATURNO" project financed by *Regione Piemonte*, an electro-enzymatic system has been constructed involving the consecutive action of carboxylic acid reductase (CAR, EC 1.2.99.6), originating aldehyde intermediates, and alcohol dehydrogenase producing alcohols [17].

The surroundings in which reactions take place is fundamental both for stability of proteins and for methanol productivity. The target is to recreate a suitable microenvironment in which enzymes can find optimal conditions of confinement and concentration of substrates. Obert and Dave [13] are considered to be pioneers in this field, since they first studied the utilization of this DH cascade, also reporting the benefits of encapsulation procedure in silica sol-gel matrices. As a result, confinement into porous carrier allows to shift equilibrium more towards products, thus significantly increases the production of methanol in comparison with the free enzymes in solution. Notwithstanding, methanol production remains low even after 3 hours of batch reaction, barely reaching 15 µmol of CH_3OH with 50 µmol of NADH. This can be imputable to inhibition effects of alcohol, which thereby must be rapidly removed from the reacting solution [13]. Likewise, concentration of oxidised NAD^+ nearby active sites contribute to act against conversion. Restoring of cofactor is also needed in order to thrust this process in

the direction of industrial application in affordable way. In section 2.3 various techniques for NADH restoring are proposed.

2.2 Enzyme immobilization

One of the foremost priorities for the purpose of enabling a worthwhile utilization of enzymes lies in their reusability. Being high-priced commodities, it would be inconceivable to lose them as waste at the end of every reaction cycle; at the same time, if enzymes are dissolved into the reaction medium, their retain and recovery would be most unlikely, ending up in this undesirable situation. The optimal way to ensure the lowest possible enzyme loss, enhancing the economic competitiveness of the overall process, is to immobilize them on some kind of support [18].

In the process of selection of the best strategy of immobilization, in terms of method and implied materials, several aspects have to be taken into account: the three-dimensional structure of the enzyme is of paramount importance, since it reflects the biocatalytic properties and therefore has to be preserved, but also it determines the actual dimension of the protein. In this view, the surface of the carrier must be compatible to host the enzyme [18]. Immobilization may have both beneficial and adverse effects. Since it involves some sort of bond between the protein and the carrier, notably ionic or covalent bonds, it can induce a variation in the structure of the active site and therefore an alteration of catalytic activity. Secondly, as mentioned above, recreating a suitable surrounding environment may increase the stability of the enzymes, in addition to the main goal of the procedure, that is their recycling. In addition, effective immobilization is required to facilitate the downstream separation of the biocatalyst from the reactive media, thus providing purer products [18].

Since the conversion of carbon dioxide to methanol involves a cascade reaction, carried out by multiple enzymes, the differences between these latter, in terms of shapes, dimensions and catalytic features, must be considered. A number of different immobilization approaches and types of support have been intensively investigated during the last decades. Luo *et al*. [19] explored different strategies of deposition to carry out co-immobilization and sequential immobilization, comparing them with free enzymes as well in terms of methanol production. Enzymes have been filtered over porous polypropylene membranes by applying a pressure of 2 bar promoting proteins fouling. In this way, immobilization is achieved by the formation of low-energy secondary bonds, i.e. hydrogen bonds or electrostatic forces, rather than strong covalent bonds. In fact, as already stated, although this latter highly prevent leakage, in some cases it can lead to activity loss caused by structural changes in the active sites [7]. Nonetheless, the drawback of secondary bonds is their poor stability over time, that leads to enzyme inactivation after a few cycles of utilization. By separating this operation into multiple stages, layer-by-layer sequential deposition of different enzymes, namely FDH, F_{ald}DH, ADH, has been conducted (Figure 2.2). This method resulted to be the best choice of immobilization, leading to concentrations of the order of 0.7 mM of CH_3OH with 50 mM of NADH after 30 minutes of reaction, compared to co-immobilization which remains around 0.5 mM. This outcome is due to the fact that spatial separation allowed to better regulate each reaction step,

overtaking the effect of the longer separation between two subsequent enzymes in the cascade [19].

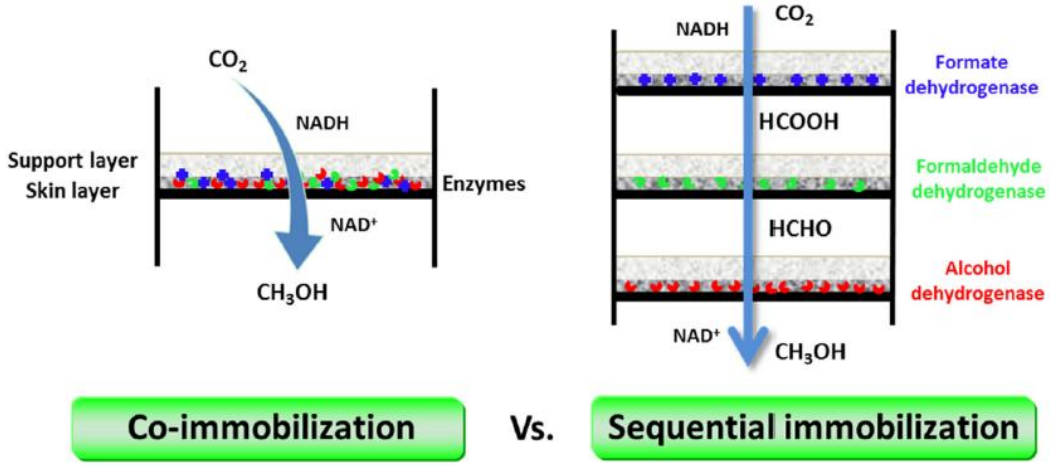

Figure 2.2 Comparison between filtration procedures for performing co-immobilization and sequential immobilization, from ref. [19]

2.2.1 Covalent attachment over functionalized supports

Introducing functional groups on the surface of the carrier constitutes a practical and effective way, often employed to establish covalent bonds with the desired enzyme. The most common reactive groups are aldehydes, epoxides, amines, and thiols, and are selected to react with as many terminal groups belonging to amino acids residues that are abundant on the surface of the protein, such as lysine, cysteine, aspartate, and glutamate [18]. In contrast to other attachment methods that involve weaker bonds, such as ionic binding, adsorption [19], encapsulation [13], and aggregation, covalent attachment is highly specific, generally easier to realize, and minimizes the risk of leaching. Besides, some of these immobilization techniques can be coupled in order to obtain better enzymatic performances; this is possible, for example, by adding to the support ù more than one reactive group, hence producing a hetero-functionalized carrier [18].

2.2.2 Porous aluminosilicate as supports for immobilization

Among all the possible materials to constitute the support for the immobilization of enzymes, great interest has been displayed towards porous aluminosilicates, namely zeolites and silicas [18]. More in general, inorganic solids are characterized by higher thermal stability and mechanical resistance, therefore they are frequently preferred over organic ones. This feature acquires even more significance for porous materials, which have thinner walls and need to withstand mechanical stresses without breaking. Depending on the diameter of the cavities, commonly referring to interparticle voids, three classes of supports can be identified: microporous if the size is smaller than 2 nm, macroporous if the diameter is bigger than 50 nm and mesoporous if it is in between [18]. In particular, zeolites and silicas are respectively

microporous and mesoporous substrates that are commonly used for this purpose since they exhibit remarkable supporting performances. The greatest advantage stands in their considerable surface area.

Zeolites are built over a tetrahedral structure of alumina and silica units AlO_4 and SiO_4 which, by its very nature, can be characterized by both in-framework and extra-framework heteroatoms, frequently cations [18]. This situation is common regarding natural zeolites, the most prevalent of which are clinoptilolite and mordenite. Synthetic zeolites are also interesting due to peculiar customizable structure which depends directly on the method of preparation and permit to obtain pores of controlled size and distribution. In addition, zeolites surface area is not only very extensive but also host several acid or basic sites which may interact electrostatically with biocatalysts [18]. On the downside, zeolites are substantially microporous, with cavity diameter of less than 2 nm that act as molecular sieve. Consequently, since enzymes have generally equal or larger size, they are not able to penetrate inside the porosity and turn out to be immobilized commonly on the outer surface of the particles.

With the intention of improving these aspects, along with deleting the limitations attributable to the mass transfer of bulky molecules, the introduction of larger channels, constituting a secondary porosity in the zeolitic framework, appears to be a convenient choice. Hierarchization can be conducted through different strategies, that can be divided into two groups, namely bottom-up and top-down approaches. The first group of methods concerns the synthesis of hierarchical zeolites starting from their precursors and adding templating agents. The second ones, instead, provides for using strong acids or bases to remove aluminium or silica atoms, hence digging new cavities, into the preformed zeolite [20]. This latter strategy is notably remarkable, considering that it can be applied to inexpensive natural zeolites with simple procedure and reagents.

2.3 Regeneration of cofactor NADH

Almost every oxidoreductase relies on cofactors to carry on reactions that imply electron, hydrogen or oxygen transfer. Among these, NADH and NADPH are involved in almost 90% of known enzymes-driven redox reactions [21]. With a view to improve the feasibility of large-scale application of carbon dioxide conversion to methanol through oxidoreductases one main obstacle to overcome is the efficient continuous reduction of oxidised cofactor $NAD(P)^+$ to NAD(P)H. This cofactor is economically impactful because it is needed in large amount and it has high costs, from few hundred to several thousand dollars per gram. This is explained, in the same way as pure enzymes, by the fact that pyridine cofactors are biosynthesized inside cells and their industrial production process goes through complex steps of purification [21]. Furthermore, in addition to shifting equilibrium towards products, avoiding inhibition caused by oxidized cofactor and thereby enhancing conversion, regeneration may also induce the formation of additional valuable products. Improvements in these methods is the way to accomplish a further advantage compared to whole-cells microbial conversion, for the purpose of making enzymes' ones more worthwhile that the others.

NADH restoring stands basically for an electron transfer issue, that can be fulfilled by biochemical, chemical, electrochemical or photochemical approaches [21]. Compared to these latter, enzymes are characterized by unique selectivity and total turnover number (defined as the moles of the product of interest formed by one mole of NADH consumed during the complete reaction). Also, they are the most environmentally sustainable and simple due to their application to biological-friendly mild operative conditions. Although both photochemical and electrochemical can be powered by clean and green energy sources (respectively direct solar energy or renewables converted into electricity), their low efficiency is slightly detrimental. In particular, photochemical application is often limited to a certain range of wavelength, usually beyond visible light, requiring some mediators such as photosensitizers [21]. Electrochemical systems are also electron mediators-dependent and might suffer from electrode fouling. Besides, pollutants formation may derive from chemical methods employing inorganic salts. Nevertheless, in light of this, cost-benefits analysis is indispensable to select a proper method, given that none of them turned out to be optimum in an absolute way.

2.3.1 Enzymatic methods for NADH regeneration

A valid strategy has been found in exploiting auxiliary enzymes to simultaneously catalyse the reduction of NADH, in parallel to the conversion of CO_2 [21]. This allows to both remove NAD^+, which is somehow a product of the reaction, from the proximity of the active site and to have a certain amount of NADH, that can be considered a reagent, available for a more lasting process. Actually, some of these enzymes are "substrate-driven", so they employ a support molecule to be oxidised providing electrons for the reduction of cofactor.

Among these, glutamate dehydrogenase (GDH, EC 1.4.1.2) is a promising enzyme which catalyses the conversion of glutamic acid into α-ketoglutaric acid yielding ammonia, meanwhile transferring one electron and a proton to NAD^+ (Figure 2.3). Magnification of the interaction between glutamate dehydrogenase active site and ligand nicotinamide adenine dinucleotide (NAD) is also reported in Figure 2.4. This enzyme can be co-immobilized within the same carrier of FDH, $F_{ald}DH$ and ADH resulting in profitable retain of activity even after recycling ten times, as proposed by El-Zahab *et al.* [22]. This process has also a double benefit: not only it reconstitutes the cofactor, but it produces ketoglutaric acid, which is a valuable product itself, finding application as precursor for pentane-1,5-diol for polyesters synthesis.

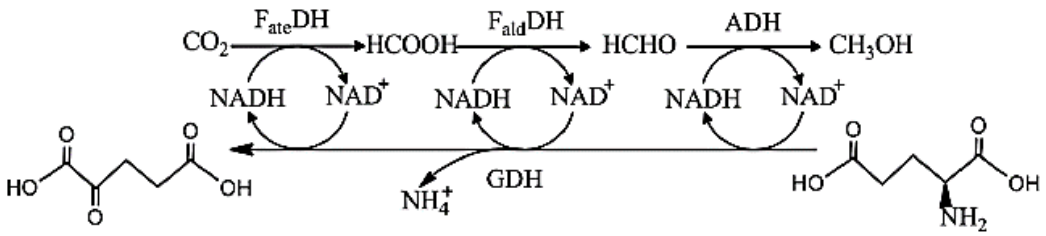

Figure 2.3 Glutamate dehydrogenase (GDH) for NADH restoring, from ref. [6]

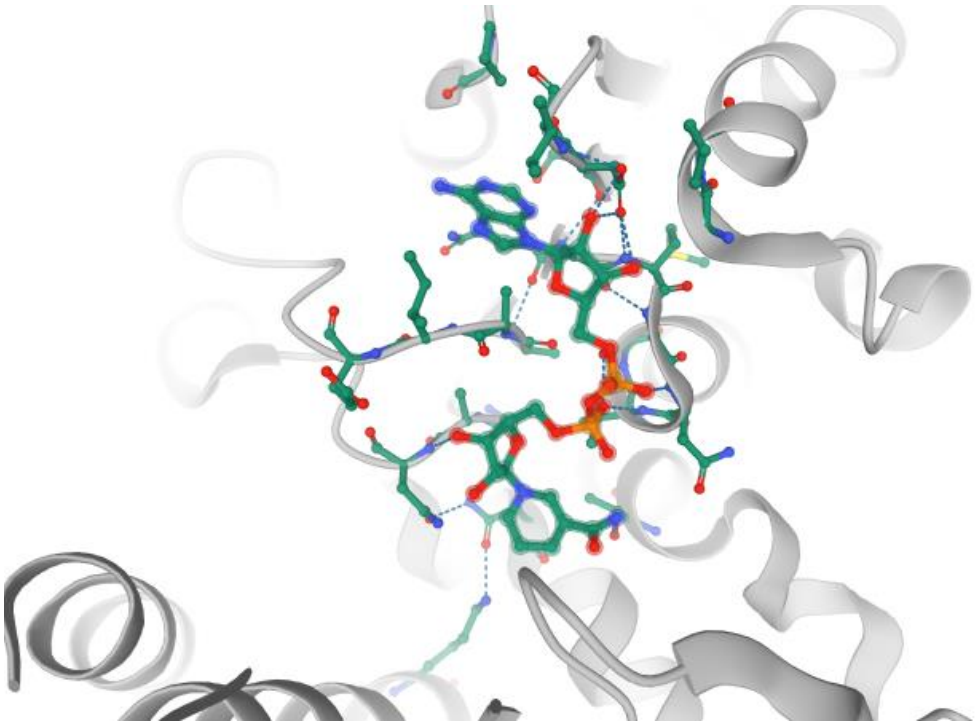

Figure 2.4 Focus on glutamate dehydrogenase active site with bounded nicotinamide adenine dinucleotide (NAD) ligand, from PDB code: 1V9L [23].

Enzyme phosphite dehydrogenase (PtDH, EC 1.20.1.1), sometimes referred to as phosphonate:NAD^+ oxidoreductase, has been applied to this task by Vrtis *et al.* [24] to increase the activity of the regenerative system. This enzyme is much less expensive compared to GDH, and the substrate can be fed directly by phosphate-buffered solution (PBS) commonly used for pH adjustment. In this sense, phosphite is converted into phosphate (Figure 2.5), and it has been shown that this latter doesn't affect the activity by any inhibition effect [24] and can be easily precipitated, if necessary, by calcium. Some years later, Cazelles *et al.* [25] compared phosphite dehydrogenase with another enzyme, glycerol dehydrogenase (GlDH, EC 1.1.1.6), and a natural photosystem, a chloroplast, concluding that PtDH is proven to be much more efficient at neutral pH than all the others. Although, due to marked susceptibility even to mild temperatures of wild-type PtDH, research has been rerouted towards the screening of enzymes obtained by site-directed mutagenesis [24,25].

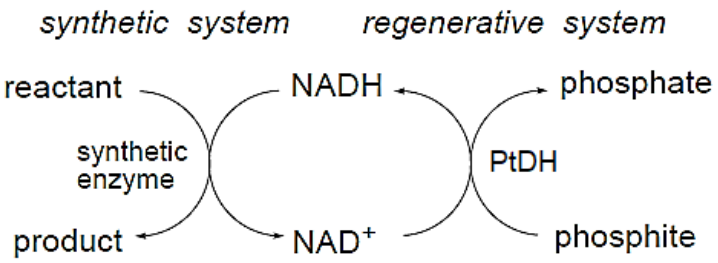

Figure 2.5 Phosphite dehydrogenase (PtDH) for NADH regeneration, from ref. [24]

With a view to organic waste valorization, glycerol dehydrogenase (GlyDH, EC 1.1.1.6) represents a convenient way to combine enzymatic NADH regeneration, for the enhancement or primary CO_2 reduction, with the conversion of glycerol, which is indeed the main by-product of biodiesel industry [26]. Dihydroxyacetone (DHA) is obtained from this reaction as a value-added product, having a price more than 400 times higher than the reagent [26]. Figure 2.7 reports the scheme of the enzymatic conversion of glycerol into dihydroxyacetone with the employment of one mole of NAD^+, while Figure 2.6 shows the common shape of GlyDH from *Geobacillus stearothermophilus*, and a focus on the structure of the active site of the enzyme.

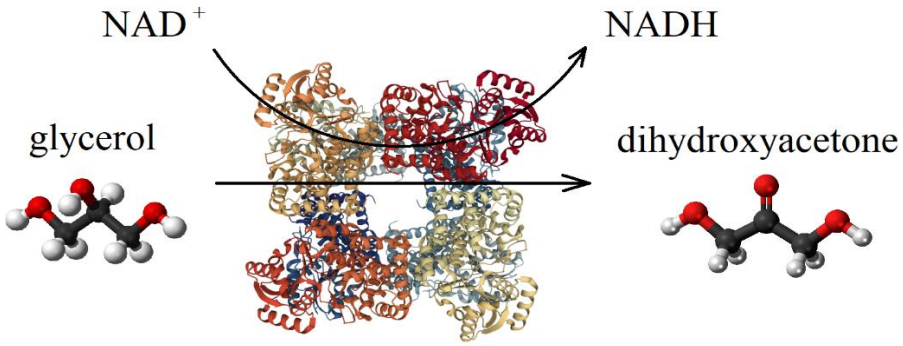

Figure 2.6 Glycerol dehydrogenase (GlyDH) for NADH regeneration.

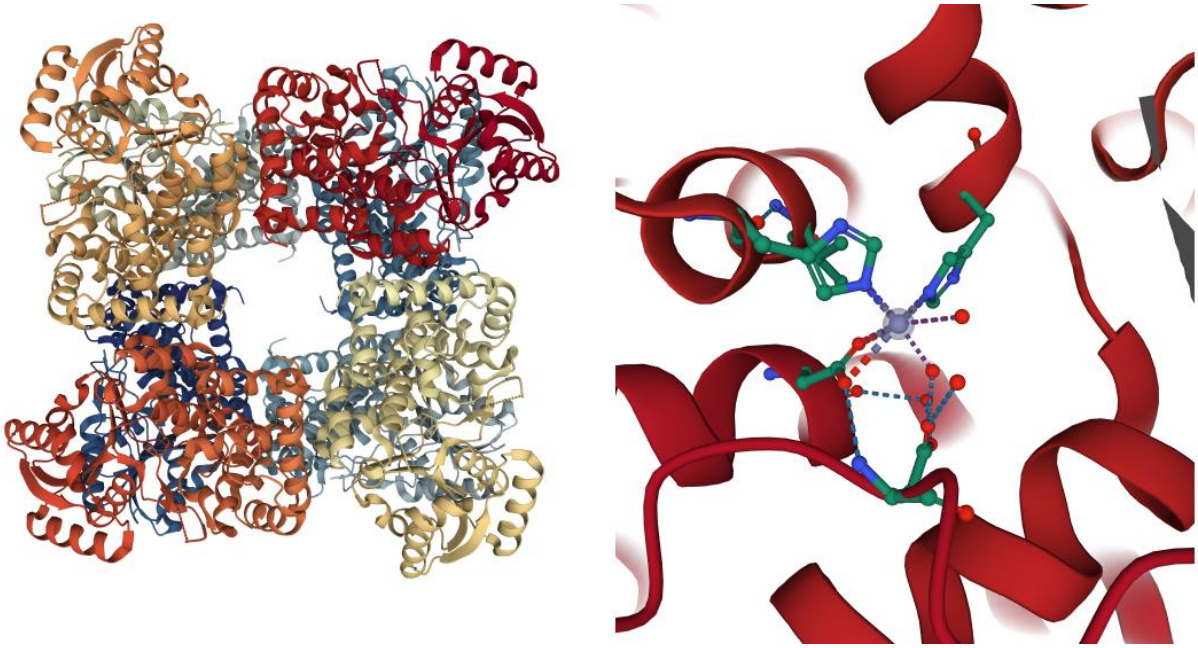

Figure 2.7 Focus on the eight subunit that constitute glycerol dehydrogenase (on the left) and on the active site (on the right), in which a zinc atom (in violet) can be found, bounded to two histidine and two aspartate residues, from PDB code: 1JPU [27].

In principle, the most used enzyme for NADH regeneration is actually formate dehydrogenase FDH, in large excess of reactants $HCOO^-$ and NAD^+ [21]. Obviously, this can't

be applied to carbon dioxide conversion since the desired reaction is exactly the reverse one. This is evidence that during the complete conversion process it is necessary to work with high concentrations of carbon dioxide and cofactor, but also to quickly remove the products in order to shift the equilibrium towards the desired direction.

A deep search of the relevant literature ensued that substrate-independent enzymes, e.g. NADH oxidases (Nox, EC 1.6.99.3) have been studied only to regenerate oxidised coenzymes NAD^+ or $NADP^+$. Gao et al. [28] investigated different wild-type Nox from various microorganisms, stated that some of them give side-production of water by shuttling two electrons while four-electron reduction originates hydrogen peroxide. The first class of biocatalysts are preferred to conduct this process, considering that H_2O_2 can act as a strong denaturation agent for many enzymes, resulting in detrimental effect for global reaction. There is no evidence of a possible employment of this class of enzymes to perform the reverse reaction, thus far. For this reason, research has tended to focus predominantly on substrate-dependent enzymes rather than these latter.

2.3.2 Photo-electro-chemical processes for NADH regeneration

Chemical approach based on catalysed redox reactions often suffer from wastage issues, since inorganic salts are exhausted at the end of the process. Moreover, high concentrations of salts needed for the regeneration of NADH can cause the deactivation of process enzymes, i.e. dehydrogenases used for the conversion of CO_2. As a consequence, these two issues make it economically unfeasible on a larger scale for the time being. However, some examples of heterogenous catalysts tested at small scale are biomimetic organometallic complexes based on transition metals such as rhodium, known to be currently the most precious and expensive metal, with a price almost 10 times higher than gold [21].

Other methods for cofactors restoring also imply delivering electrons or other reducing equivalents to oxidised form NAD^+, and of course this means that any type of energy is required. One alternative arrangement has been proposed by Schlager *et al.* [29] in 2016 referring to a cofactor-independent bio-electrochemical system. In this case, the three dehydrogenases are all supported over a carbon felt electrode coated with an alginate-silicate hybrid gel matrix, so an electron flux is directly funnelled to serve the biocatalysts (Figure 2.8). In Figure 2.9 is also showed a scheme of the electrochemical cell involved in this process. Neither NADH nor other cofactors are necessary, hence the entire process is based on direct electron flow from the electrode to the enzyme. The overall reaction needs a theoretical potential of -0.38 V to move forward, besides an additional overpotential has to be prescribed. In fact, direct injection way has been effectively undertaken at -1.2 V with respect to an Ag/AgCl reference electrode, getting a Faradaic efficiency of around 10% [29].

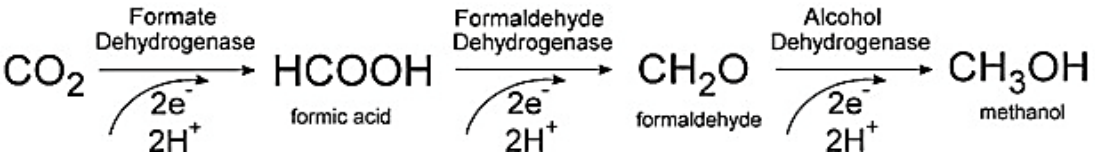

Figure 2.8 Cofactor independent mechanisms of CO_2 reduction to methanol, from ref. [29]

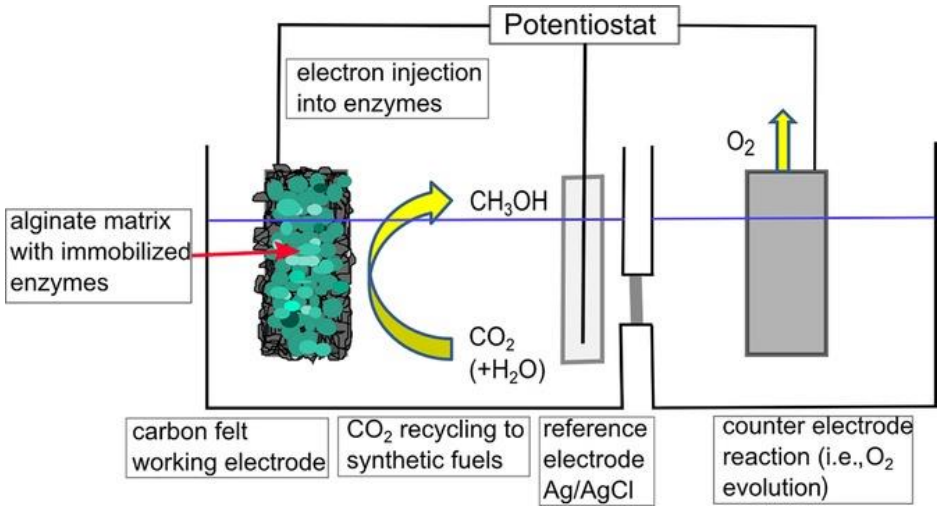

Figure 2.9 Electrochemical cell for direct electron injection method [29].

Electrocatalytic regeneration of NADH involve the two-step reduction of NAD^+ at the cathode. The first step consists in the transfer of the first electron with reversible formation of a radical species NAD•, which can undergo a further reduction and protonation to originate NADH. This second step is decisive in determining the regeneration efficiency of the process due to the slow kinetic that enables the formation of other improper-reduced compounds, namely NAD_2, which is ineffective for the production process [21]. In the light of this, electrode modification has been investigated in order to fix selectivity issues, avoiding further unfavourable loss of coenzyme, reduce the significant overpotential often required for electrons shuttling and also to mitigate electrode fouling phenomena [21]. Many approaches have been examined over the past years, including direct regeneration by contact of coenzyme with the modified electrode, mediated regeneration (i.e. reduction assisted by intermediary compounds) and ultimately enzyme-mediated regeneration [21]. Handling redox mediators may also imply their immobilization on the electrode, producing even in this case a sort of modification effect, to improve stability and downstream separation processes.

As mentioned above, the possibility to harvest clean and low-cost solar energy originated growing attention towards photochemical methods [21]. Sometimes, solar-driven devices have been possibly coupled to enzymes, recreating an artificial-photosynthesis mechanism. The aim is to mimic the efficient natural Calvin cycle, an electron transport chain which allows to store electrons inside cofactor NADH by adsorbing photons in visible light spectrum. This is possible thanks to chlorophyll that acts as a powerful photosensitizer in this range of wavelength. Although various compounds have been screened to find suitable artificial sensitizers for this

purpose, and electron mediators as well, unfortunately these are commonly quite expensive. Rhodium complexes are the most widely used mediators, while both organic and inorganic sensitizers have been tested, concluding that metal-based photocatalysts, e.g. titania (TiO_2) have broader long-term stability and corrosion resistance [21].

2.4 Alternative enzymatic ways

Multi-enzyme pathway's main drawback lies in the fact that every biological catalyst usually has medium-low productivity. This effect is amplified the greater the number of enzymes that are involved. For this reason, shorter alternative biosynthetic routes need to be investigated. However, the overwhelming majority of the literature about the reduction of carbon dioxide into methanol is capitalized by the three-enzyme cascade that has been described in detail in section 2.2. Consequently, from this point of view, to the best of our knowledge, there is a lack of investigation on innovative enzymatic routes for this process.

What is known is that for obtaining methanol starting from methane as a feedstock another oxidoreductase, namely methane monooxygenase (MMO, EC 1.14.13.25), can be exploited [30]. In the light of this, although there is no evidence that this path has ever been followed before, methane oxidation to methanol could be teamed up with carbon dioxide hydrogenation mediated by modified nitrogenase (EC 1.18.6.1) [31]. The scheme of this reaction is shown in Figure 2.10. This represents a hypothetical novel way to achieve CO_2-to-methanol conversion through 2-step enzymatic process, that will not be discussed in detail within this thesis work but can possibly provide insights for further research.

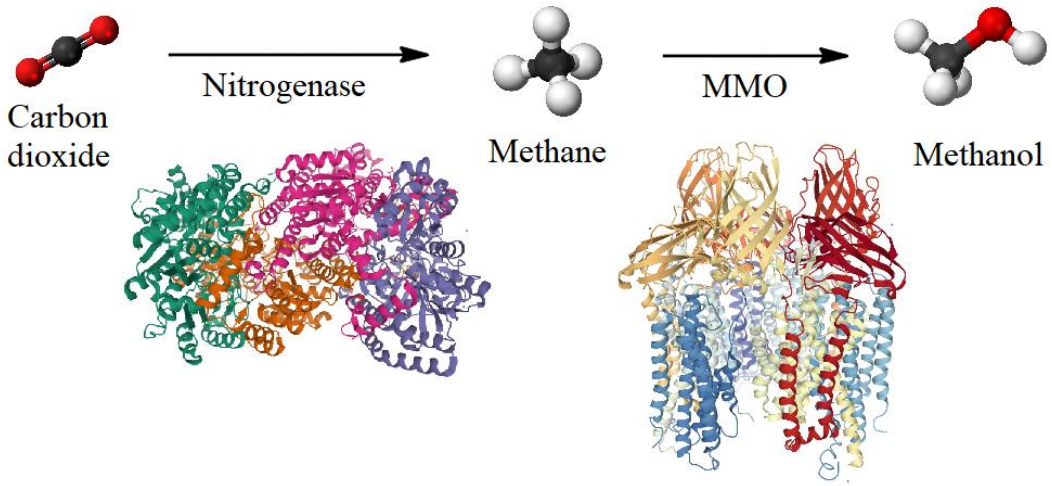

Figure 2.10 Proposed alternative enzymatic route for carbon dioxide conversion to methanol through reduction into methane by remodelled nitrogenase (PDB code: 6VXT [32]) and further oxidation by methane monooxygenase (PDB code: 3RGB [33]).

Nitrogenase is naturally utilized by cells for nitrogen (N_2) fixation into ammonia (NH_3), by transferring six electrons, for amino acids and nucleic acids biosynthesis. The feasibility of two-electrons reduction from carbon dioxide (CO_2) to carbon monoxide (CO) has also been

demonstrated with the exploitation of wild-type *Azotobacter vinelandii* nitrogenase. Instead, carbon dioxide reduction into methane (CH_4) requires an eight-electrons transfer, which turned out not to be favoured by native nitrogenases [31, 34]. This enzyme is present in nature in the form of three different metal-dependent isozymes; the preponderant one is molybdenum nitrogenase, whereas less-abundant vanadium and iron nitrogenases are considered to be alternative isozymes, whose genes are sometimes expressed by some diazotroph species in low-molybdenum availability conditions. All these isozymes are characterized by similar quaternary structure in which different subunits can be distinguished: two identical catalytic MoFe-proteins and one electron delivery Fe-protein for each. In this way, the electron flux originates from the hydrolysis of ATP bounded into this latter and is shuttled into the catalytic subunit by Fe-S clusters reaching the active site [31].

Carbon dioxide reduction through nitrogenase has the benefit to proceed without the need of any added pyridine cofactor like NADH or NADPH. Indeed, a metal cluster constituted by iron, molybdenum, sulphur and carbon (i.e. FeMo-cofactor) is the main cofactor for Mo-nitrogenase activity, and it is contained directly within enzyme's active site (Figure 2.11), bounded to amino acid Cys-275 [32]. Even so, this enzyme relies on ATP utilization, which is still less expensive than pyridine cofactors and whose regeneration has been investigated for the last fifty years [31].

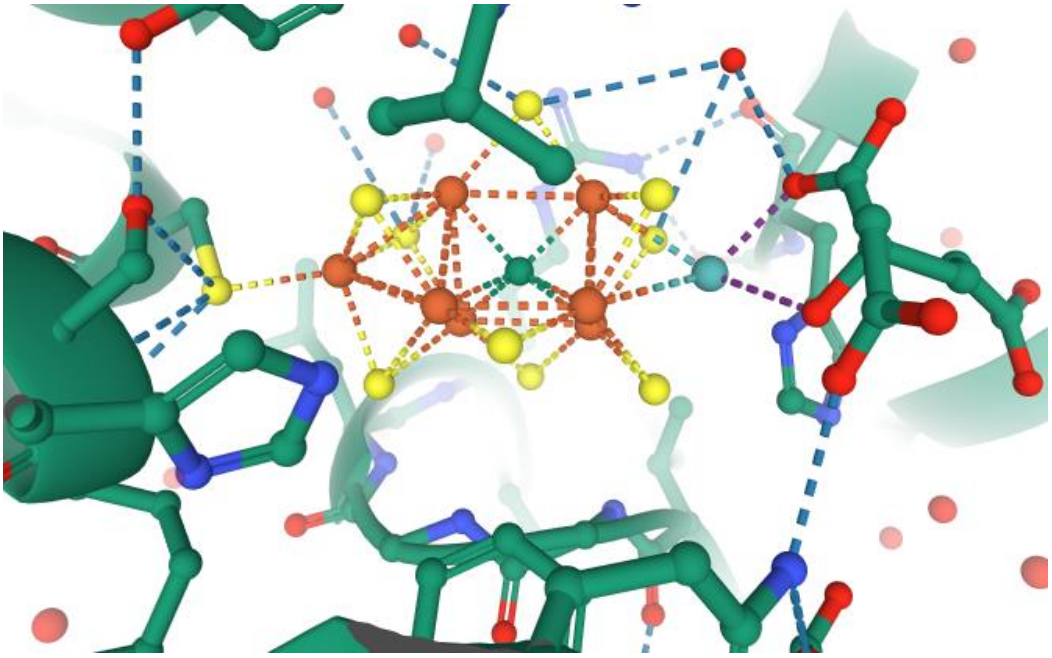

Figure 2.11 3D focus on catalytic MoFe-protein active site bounded to the central FeMo-cofactor (7Fe-9S-1Mo-1C-R-homocitrare). Light blue bead represents molybdenum atom (on the right, bounded to R-homocitrate), orange is for iron, yellow is for sulphur and green for carbon. Cys275-S bound can be observed on the left. From PDB code: 6VXT [32].

It is well known that amino acids inside or near the active site of the enzyme play key role in several steps of the catalysed reaction, notably detection, orientation and transformation

of the substrate. Methane yielding from carbon dioxide can be achieved by remodelling the active site of nitrogenase in proximity of FeMo-cofactor's location. Double substitution of amino acids α-70 Val and α-195 His has been demonstrated to permit the transfer of eight electrons to CO_2 producing CH_4 [34, 35].

The second element of this reaction is methane monooxygenase, a metalloenzyme that catalyses the addition of one oxygen atom to methane, converting it into methanol. Two forms of MMO can be found in nature, i.e. soluble MMO (s-MMO) dissolved in intracellular region, and particulate MMO (p-MMO) bond to the membrane of the cells of methanotrophic bacteria [30]. Between them, s-MMO from *Methylococchus capsulatus* is the most extensively studied one. It is composed of three different subunits, which incorporate the required cofactors, i.e. flavin adenine dinucleotide (FAD) and [2Fe-2S]-ferrodoxin, in their own structure [30]. A main challenge for the exploitation of this enzyme lies in the expression of its functional form into *Escherichia coli*, and its isolation [30].

The chain reaction, constituted by a reduction coupled with an oxidation, appears to be highly interesting since it involves only two enzymes and does not require the addition of expensive NADH cofactor for the reduction stage. Anyway, enzyme engineering becomes necessary for the adaptation of nitrogenase to a different substrate, which is CO_2, apart from the production and purification of worthwhile quantities of methane monooxygenase.

3. Materials and method

The aim of this thesis work is to deeply investigate the optimal conditions, in terms of support for immobilization and enzymatic regeneration of the cofactor, to carry on the first step of the previously mentioned multi-enzyme cascade, namely the conversion of carbon dioxide into formic acid by the enzyme formate dehydrogenase FDH. In fact, this main reaction was coupled with the simultaneous regeneration of cofactor NADH by a second enzyme, which is glycerol dehydrogenase GlyDH, and both the enzymes were co-immobilized on different types of functionalized inorganic supports. Two types of as-received microporous zeolite, namely one natural clinoptilolite and one synthetic ZSM-5, were firstly involved in this process. The choice to compare these two different types of materials is intended to research possible beneficial or detrimental effects of native cations enclosed in the framework of natural zeolite as opposed to the only alumina and silicon atoms of synthetic one. In addition, clinoptilolite is extracted from open-pit mines distributed almost all over the world, hence it is way cheaper than ZSM-5.

Furthermore, in order to enhance the supporting potential of these materials by allowing them to exploit their whole surface area, the same types of zeolites have undergone a process of hierarchization, hence micro-mesoporous clinoptilolite and ZSM-5 were prepared by following and adapting the methods reported in the literature. In fact, the main difficulty in this coupled process is that the two enzymes have different dimensions, that can be determined starting from the total structure weight of the protein expressed in Da, and then exploiting Equation 3.1.

$$R_{min} = 0.066 \cdot \left(MW_p\right)^{1/3} \tag{3.1}$$

R_{min} Minimum radius of the protein [nm]

MW_p Total structure weight of the protein [Da]

By the data reported in the literature, formate dehydrogenase from *Candida boidinii* is a homo-dimer having an average weight of 82.21 kDa [14], while glycerol dehydrogenase from *Geobacillus stearothermophilus* is formed by eight subunits of 39.70 kDa each, for a total weight of around 317.6 kDa [27]. This results in 5.73 nm and 9.00 nm of diameter, respectively. In view of this aspect, hierarchical materials are promising supports since they are supplied with pores of different dimensions, mainly original micropores and tailor-made mesopores, which can tend to meet this necessity. In particular, hierarchical materials are supposed to give rise to preferential pathways for smaller enzymes like FDH to enter the original micropores, and for bigger ones (GlyDH) to remain outside, into these kinds of mesoporous “highways” generated through the hierarchization process. Also, mesoporosities have the purpose of enhancing the mass transfer of reagents and reaction products, and therefore improving the global efficiency of the process.

3.1 Preparation of hierarchical zeolites

Base clinoptilolite (B-Clino) was supplied by Zeolado (Greece), while base ZSM-5 (B-ZSM5), with a 50:1 ratio of SiO_2/Al_2O_3, was purchased from Alfa Aesar. This latter was originally in ammonia form, therefore was brought into protonated form by calcination at 550 °C for 5 h. Hierarchical clinoptilolite (H-Clino) and hierarchical ZSM-5 (H-ZSM5) were prepared by adapting the methods reported from Moradi *et al*. [36] and Mitchell *et al*. [37], respectively.

Natural clinoptilolite involved in this process has a Si/Al ratio that ranges from 4.0 to 5.3 as reported by Dosa *et al*. in a paper that employs the same sample of zeolite [38]. Thereby, after a first washing with ultrapure water (MilliQ) at room temperature for 10 minutes under vigorous stirring, the material has undergone a preliminary process of dealumination with a solution of hydrochloric acid 1 M at 100 °C for 4 h, in order to raise this ratio and enhancing the subsequent formation of mesopores. This pre-treatment was repeated 4 times, after each of which the mixture was centrifugated at 5000 rpm for 10 minutes and the solid was washed and dried overnight in oven at 60 °C. Afterwards, desilication with a solution of sodium hydroxide 0.2 M was performed at 100 °C for 30 minutes, and then the solid was centrifugated, washed and dried overnight in oven. Finally, the last step of milder dealumination with a solution of hydrochloric acid 0.5 M at 100 °C for 4 h, aimed at removing extra-framework alumina atoms remained in excess after the previous alkaline leaching, was done. At the end, the solid was recovered by centrifugation, washed, and dried overnight in oven, obtaining H-Clino.

An extra sample of hierarchical sodium-clinoptilolite (Na-H-Clino) was obtained by replacing the first washing with an ion exchange with sodium chloride 2 M at 50 °C for 3 h. This sample was further studied and compared with the washed one in order to investigate the effects of any impurities and original framework ions on the process of hierarchization, in a view to the subsequent immobilization of enzymes, i.e. possible interactions due to the formation of charge on the surface of the zeolite.

ZSM-5 did not require any preliminary dealumination due to its high Si/Al ratio of 25, so the material was directly desilicated by putting it in contact with a solution of sodium hydroxide 0.2 M at the temperature of 65 °C for 1 h. Then the reaction was quenched with ice and the mixture was centrifugated at 5000 rpm for 10 minutes. The solid required 5 steps of washing and centrifugating to get back at neutral pH, and then it was dried overnight in oven at 60 °C. Since using NaOH for desilication some silicon atoms might have been replaced by sodium, two further steps of ion exchange with an aqueous solution of ammonium nitrate in concentration 0.1 M at 60 °C for 1 h were performed, after each of which the zeolite was dried, washed and calcinated at 550 °C for 5 h in order to obtain the protonated form of the zeolite. This additional process was not carried out for clinoptilolite because the small number of sodium ions due to the alkaline leaching with NaOH was simply additional to the greater deal of native sodium cations. It followed a dealumination step with a solution of hydrochloric acid 0.1 M at 70 °C for 6 h in order to rebalance the Si/Al ratio. At the end of this, the solid was centrifugated, washed with distilled water, and dried in oven at 60 °C, obtaining hierarchical ZSM-5 (H-ZSM5).

3.2 Characterization of materials

All samples (B-Clino, B-ZSM5, H-Clino, H-Na-Clino and H-ZSM5) were examined and tested to determine the structural and morphological features of both the base materials and of hierarchical ones, and finally assessing the proper formation of mesopores.

In view of the functionalization and the immobilization of enzymes, specific surface area represents a key property for the support, since it determines a higher number of sites for the formation of functional groups and therefore a larger immobilization capability. The specific surface area S_{BET} of the samples of zeolite involved in this work was evaluated by exploiting the technique of nitrogen physisorption at its boiling temperature of 77 K, with a Micromeritics TriStar II 3020 instrument (shown in Figure 3.1), and then by processing the results with the Braunauer-Emmet-Teller (BET) method. However, for zeolites, BET usually provides quite underestimated values of surface area, hence it was calculated also with the Langmuir method S_{LAN}. This technique is also able to give an estimation of the global pores volume V_p, the micropores volume V_{micro} and the average pores dimension d_{avg} by analysing the desorption stage with the Barrett-Joyner-Halenda (BJH) method.

Figure 3.1 Picture of the laboratory instrument used for the evaluation of the specific surface area of the samples: Micromeritics TriStar II 3020 (on the right) and the pre-treatment instrument (on the left).

Before the testing, all the samples were subjected to an outgassing pre-treatment at a high temperature (400 °C) for 2 h with the intention to remove the great majority of molecules that could be physisorbed or chemisorbed on the surface of the support. One of the main issues in this process is related to carbonate ions CO_3^{2-}, which are substantially basic molecules and tent to strongly attach to the acidic sites of the zeolites: for this reason, these kinds of supports must undergo a more stringent treatment than others, which instead are usually subjected to temperatures up to 200 °C.

The crystalline structure of materials was determined with X-ray diffractometry (XRD) by using a Philips PW3040 X'Pert diffractometer. For zeolitic samples, diffraction angles 2θ were analysed in a range between 5° and 50°. Eventually, the resulting patterns were compared with the ones contained in the Powder Data Files (PDF) database.

Finally, the morphology of the granules that compose the zeolites and the shape of the cavities were observed through Field-Emission Scanning Electron Microscopy (FE-SEM) and High-Resolution Transmission Electron Microscopy (HR-TEM) techniques, respectively. FE-SEM instrument was a Zeiss SUPRA 40, which usually employs a GEMINI column with low magnetic field. Whereas, for HR-TEM analysis, a JEM-3100F equipped with Field Emission LaB_6 gun was used, and the imaging was carried out at 200kV.

3.3 Supports functionalization

In order to allow the attachment of enzymes on the surface of inorganic supports, there is the necessity to generate some kinds of functional groups on these latter, which would be able to establish physical or chemical bonds with as many groups in the amino acids of the enzymes. To do this, all the zeolites (B-Clino, B-ZSM5, H-Clino, H-ZSM5) were hetero-functionalized with aldehydic (glyoxyl) and amino groups by adapting the method reported by Bernal *et al*. [39] in 2012 and later by Pietricola *et al*. [40]. The formation of glyoxyl groups went through a series of three reactions: firstly, the generation of epoxydic groups on the surface of the support, then the hydrolysis with sulphuric acid, with the opening of the ring structure to form diols, and finally the oxidation of these latter with sodium periodate to yield glyoxyl groups. A scheme of functionalization is shown in Figure 3.2, alongside to the formation of amino groups on the surface of the support.

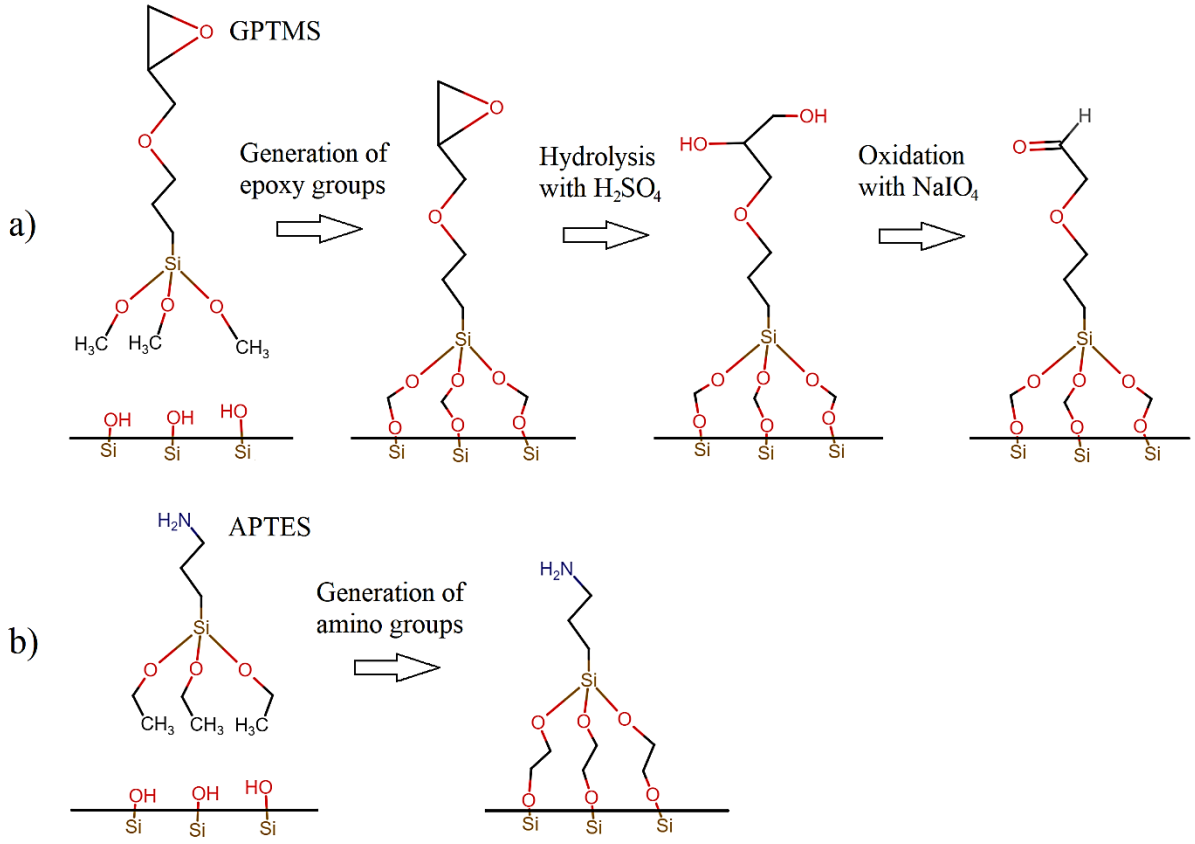

Figure 3.2 Reaction scheme for hetero-functionalization with glyoxyl and amino groups: scheme above (a) shows the three steps of the formation of aldehydic groups on the surface of aluminosilicate supports (i.e. formation of epoxy group by GPTMS, hydrolysis into diol and oxidation into aldehyde); below (b) it is represented the result of the reaction between APTES and the support.

For each sample, 1 g of zeolite was put into a balloon with 30 mL of toluene and the temperature was brought to 105 °C with an oil bath. In order to avoid the evaporation of the solvent, the balloon was connected to a cooling column. The two functionalizing solutions, i.e. APTES and GPTMS, were added in equal quantities of 1.5 mL and the mixture was allowed to react for 5 h. Then, the solid was filtered and thoroughly washed with acetone and water. Subsequently, hydrolysis of epoxy groups was carried out by putting the powder in contact with 30 mL of aqueous solution of sulphuric acid in concentration of 0.1 M at 85 °C for 2 h. Again, it followed a step of filtration and deep washing with abundant distilled water. The last stage of functionalization was the oxidation of diol groups by 30 mL of sodium periodate aqueous solution 0.1 M at room temperature for 2 h more, followed by one last filtration and washing with distilled water, in order to remove periodate ions from the surface, and phosphate buffer 25 mM pH 7. The process scheme is showed in Figure 3.3.

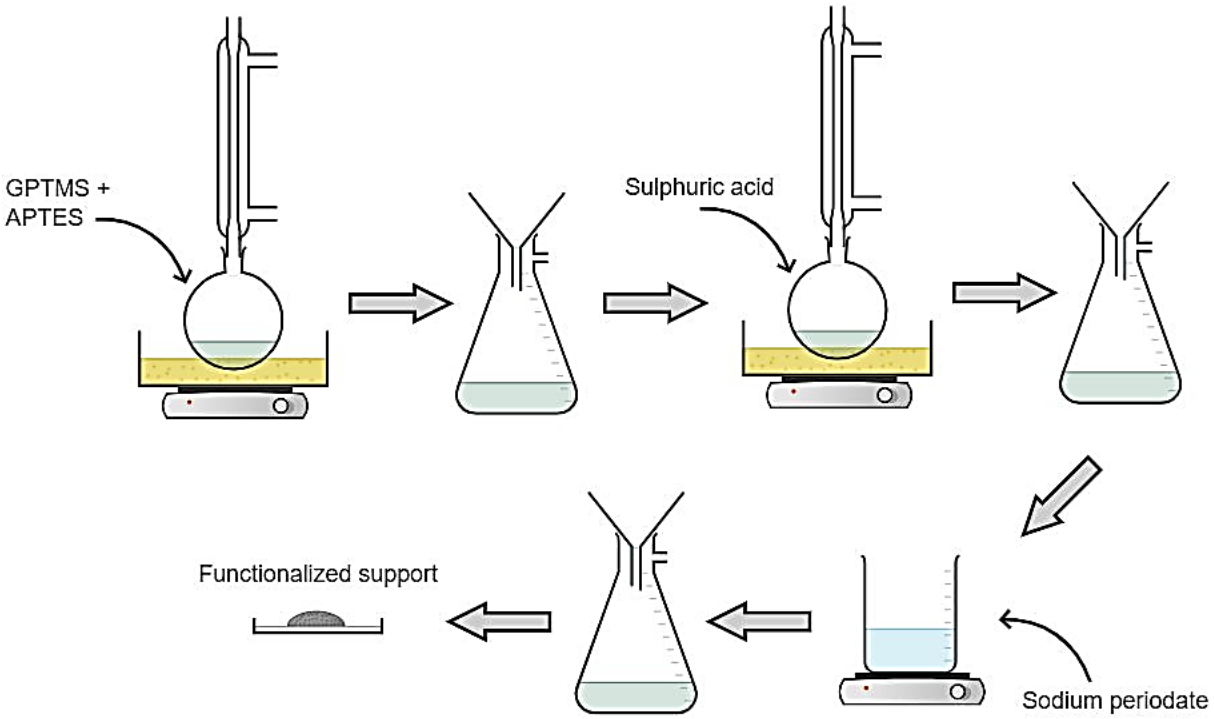

Figure 3.3 Scheme of the experimental procedure of hetero-functionalization, with the formation of glyoxyl and amino groups, as modified by literature [39, 40].

3.3.1 Quantification of glyoxyl groups

Before the last reaction step, 1 mL of sodium periodate was collected, and, through a back titration method, the absorbance at 420 nm of 100 µL of the sample in 1 mL of a mixture of 10% KI solution and saturated sodium bicarbonate solution in a 1:1 ratio was measured and related to the concentration of periodate ions in solution at the initial time. Likewise, 1 mL of supernatant was sampled after the last step of reaction, centrifugated and observed to quantify the concentration of periodate ions at the end of the functionalization, in the same way described above. This latter was compared to the first data in order to evaluate the moles of glyoxyl groups formed on the surface of the zeolite, exploiting Equation 3.2. The mixture of 10% KI solution and saturated sodium bicarbonate solution in a 1:1 ratio was also used as the blank.

$$\frac{mol_{gly}}{m_{sup}} = \frac{1}{m_{sup}} V_{IO_4^-}\, C_{IO_4^-,in} \left(1 - \frac{Abs_{final}}{Abs_{init}}\right) \cdot 1000 \qquad (3.2)$$

mol_{gly} Quantity of glyoxyl groups formed on the surface of the support [µmol]

m_{sup} Mass of support [g]

$V_{IO_4^-}$ Volume of periodate solution involved in the reaction [mL]

$[IO_4^-]_{in}$ Initial concentration of periodate into the solution [mmol/mL]

Abs Absorbance value of the sample at 420 nm

The samples were diluted 50 times to obtain a detectable absorbance value, using a Jasco V-730 spectrophotometer (Figure 3.4).

Figure 3.4 Picture of the spectrophotometer Jasco V-730 involved in all the absorbance tests within this thesis work; on the right, the thermostatic water bath is visible with the piping system that brings water to the spectrophotometer chamber.

3.4 Characterization of FDH and GlyDH

Formate dehydrogenase from *Candida boidinii* (25 mg_{enz}/mL) was purchased from Megazyme, while glycerol dehydrogenase from *Geobacillus stearothermophilus* (10.65 mg_{enz}/mL) was expressed in *Escherichia coli*, purified, and kindly provided by the Bioprocess Engineering and Applied Biocatalysis Group of the Autonomous University of Barcelona.

3.4.1 Activity assay of free enzymes

Before starting with the immobilization, the activity of free enzymes was tested in order to have a benchmark for further activity assessment during the whole process. Reactions of oxidation of sodium formate (Equation 3.3) and oxidation of glycerol (Equation 3.4) were considered.

$$HCOO^{-}Na^{+} + NAD^{+} \overset{FDH}{\Longleftrightarrow} CO_2 + NADH \tag{3.3}$$

$$glycerol + NAD^{+} \overset{GlyDH}{\Longleftrightarrow} DHA + NADH \tag{3.4}$$

Operatively, 50 µL of FDH solution was added to a solution constituted of 2.3 mL of phosphate buffer 0.1 M pH 7.5, 100 µL of cofactor NAD^+ 50 mM and 500 µL of sodium formate 0.3 M. Similarly, 100 µL of GlyDH solution was added to 1.850 mL of glycerol solution 100 mM (in phosphate buffer 0.1 M pH 7) and 50 µL of NAD^+ 100 mM. The variation of absorbance at a wavelength of 340 nm, corresponding to the peak of NADH produced, was recorded as time-course measurement, and put inside Equation 3.5.

$$A_{FE} = \frac{(\Delta Abs/\Delta t)_{FE}}{\varepsilon}\frac{V}{m_{enz}} \tag{3.5}$$

A_{FE}	Activity of the free enzyme [IU/mg_{enz}]
$(\Delta Abs/\Delta t)_{FE}$	Time course absorbance of the free enzyme [abs/min]
ε	Molar extinction coefficient [abs L/µmol]
V	Volume of the solution into the cuvette [L]
m_{enz}	Mass of enzyme into the solution [mg]

The unit of measurement of enzymatic catalytic activity is the International Unit (IU), which basically stands for the amount of enzyme that catalyses the conversion of one micromole of substrate (formate or glycerol) per minute (µmol/min).

3.5 Immobilization of enzymes on supports

Both enzymes were subjected to an immobilization technique that relies on multipoint covalent attachment of the enzyme on aldehydic and amino sites generated on the carrier. In particular, in the first part of the reaction, at neutral pH, amino groups on the support favour the physical adsorption of the enzyme, generating weak intermolecular bonds that would not be able to retain the protein for a long time. In the second part, indeed, the formation of covalent bond occurs at alkaline pH, since these conditions allow to deprotonate the majority of primary amino groups present in the lysine residues, which are usually abundant on the surface of a large group of enzymes [18, 41]. In this way, deprotonated amino groups of the protein turn out to be more reactive towards glyoxyl groups added to the support, and this leads to the formation of an imine, otherwise known as Schiff's base (C=N). By adding sodium borohydride, the reduction of Schiff's bases occurs hence it leads to the formation of a single bond between the protein

and support, which reduces the risk of modifications in the conformation of the protein but still preventing leaching phenomena [41]. This reaction mechanism is shown in Figure 3.5.

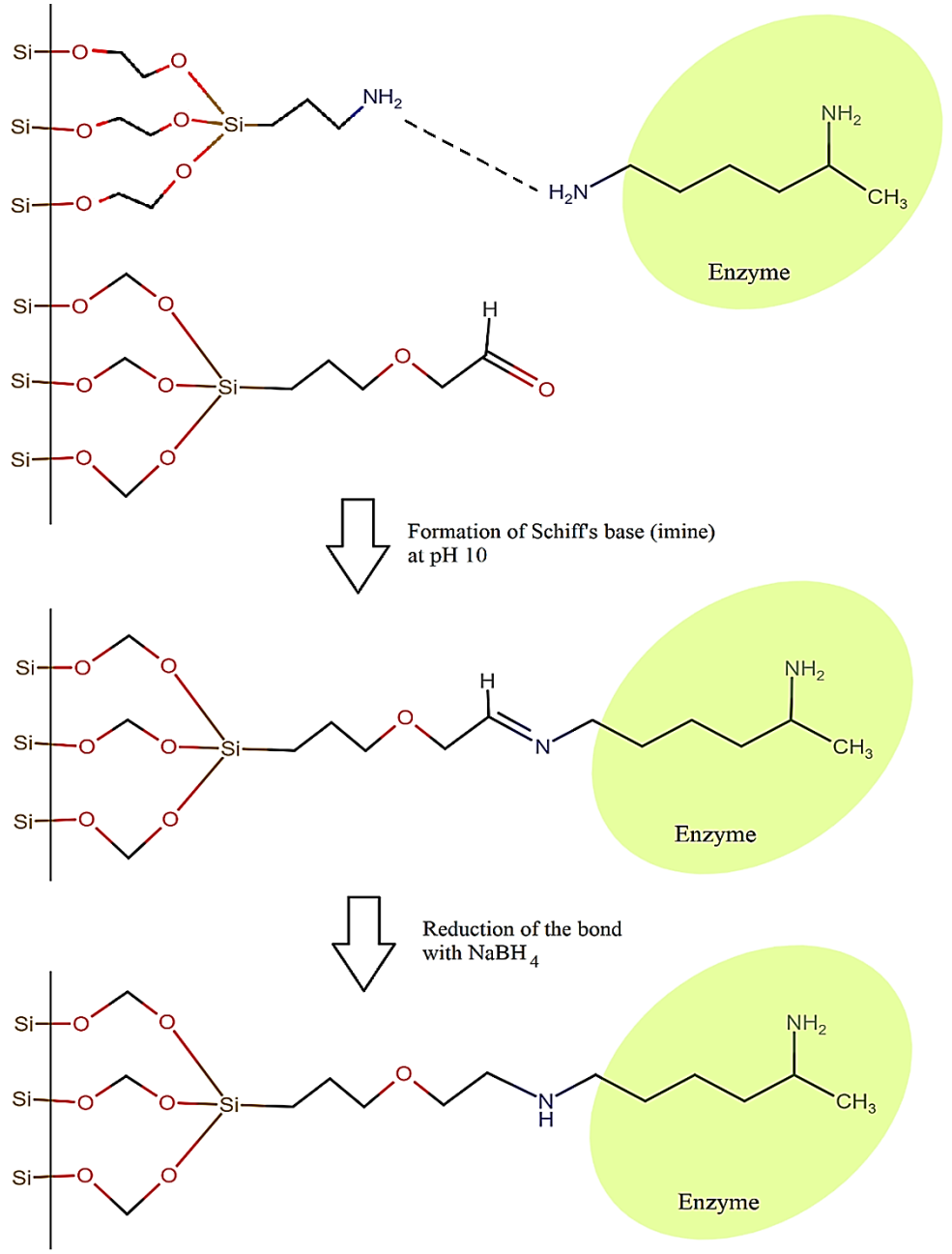

Figure 3.5 Reaction scheme of the process of immobilization on functionalized support [41] after the first interaction between amino groups at neutral pH: formation of imine at pH 10 and further reduction of the C=N bond by sodium borohydride.

FDH and GlyDH were immobilized alone on each support. In this way, 200 mg of support were put in contact with 0.4 mg of FDH or GlyDH (2 mg_{enz}/g_{sup}). The process is adapted from the ones reported by Pietricola *et al.* [40] and Rocha-Martin *et al.* [42], and a scheme of it is reported in Figure 3.6.

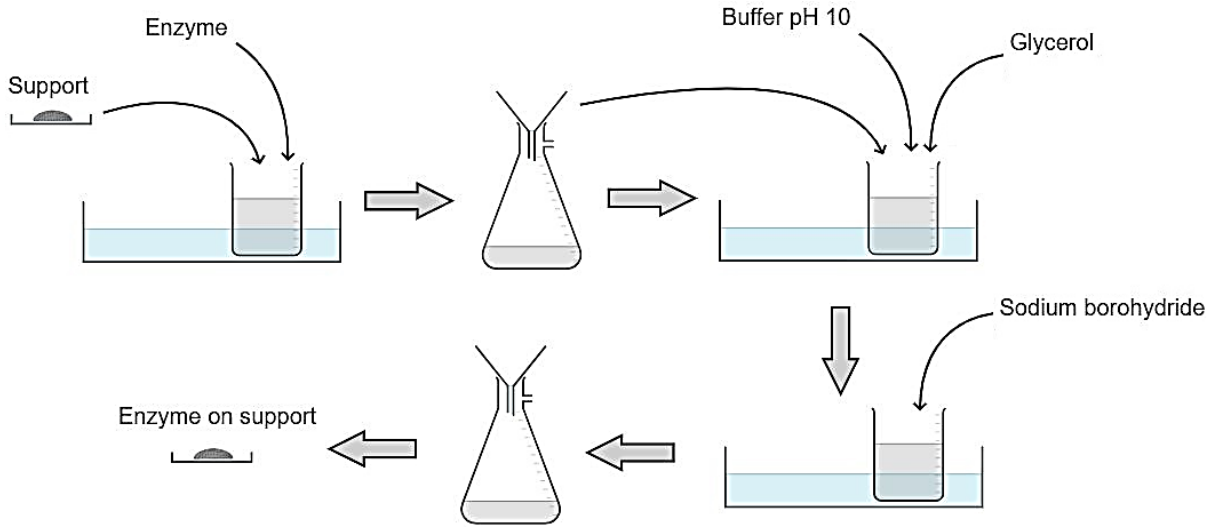

Figure 3.6 Scheme for the process of immobilization of FDH and GlyDH on hetero-functionalized supports, as modified from literature [40,42].

First, the enzyme was dissolved in 8 mL of phosphate buffer 25 mM pH 7 into a vial and the mixture was maintained at a temperature of 4 °C in an ice bath, with gentle stirring. The support was added, and the immobilization took place in a time that was estimated by collecting samples of the supernatant and monitoring the activity of the enzyme still in solution. When the activity of the supernatant dropped to zero or remained constant for two consecutive measurements, the mixture was filtered under vacuum in a Buchner funnel.

Subsequently, the solid was resuspended in 8 mL of carbonate buffer 100 mM pH 10 with 2.3 mL of glycerol, which has the purpose of stabilizing the enzyme at alkaline pH [18], and let in mild stirring for 30 minutes. The role of polyalcohols in this step is particularly important for GlyDH from *Geobacillus stearothermophilus* since this specific enzyme is sensible at pH between 9.5 and 10, at which it was observed that, for long contact times, it loses its quaternary structure [42]. Then, 4 mg of sodium borohydride were added to the mixture and let react for 10 minutes. Afterwards, the immobilization process is completed and the solid is filtered under vacuum, washed with abundant water and phosphate buffer 100 mM pH 7.5 and dried in refrigerated desiccator at the temperature of 4 °C.

With the purpose of evaluating the yield of immobilization, standard Bradford assay was carried out, determining the amount of enzyme that was successfully bonded to the support without leaching back into the solution. The measures of absorbance, revealed at the Uv-vis SP at the fixed wavelength of 596 nm, were put in correlation with the concentration of protein using a calibration line. Lastly, immobilization yield was determined through Equation 3.6.

$$Y_I = 1 - \frac{C_{e,1}}{C_{e,0}} \tag{3.6}$$

Y_I Yield of immobilization [%]

$C_{e,0}$ Concentration of enzyme in solution before the immobilization [mg/mL]

$C_{e,1}$ Concentration of enzyme in solution after the immobilization [mg/mL]

3.5.1 Activity assay of immobilized enzymes

The activity of the enzymes measures the amount of reagent that is converted into product per unit of time and, usually, per unit of mass of enzyme or mass of support. As already described in Section 3.4.1, UV-vis spectroscopy is applied to perform time-course measurements at 340 nm of the production of cofactor NADH due to the two corresponding oxidation reactions: the conversion of formate to carbon dioxide by FDH and the conversion of glycerol to dihydroxyacetone by GlyDH, involving oxidised cofactor NAD^+. The measurement was basically analogous to the one performed before the immobilization, with the only difference that in this case 5 mg of supported enzyme were added to the respective solution of substrate and cofactor. Equation 3.7 was employed to determine the value of activity referred to the mass of support.

$$A_{IE} = \frac{(\Delta Abs/\Delta t)_{IE}}{\varepsilon} \frac{V}{m_{sup}} \tag{3.7}$$

A_{IE} Activity of the immobilized enzyme [IU/g_{sup}]

$(\Delta Abs/\Delta t)_{IE}$ Time course absorbance of the immobilized enzyme [abs/min]

ε Molar extinction coefficient [abs L/µmol]

V Volume of the solution into the cuvette [L]

m_{sup} Mass of support [g]

Usually, the activity of immobilized enzymes is lower than the activity of soluble ones. This may be related to some changes in the structure of their active site, caused by the bonds established with the supports. In fact, this effect is more pronounced the stronger the bonds are. Against this background, the retained activity of the immobilized enzyme was assessed through Equation 3.8.

$$R_{act} = \frac{A_{IE}}{A_{FE}} \cdot \frac{100}{q_E} \tag{3.8}$$

R_{act} Retained activity of the immobilized enzyme [%]

q_E Enzymatic load on the support [mg_{enz}/g_{sup}]

3.5.2 Evaluation of optimal temperature and pH

An array of activity assays was conducted at different temperatures and pH in order to evaluate the optimal conditions for both the enzymes. In particular, optimal temperature measurements were performed by warming up the buffer (0.1 M pH 7.5) in which the reaction took place, and by maintaining it at the set-point temperature during the whole test by means of a thermostatic system inside the spectrophotometer. Instead, for optimal pH measurements, the buffer solution was modified with HCl or NaOH solutions, or substituted, in order to reach the desired value of pH, at a constant temperature of 30 °C. Then, the activity was assessed in similar way as described in Section 3.5.1.

3.5.3 Thermal stability tests

Thermal deactivation of the immobilized enzymes over time was assessed by incubating an array of samples of 5 mg each in a thermostatic water bath at 50 °C for 4 days. Then, the activity was measured by spectroscopic technique, as described in Section 3.5.1. Similarly, thermal deactivation of soluble enzymes was evaluated by incubating diluted enzyme solutions at 50 °C and then sampling 50 µL for FDH or 100 µL for GlyDH, and the activity was measured as described in Section 3.4.1. FDH solution was diluted 1:400, while GlyDH solution was diluted 1:200, in order to obtain approximately the same concentration of enzyme (around 0.05 – 0.06 mg/mL).

Generally, deactivation kinetics for free enzymes follow a first order exponential decay law, which can be written as Equation 3.9.

$$\frac{A_t}{A_0} = \exp(-kt) \tag{3.9}$$

A_t	Activity at time t [IU]
A_0	Initial activity [IU]
k	Thermal decay constant [h^{-1}]
t	Time [h]

More complex models are reported in the literature [43], such as asymptotic deactivation kinetics, which assume residual activity at infinite time. These models can be described by Equation 3.10.

$$\frac{A}{A_0} = (1-\alpha)\exp(-kt) + \alpha \tag{3.10}$$

α	Residual activity [-]

For each model, different parameters were considered to be most relevant for further speculations on the stability of free and immobilized enzymes. In particular, the time at which the residual activity is 50% of the maximum value, i.e. half-life $t_{1/2}$, and the ratio between the half-life of the immobilized enzymes and the same parameter of the free enzyme, which is the stability factor F_S, were considered. Expressions for the half-time for the two exponential models (the first order law and the model with residual activity) are reported in Equation 3.11 and Equation 3.12, respectively; meanwhile, an expression for the stability factor is written in Equation 3.13.

$$t_{1/2} = -\frac{\ln(0.5)}{k} \tag{3.11}$$

$$t_{1/2} = -\frac{1}{k}\ln\left(\frac{0.5-\alpha}{1-\alpha}\right) \tag{3.12}$$

$$F_S = \frac{t_{1/2,IE}}{t_{1/2,FE}} \tag{3.13}$$

$t_{1/2,IE}$ Half-life of immobilized enzyme [h]

$t_{1/2,FE}$ Half-life of free enzyme [h]

3.6 Co-immobilization of fluorescence-labelled FDH and GlyDH

The two enzymes were labelled with two different hydrophilic fluorescent dyes. In particular, FDH was coloured with ATTO 488, while GlyDH with ATTO 550. Both the labelling kits were purchased by Merck.

First, each soluble enzyme was put in contact with the respective colourant in carbonate buffer pH 9.5 and incubated for 2 h in gentle stirring. This allows to establish bonds between the reactive molecule of the dye, and the primary amino groups of the proteins. The two dyes molecules belong both to the family of rhodamine (Figure 3.7) [44]. Then, the labelled enzymes were purified through a separation column and the resulting mixture was later characterized by Bradford assay.

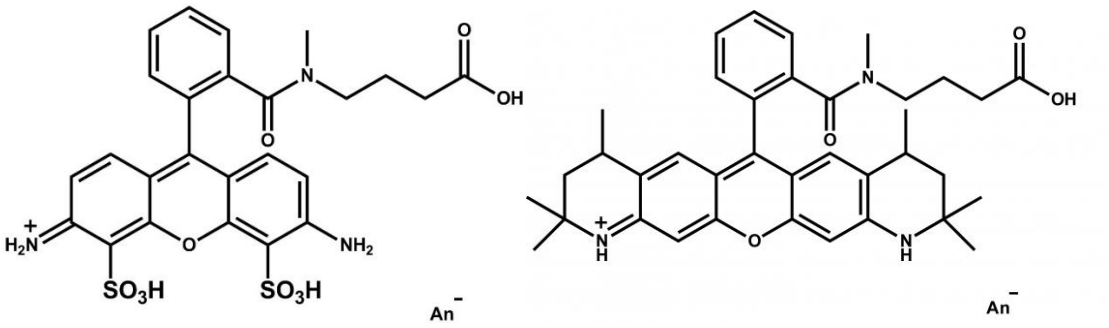

Figure 3.7 Reactive molecules of the fluorescent labelling dyes, reported by the manufacturer's technical sheets [44]: ATTO 448 on the left, ATTO 550 on the right.

Co-immobilization of the two labelled enzymes was performed in a similar way as the single immobilization, by adding 2 mg of each enzyme per gram of support, simultaneously. B-Clino was chosen to be used for the test because it did not show any fluorescence emittance in the considered wavelength. Instead, all the other supports (B-ZSM5, H-Clino and H-Na-Clino) showed strong fluorescent emissions in several channels, both in green and red, which are the ones of interest, but also in blue. The whole process of immobilization was carried out in dark environment, paying attention to avoid reducing the performances of the dyes. The resulting loaded support was left in buffer 25 mM pH 7 overnight, and then filtered and resuspended into the same buffer, with the intent to wash away any possible trace of dye weakly adsorbed on the surface of the support. Finally, the sample was observed with a Nikon Eclipse Ti fluorescence microscope at a magnification of 100x.

3.7 Reduction of CO_2 into formic acid

In order to evaluate the production of formic acid by FDH, the reaction of reduction of carbon dioxide was carried out into a sealed glass bottle, at the standard temperature of 30 °C. Operatively, 500 mg of biocatalyst, namely FDH over H-Clino, were suspended in 30 mL of phosphate buffer 100 mM pH 7.5 with NADH in concentration 10 mM as cofactor. Also, in order to assess the proper regeneration of the cofactor by GlyDH, the same procedure was applied to the two co-immobilized enzymes over H-Clino, by substituting the reduced cofactor NADH with NAD^+ in the same concentration and by adding equimolar glycerol. In this way, a chain reaction mechanism is supposed to be carried out, with GlyDH producing NADH, which is necessary to FDH to reduce CO_2 (Figure 3.8). In each reaction, a flux of 100 mL/min of carbon dioxide was then bubbled into the bottle by means of a needle, inserted into the cap with a second needle that acts instead as a pressure control vent. Due to the solubilization of CO_2 in the liquid phase, a decrease in pH was observed after 6 hours of reaction, from 7.5 to 6.5. The reactor was maintained in mild stirring for the entire experiment. The operative configuration is displayed in Figure 3.9.

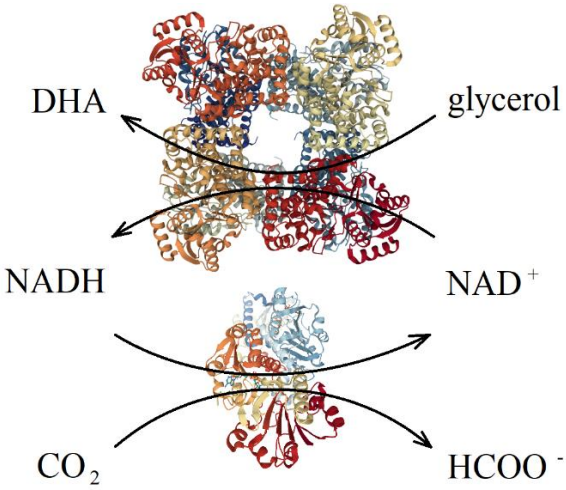

Figure 3.8 Chain-reaction scheme: glycerol and NAD^+ are converted into DHA and NADH by enzyme GlyDH, while FDH utilizes NADH to carry out the conversion of CO_2 into formic acid.

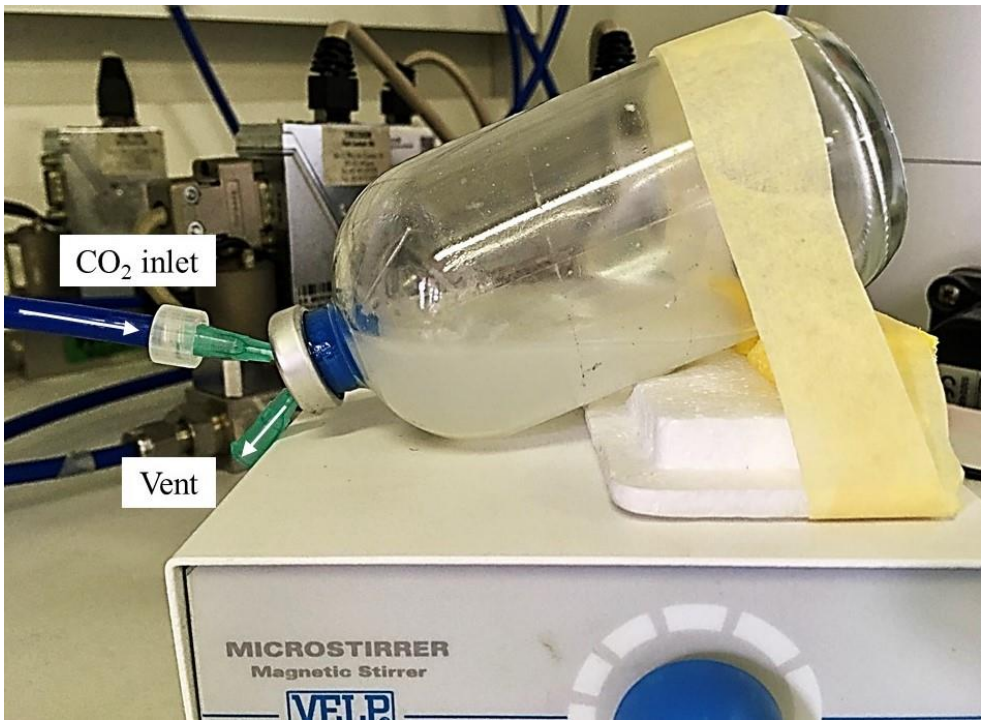

Figure 3.9 Reactor configuration for the reduction of CO_2. The two needles are visible on the left side: the one above is the carbon dioxide inlet, while the one below is the pressure control vent.

The proceeding of the reaction was assessed by collecting 1 mL of the reaction mixture every 30-60 min and then monitoring the variation in the concentration of formic acid by chromatographic technique. The analysis was carried out in a Shimadzu RID-20A High-Performance Liquid Chromatography (HPLC) device, with a C18 column, at a constant temperature of 30 °C and using H_2SO_4 5mM as mobile phase, with a flow rate of 0.4 mL/min. The calibration line used is described by Equation 3.14.

$$C_f = 1.55 \cdot 10^{-5} \cdot I \quad (3.14)$$

C_f	Concentration of formic acid [mM]
I	Integral of the peak obtained at the HPLC analysis [-]

4. Results and discussion

4.1 Support characterization: porosity and morphological features

4.1.1 BET surface area and pore size distribution

A global overview of the results obtained with nitrogen physisorption tests on the supports is reported in Table 4.1: BET surface area S_{BET}, Langmuir surface area S_{Lang}, cumulative pore volume V_p as calculated in the desorption stage with BJH method, micropore volume deduced by t-plot V_{micro} and average diameter of pores d_{avg} evaluated with the same method.

Table 4.1 Results of nitrogen physisorption tests for all the samples.

	$S_{BET}\ [m^2/g]$	$S_{Lang}\ [m^2/g]$	$V_p\ [cm^3/g]$	$V_{micro}\ [cm^3/g\ ]$	$d_{avg}\ [nm]$
B-Clino	37	39	0.14	0.005	11
B-ZSM5	312	521	0.15	0.120	7
H-Clino	195	282	0.22	0.064	15
H-Na-Clino	216	311	0.25	0.066	13
H-ZSM5	411	623	0.42	0.114	11

From these values of surface area, the effect of hierarchization is clearly visible for both zeolites: clinoptilolite increased its surface area by 600% compared to the base material, while ZSM-5 showed a 20% increase in its surface area, which, however, was already quite high. The resulting surface area of hierarchical samples is in line with the values present in the literature [36, 37]. The total pore volume increased, with a greater extent for synthetic zeolites compared to the natural ones. Simultaneously, the microporous volume did not increase much concerning the total volume, hence this implied that some mesopores and macropores were generated.

Isotherm graphs (of the adsorption and desorption stages of the test) allow evaluating the entity of the hierarchization process. Figure 4.1 and Figure 4.2 refer to the base and hierarchical samples of clinoptilolite, both only-washed and ion exchanged ones (B-Clino, H-Clino, H-Na-Clino), and of ZSM-5 (B-ZSM5, H-ZSM5), respectively.

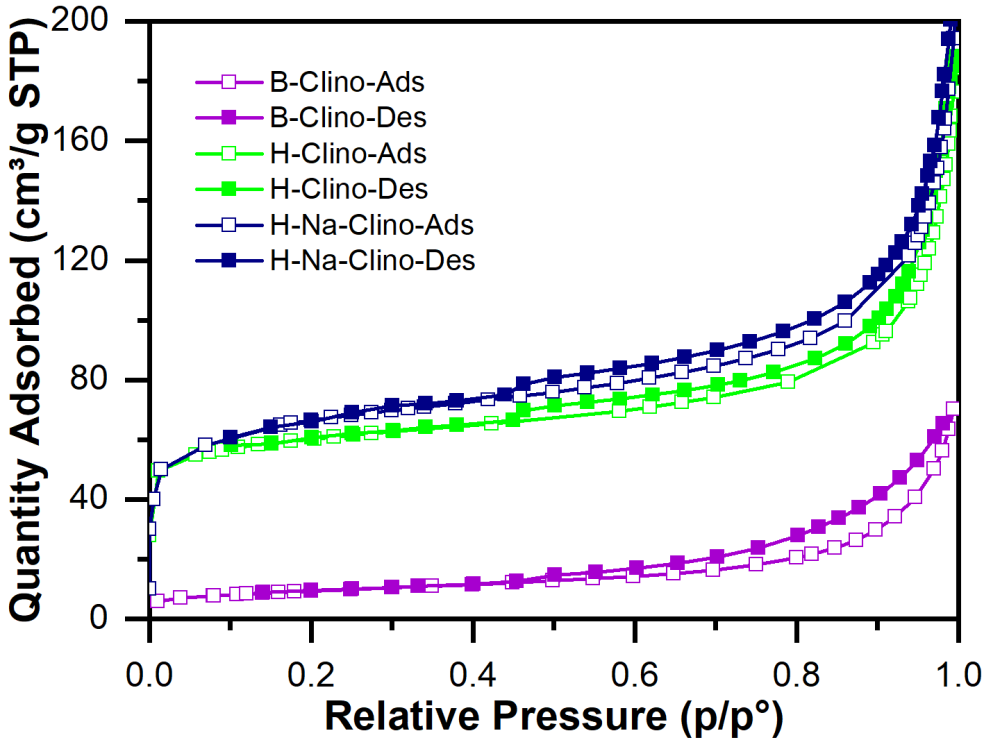

Figure 4.1 Isotherms of nitrogen physisorption tests for base and hierarchical clinoptilolite: B-Clino (purple), H-Clino (green) and H-Na-Clino (blue). Adsorption curve is marked with empty square symbols, whereas desorption ones with full square symbols

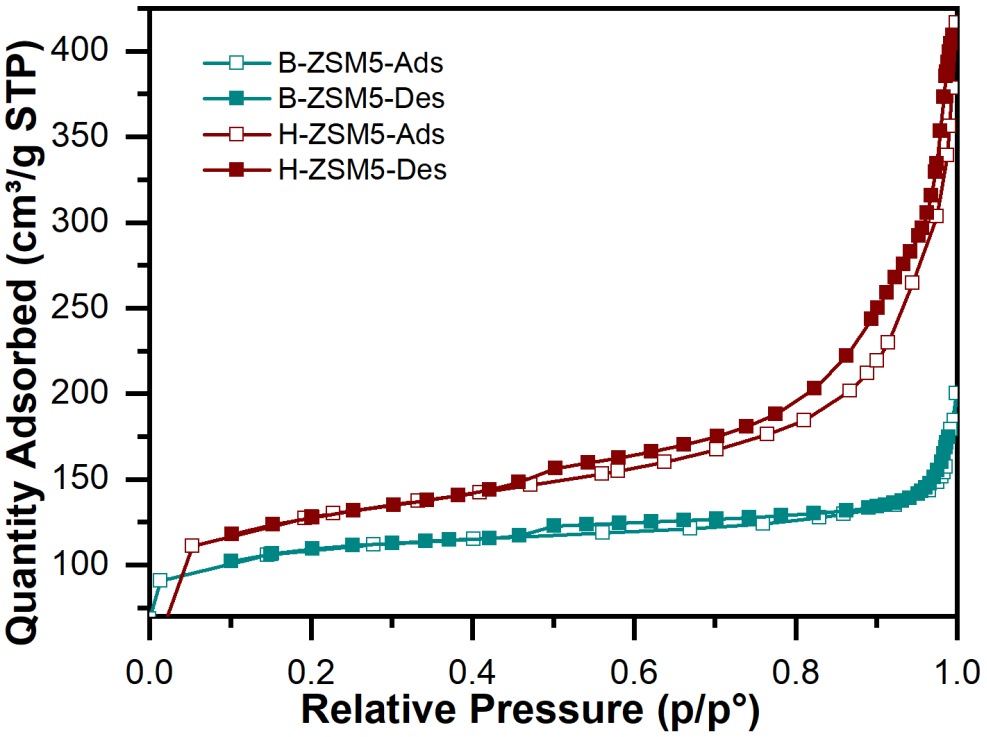

Figure 4.2 Isotherms of nitrogen physisorption tests for the base and hierarchical ZSM-5: B-ZSM5 (turquoise) and H-ZSM5 (brown).

In addition, Figure 4.3 and Figure 4.4 report the distributions of pore dimensions, comparing base materials with the ones subjected to hierarchization.

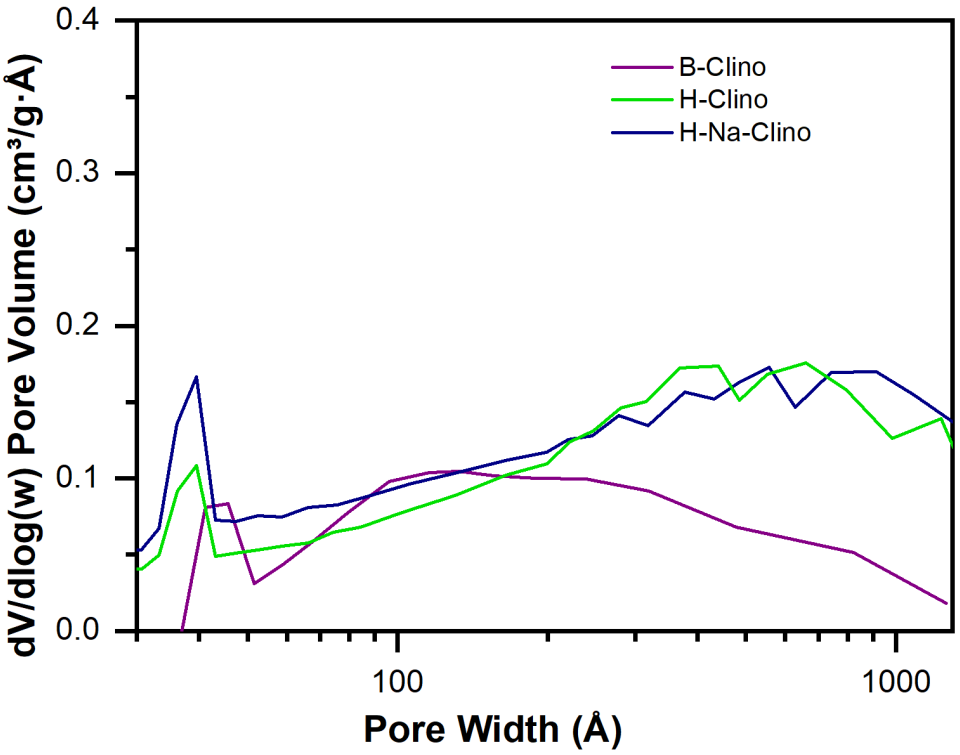

Figure 4.3 Distribution of pore dimensions for base and hierarchical clinoptilolite.

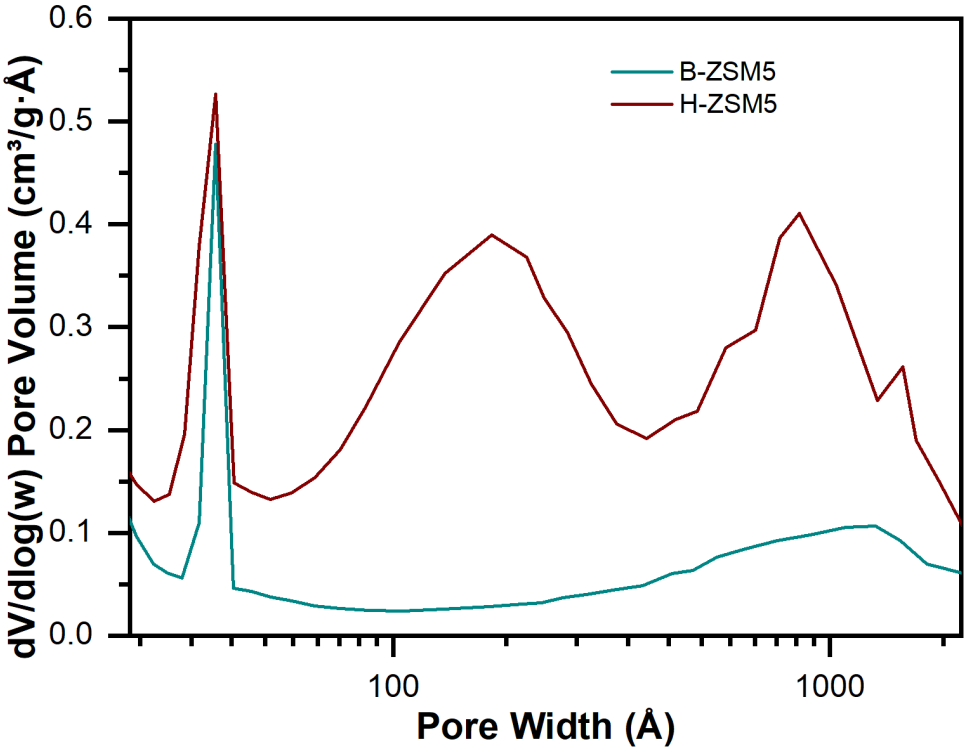

Figure 4.4 Distribution of pore dimensions for base and hierarchical ZSM-5.

The isotherms clearly show the changes in the position of the curve and in the shape of the hysteresis. Accordingly, the distributions of pore dimensions reflect the outcomes of the alkaline leaching. It turns out that predominantly macropores were generated inside the structure of H-Clino and H-Na-Clino, as can be seen from the shape of the isotherms (Figure 4.1) and from the multi-modal behaviour of the distribution, which displays multiple peaks between 30 nm and 200 nm (Figure 4.3). The shape of the hysteresis for all the samples of clinoptilolite reflects the original morphological features of this type of zeolite, which shows slits-like porosity generated by plates [45]. Instead, the structure of H-ZSM5 seems to be closer to the desired one, having a more pronounced hysteresis (Figure 4.2), which can describe more likely bottle-neck pores [45], and a bi-modal distribution with a distinct peak in the mesoporous range, at 20 nm, and another one in the macroporous range, at 80 nm (Figure 4.4).

4.1.2 X-ray diffraction

The crystalline structure of each hierarchical material was compared to the corresponding base material by overlapping the XRD patterns and identifying the matching of the distinctive peaks. Figure 4.5 and Figure 4.6 refer to the patterns for clinoptilolite (B-Clino/H-Clino/H-Na-Clino) and ZSM-5 (B-ZSM5/H-ZSM5), respectively.

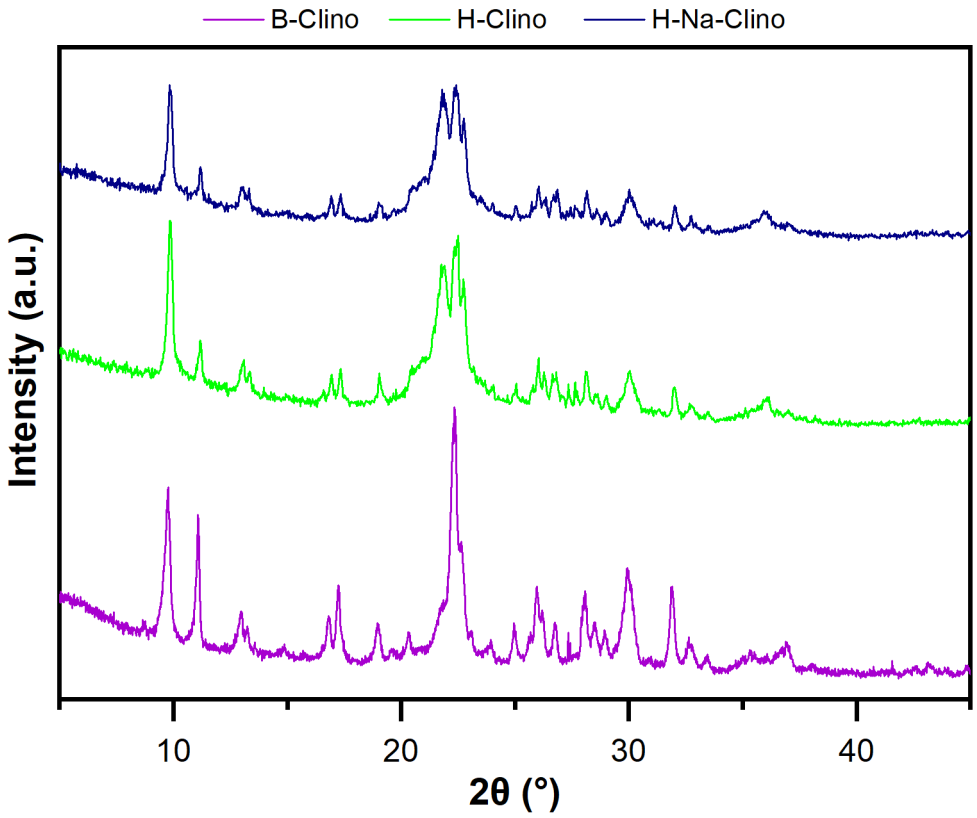

Figure 4.5 Comparison between B-Clino (purple), H-Clino (green), and H-Na-Clino (blue) XRD patterns.

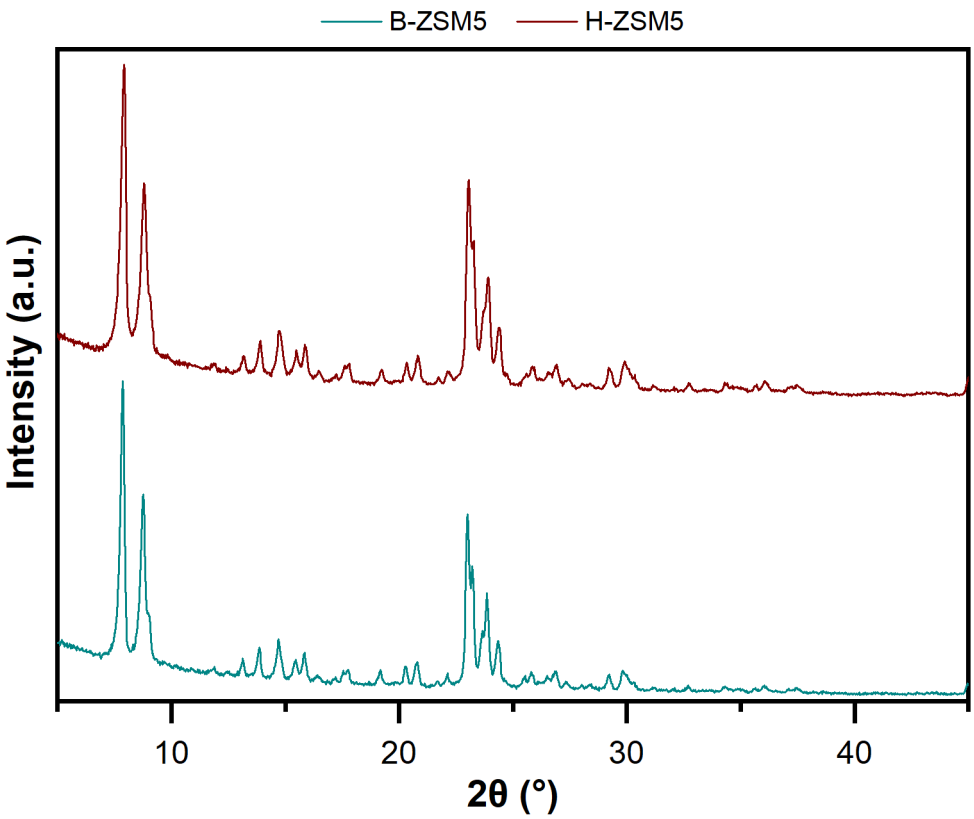

Figure 4.6 Comparison between B-ZSM5 (turquoise) and H-ZSM5 (brown) XRD patterns.

From these latter figures can be observed that the crystallinity was successfully preserved in good part for H-Clino and H-Na-Clino, and almost entirely for H-ZSM5. The main peaks related to clinoptilolite pattern (reference code 00-039-1383) are 2θ = 22.43°, 9.92°, and 30.50° [38]. The most intense one (at 22.43°) is slightly lower in hierarchical materials pattern, with respect to B-Clino, as well as the peak at 30.50°, whereas the one at 9.92° is unchanged. On the other hand, the pattern of H-ZSM5 happens to be practically identical to B-ZSM5, maintaining the main characteristic peaks at 2θ = 7.94°, 8.90°, 23.10° and 23.98° [46]. These results may lead to suppose that, as foreseen by Moradi *et al.* and Mitchell *et al.* [36, 37], the adjustment of the Si/Al ratio in a range between 25-50, along with the involvement of mild conditions in terms of acid/base concentrations and temperature, played a critical role in preventing the material to lose or damage its crystalline structure.

4.1.3 Field-Emission Scanning Electron Microscopy (FE-SEM)

Electron microscopy analysis is intended to define the morphology of the support at different levels of magnification. Figure 4.7 and Figure 4.8 report the images taken from FE-SEM analysis at 1kx and 10kx, comparing the base materials with their hierarchical counterparts. This level of magnification can illustrate only the shape of the granules of the zeolite, up to smaller particles.

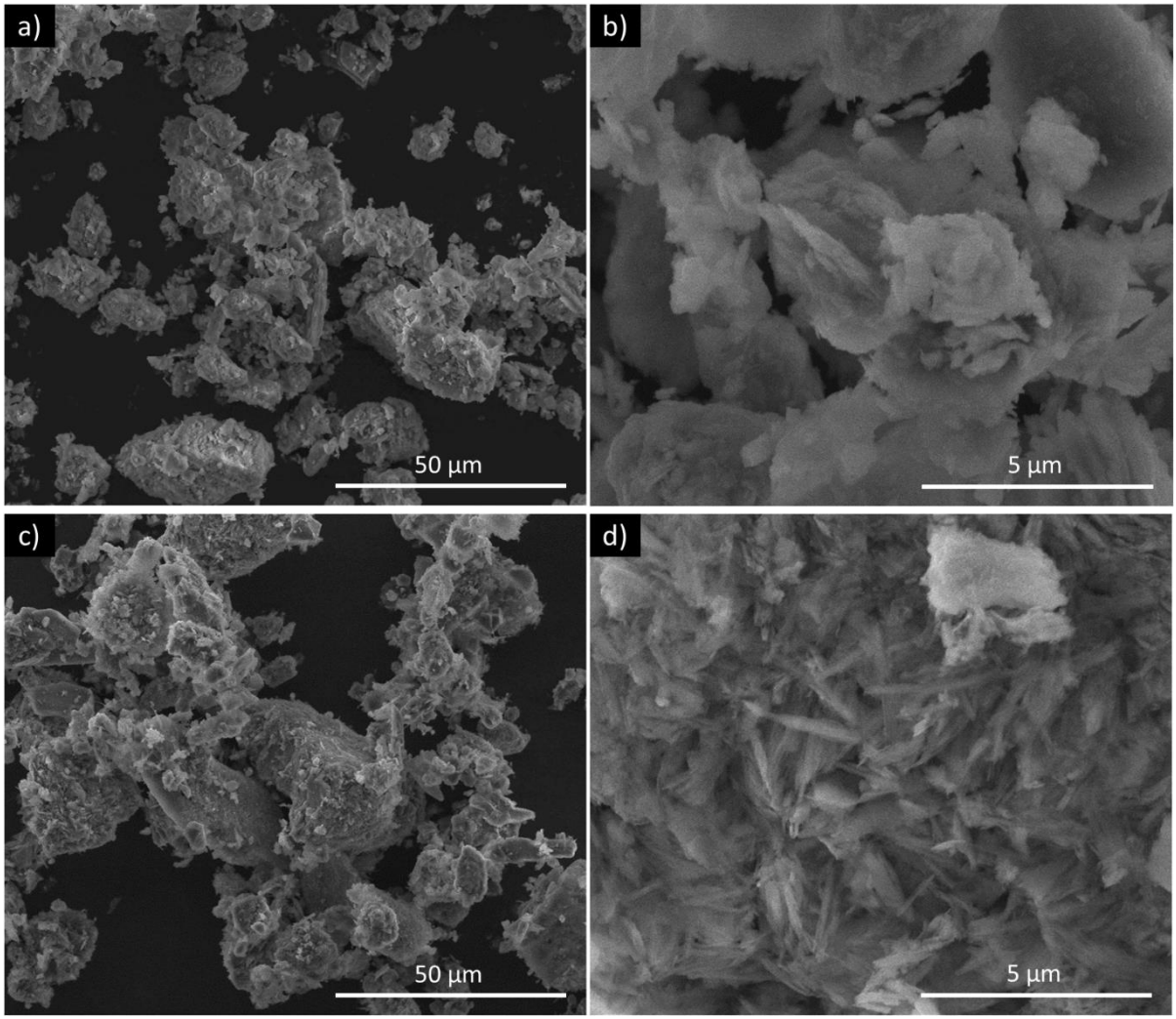

Figure 4.7 FE-SEM images for B-Clino (a,b) and H-Clino (c,d) at magnification 1kx and 10kx, respectively.

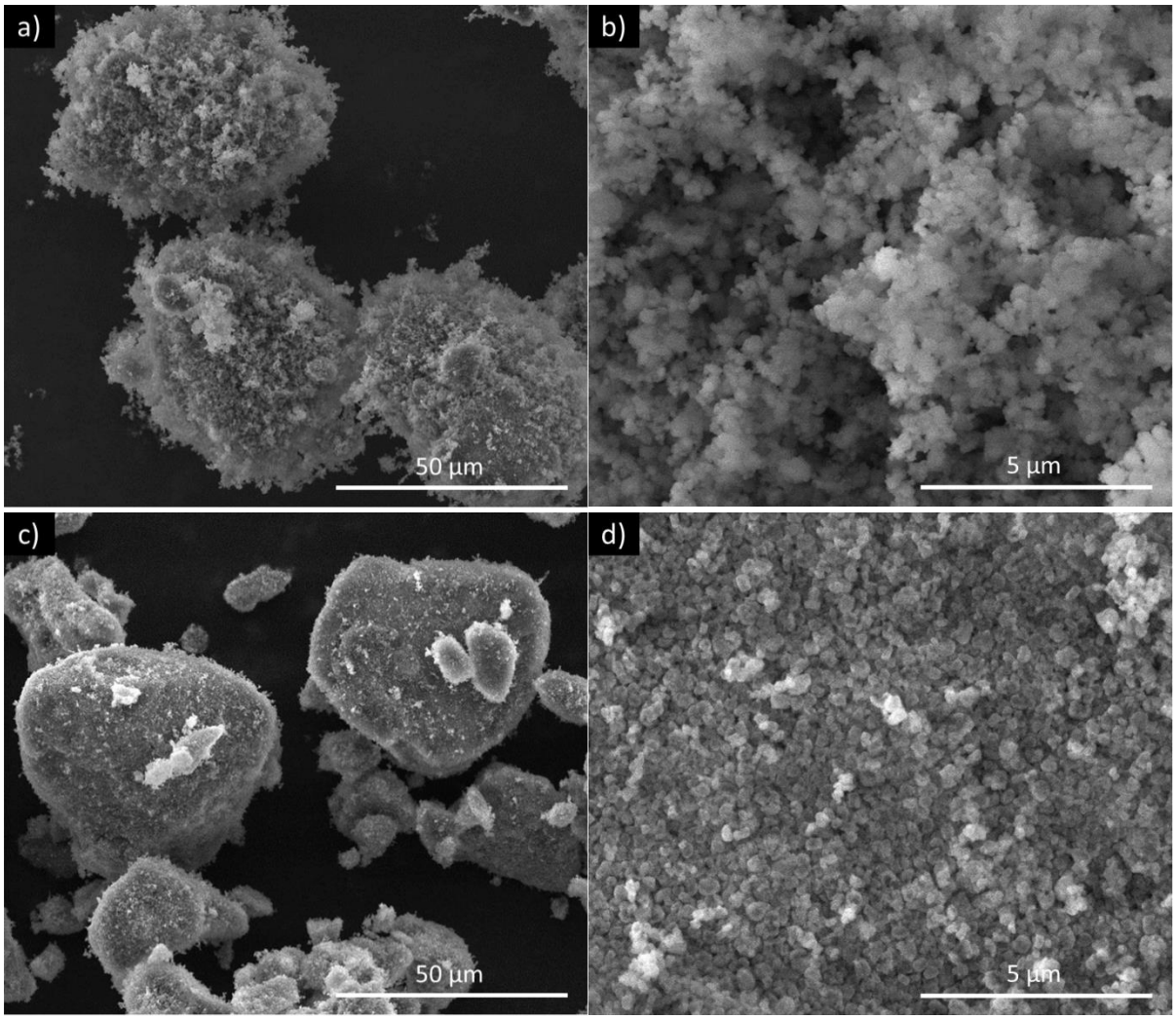

Figure 4.8 FE-SEM images for B-ZSM5 (a,b) and H-ZSM5 (c,d) at magnification 1kx and 10kx, respectively.

For all the samples, we can see that, despite several acid/alkaline attacks were carried out to remove aluminium and silicon atoms, the microscopic morphological features of the zeolites were maintained. In particular, clinoptilolite, which is generally in the form of flakes, reduces the dimensions of its particles in the hierarchical sample, probably due to the processes of dealumination/desilication. This outcome can be observed also for ZSM-5, which particles are instead more round-shaped.

4.1.4 Transmission Electron Microscopy (TEM)

TEM analysis is a burdensome and cost-intensive technique, so it was executed only on clinoptilolite samples (B-Clino, H-Clino and H-Na-Clino), which resulted to be, as it will be shown in the following sections, the best materials in terms of retained activity of enzymes. Images are collected in Figure 4.9.

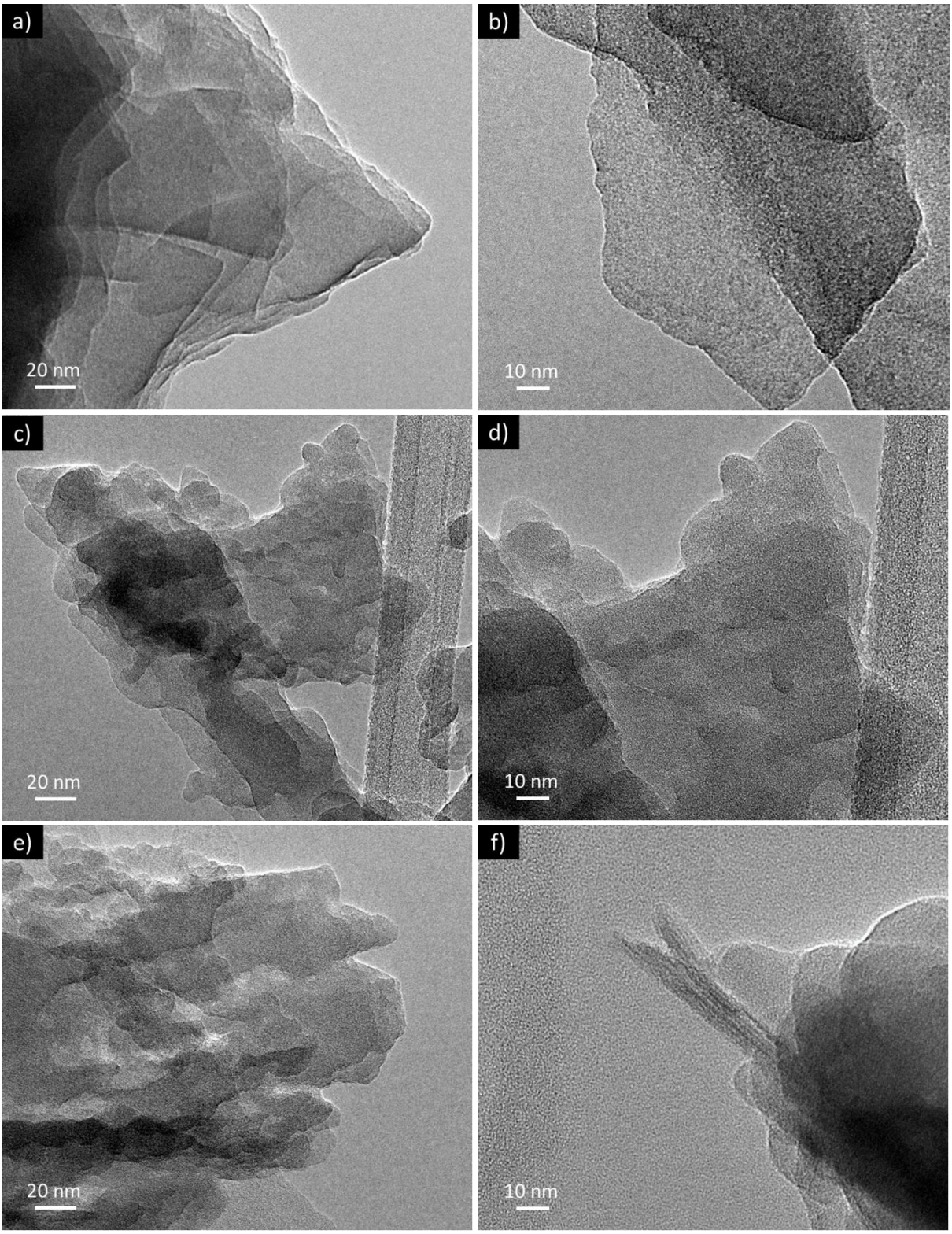

Figure 4.9 TEM images for B-Clino (a,b), H-Clino (c,d), and H-Na-Clino (e,f) at magnification 100kx and 150kx, respectively.

At a nanoscopic level, the variation in the surface texture of the material is immediately observable. In particular, B-Clino at magnification 100kx (Figure 4.9a) displays its lamellar structure, composed of several parallel overlapping scales, with a noticeably smooth surface.

Instead, H-Clino (Figure 4.9c) and H-Na-Clino (Figure 4.9e) exhibit uneven textured surfaces with rugged edges, evidencing the presence of multiple and diverse holes in the mesoscopic range, in compliance with that already observed after nitrogen physisorption test (Figure 4.3). Another effect of the acid/alkaline attacks on the base material may be the increase of distancing between the scales in the structure, which resulted in an enlargement of the original slits-like pores of clinoptilolite. This is a further validation of the positive outcome of the hierarchization process on this material.

Lastly, in H-Na-Clino at magnification 150kx (Figure 4.9f), some prismatic crystals can be distinguished from the structure of the zeolite.

4.2 Efficiency of functionalization and immobilization

Immediately after the end of the process of functionalization, the moles of glyoxyl groups that have formed on the surface of the support was evaluated by exploiting Equation (3.2). The results for each support are reported in Table 4.2.

Table 4.2 Absorbance measurements for every support and results in terms of moles of glyoxyl groups formed per unit mass of support, and the moles per unit surface.

	mol_{gly}/m_{sup} $[\mu mol/g]$	mol_{gly}/S_{sup} $[\mu mol/m^2]$
B-Clino	273	5.6
B-ZSM5	305	0.6
H-Clino	332	1.2
H-Na-Clino	304	1.0
H-ZSM5	213	0.3

These values are associated to relatively high surface densities of glyoxyl groups available for the immobilization of the enzyme; to give an example, in the literature it is reported that, in general, 1.5 $\mu mol_{gly}/m^2$ can provide on average around 40 – 80 sites per molecule of protein to carry out the immobilization [41].

4.2.1 Immobilization yield

The values of concentration of protein in solution before and after the immobilization were obtained with the Bradford assay. Using Equation (3.6), the immobilization yield was calculated, and the results are summarized in Table 4.3. The yield of immobilization after the first step at pH 7, which lasted approximately 60 minutes, was around 95-100% for almost every biocatalyst.

Table 4.3 Amount of enzyme that was immobilized with respect to its initial concentration in the solution, expressed as immobilization yield, as resulted from Bradford assay.

	$Y_{I,pH7}$ *of FDH* [%]	$Y_{I,pH7}$ *of GlyDH* [%]
B-Clino	97,2	90.5
B-ZSM5	100	97.2
H-Clino	96.9	97.5
H-Na-Clino	100	93.5
H-ZSM5	92.4	95.6

These values of yield were obtained by comparing the supernatant at time zero of the process and at the end of the first step of immobilization, namely the contacting between the enzyme and the support at neutral pH. This first stage of the process involves the physical adsorption of the enzyme on the support, mediated by the interaction between amino groups on both the engaged surfaces.

It was observed from further tests that a non-negligible amount of enzyme was subjected to leaching during the second step at pH 10. The amount of protein lost was estimated in about 20-30% for FDH, hence ending up in a 70-80% global yield of immobilization, and up to 40% for GlyDH, with a global yield of 60% (Table 4.4).

Table 4.4 Yield of immobilization as resulted from Bradford assay after the second step at pH 10.

	$Y_{I,pH10}$ *of FDH* [%]	$Y_{I,pH10}$ *of GlyDH* [%]
B-Clino	71.7	60.0
B-ZSM5	81.5	60.9
H-Clino	74.9	67.7
H-Na-Clino	72.1	73.0
H-ZSM5	69.1	64.8

On the whole, slightly higher immobilization yields at the end of the process were exhibited by H-Clino and H-Na-Clino as compared to their equivalent base material, B-Clino. Probably hierarchical clinoptilolite has a mild stabilizing effect on FDH, and a bit more on GlyDH, towards alkaline pH.

4.2.2 Activity of FDH and GlyDH

The activity of the enzyme in the supernatant was measured after the immobilization and put in a relationship with the original activity of the dissolved enzyme, which is 2.51 IU/mg_{enz} for FDH and 1.20 IU/ mg_{enz} for GlyDH. To perform this assessment, Equation (3.5) and Equation (3.7), were employed. Activity tests were performed as described in Section 3.5.1. However, the support gave interference in the absorbance at the same wavelength of NADH, showing a growing curve with decreasing slope over time. Due to this issue, a "stabilization period" was necessary between the adding of the support into the cuvette and the injection of NAD solution. It was chosen to assume that the curve was fairly stable when the slope was 0.0001 min^{-1}, so the measurements were all done after this variable time. Table 4.5 refers to the values of the retained activity observed after the immobilization of the two single enzymes, FDH and GlyDH, as results from Equation (3.8).

Table 4.5 Retained activity of enzymes immobilized over zeolitic supports.

	R_{act} *of FDH* [%]	R_{act} *of GlyDH* [%]
B-Clino	10.7	44.9
B-ZSM5	50.4	35.0
H-Clino	47.6	41.0
H-Na-Clino	26.7	36.5
H-ZSM5	21.8	37.1

By looking at the results for FDH, it can be observed that hierarchization of natural zeolite (clinoptilolite) had a beneficial effect on the retained activity, since it increased from 10% up to nearly 50%. This can be attributable to the fact that this enzyme, which has smaller dimensions, may change its shape by elongating and reducing its diameter and, in this way, it should be able to enter some micropores; however, when the bond with the support is formed, it regains its original active conformation and blocks the access to the pores to reagents, ending up in mass transfer issues and low activity. Besides, the retained activity of FDH over B-Clino is very similar to the value obtained by Pietricola *et al.* [40] by immobilizing it over a mono-functionalized (glyoxyl) milled natural mordenite, with similar properties (specific surface area, average diameter), which was 14%, with 76% of immobilization yield. Due to hierarchization, instead, it is probable that FDH fits better into the meso-macropores, and molecules, in particular the cofactor NADH, which has larger steric footprint, have the possibility to reach the enzyme faster, increasing the overall activity. Furthermore, the value corresponding to the enzyme supported on the only-washed sample (H-Clino) is higher than the ionic exchanged one (H-Na-Clino). It is probable that the native cations of the zeolite, which are mainly potassium, calcium, iron and magnesium [38], may contribute to the stabilization of the biocatalyst on the support, maybe due to electrostatic interactions, providing better enzymatic performances.

As far as B-ZSM-5 is concerned, the higher retained activity of FDH can be attributable to the immobilization of the enzyme only outside of the micropores (which have a precise diameter of 0.5 nm), without blocking the passage of reagent/products molecules, therefore the mass transfer issues are less impactful. This explanation can be applied also to GlyDH, which have bigger dimensions, and seemed not to be affected by the different support, maintaining a retained activity around 35-40% over all the samples. It is probable that, despite the bi-modal distribution of pores, H-ZSM5 did not achieve a proper "branching" structure, but more likely dead-end cylindrical mesopores and macropores, similar to silica [47], surrounded by the microporous framework. As opposed to H-Clino, this did not enhance the mass transfer, but it exacerbated the issue. The behaviour of enzymes over H-ZSM5 might be similar to the one over H-Na-Clino, since the retained activity value is comparable. Also, the effect of ions is not present since ZSM-5 is synthetic, hence it is composed only of aluminium and silicon atoms.

4.2.3 Optimal temperature and pH of FDH and GlyDH

The results for the optimal temperature of the biocatalysts are reported in Figure 4.10 while the corresponding values of optimal pH are in Figure 4.11. The graphs show a comparison between the activity of the enzyme immobilized on B-Clino and H-Clino and the free enzyme in solution. The values of activity are normalized with respect to the higher ones measured in the same test. A comparison between the value of activity of the free enzymes and the immobilized ones resulted to be not feasible, due to the previously mentioned absorbance interference issue of the support at 340 nm. In this case, the stabilization period was chosen to be equal to 2 minutes for every test, so that the interfering curve was approximately at the same slope.

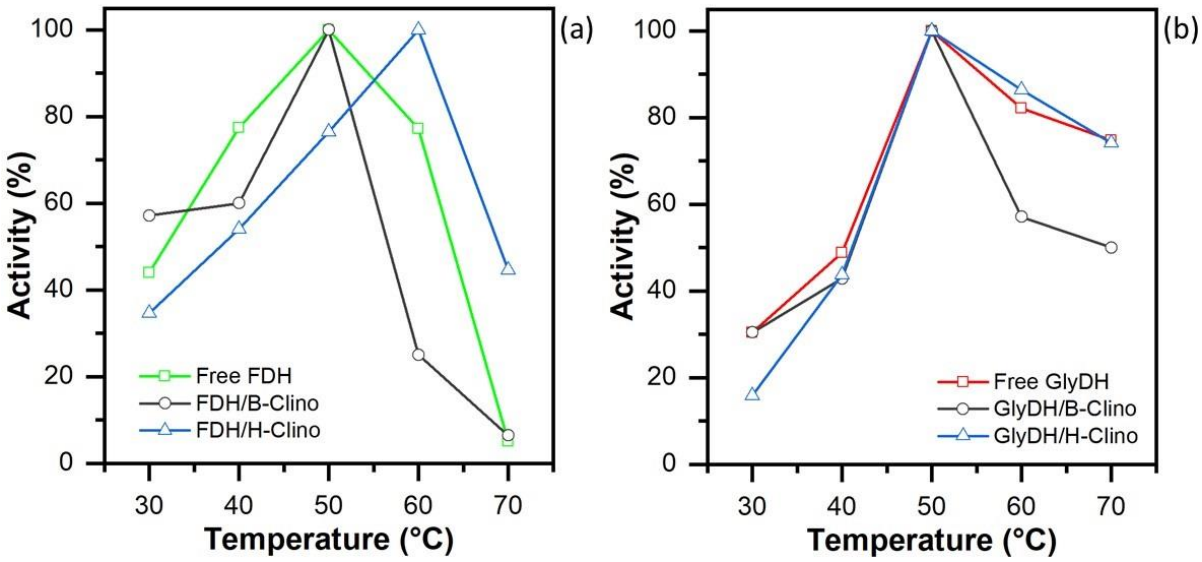

Figure 4.10 Optimal temperature for FDH (a) and GlyDH (b) in different conditions: soluble FDH (green), soluble GlyDH (red), enzymes immobilized over B-Clino (grey) and over H-Clino (blue).

The optimal value of temperature, at which both free FDH and free GlyDH show the highest activity, is around 50 °C. The stabilizing effect of immobilization is visible for FDH, which optimal temperature over H-Clino is shifted towards 60 °C; however, GlyDH seems to be not affected by the same effect, maintaining its higher activity at 50 °C. Moreover, B-Clino did not change the optimal temperature of either enzyme.

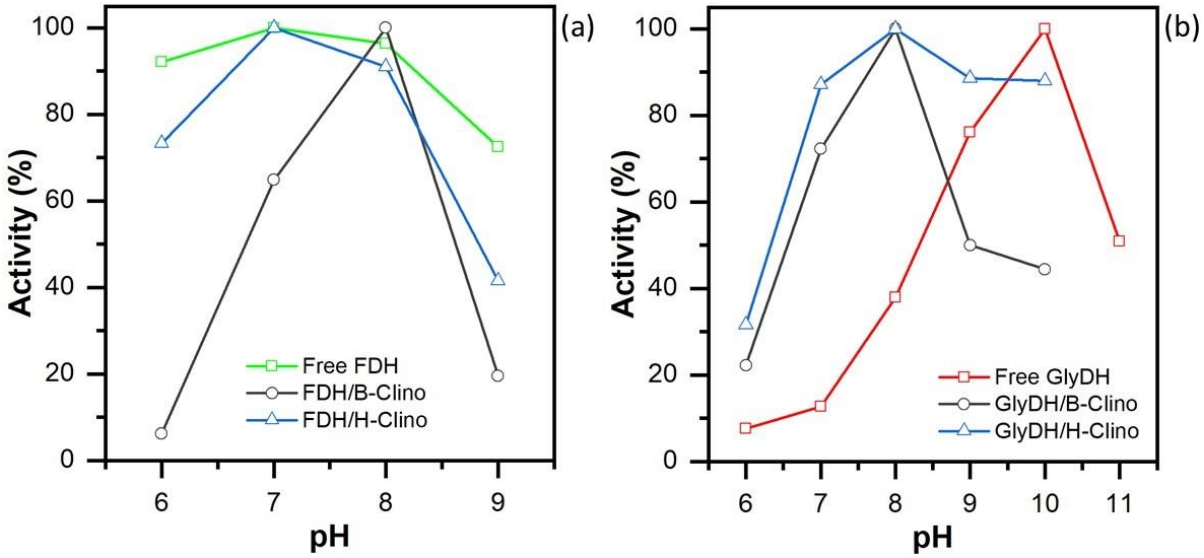

Figure 4.11 Optimal pH for FDH (a) and GlyDH (b); the notation in the same as Figure 4.9.

Free FDH showed its highest activity at pH 7, while GlyDH was more active at pH 10. This represented an additional problem that could be overcome by immobilizing the two enzymes over B-Clino or H-Clino. In fact, on both the supports the optimal pH of GlyDH shifted towards pH 8, at which the enzyme is more stable and did not show any pH-related deactivation phenomena. Meanwhile, the optimal value for FDH moved to pH 8 on B-Clino and remained fixed at pH 7 on H-Clino; however, the activity of FDH on H-Clino at pH 8 was still 90% of its highest value.

4.2.4 Thermal stability of FDH and GlyDH

Enzyme's deactivation kinetic due to high temperature was represented as the loss of activity with respect to initial time (100%). These results are reported in Figure 4.12 and Figure 4.13.

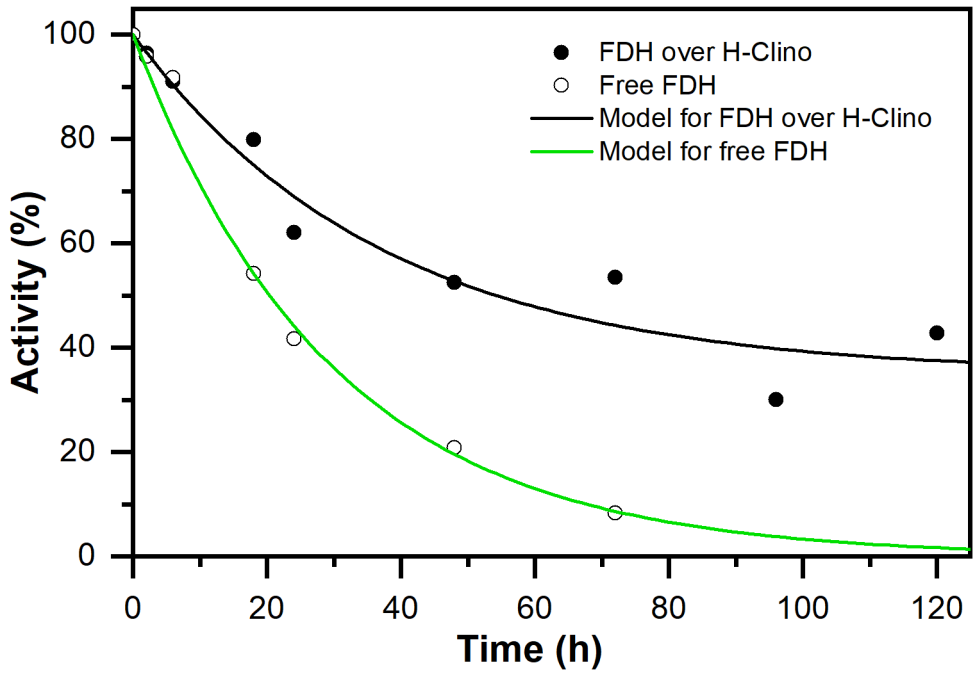

Figure 4.12 Thermal deactivation of FDH: model for the soluble enzyme (green curve) and for the enzyme immobilized over H-Clino (black curve).

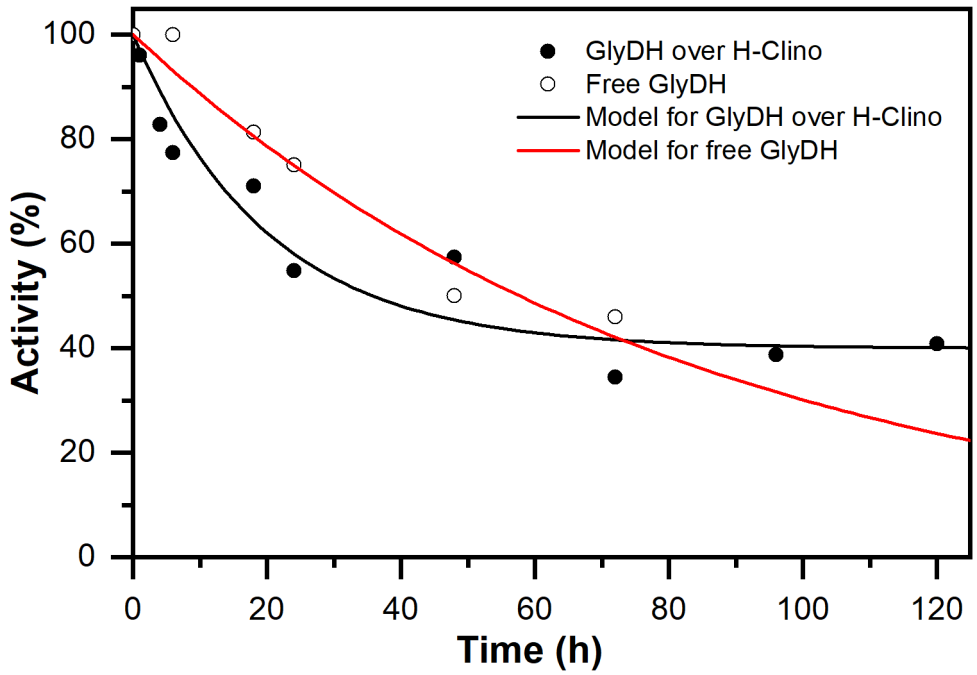

Figure 4.13 Thermal deactivation of GlyDH: model for the soluble enzyme (red curve) and for the enzyme immobilized over H-Clino (black curve).

Both enzymes displayed different behaviour when they were in soluble form with respect to the immobilized ones. As expected, free enzymes' activity followed exponential deactivation kinetic as described in Equation (3.9). Immobilized enzymes, instead, showed more likely asymptotic deactivation kinetics with residual activity, as Equation (3.10).

Table 4.6 is intended to summarize the main parameters for the models that were used to describe thermal deactivation of the different biocatalysts, namely exponential constant k, residual activity α, half-life $t_{1/2}$, stability factor F_S, and the coefficient of determination R^2.

Table 4.6 Thermal deactivation kinetic parameters for FDH and GlyDH at 50°C.

	Decay constant k *[h^{-1}]*	*Residual activity* α *[-]*	*Half-life* $t_{1/2}$ *[h]*	*Stability factor* F_S *[-]*	R^2 *[-]*
Free FDH	0.034	-	20	-	0.99
FDH over H-Clino	0.027	0.35	54	2.7	0.97
Free GlyDH	0.012	-	58	-	0.97
GlyDH over H-Clino	0.050	0.40	36	0.6	0.96

The main advantage of the immobilization of enzymes on porous supports is the increase in their stability. In general, this was clearly visible for FDH, since the thermal decay constant for the soluble enzyme was higher than the one related to the immobilized one. This latter also showed a residual activity at infinite time, approximately around 35%, with respect to soluble FDH which tended to completely deactivate.

The behaviour of GlyDH, which seemed to be quite more stable in its soluble form with respect to the immobilized one, may be connected to the microorganism from which the enzyme originally was obtained, that is a thermophile (i.e. *Geobacillus stearothermophilus*). However, also in this case the soluble enzyme showed no residual activity as opposed to the immobilized enzyme, which was still 40% active.

4.3 Fluorescence microscopy imaging

The images taken with the fluorescence microscope are collected in Figure 4.14 and Figure 4.15. The first series of images (Figure 4.14) depicts the two labelled enzymes co-immobilized over B-Clino. FDH is labelled with ATTO 488 dye, so its emission in fluorescence is in the green channel, while for GlyDH the colourant ATTO 550 was used, which emits in the red channel. Also, the brightfield showing the support granules and the multiple channel (red/green) images were produced. Besides, unloaded B-Clino was observed with the same parameters to check that the support did not emit (Figure 4.15) by itself.

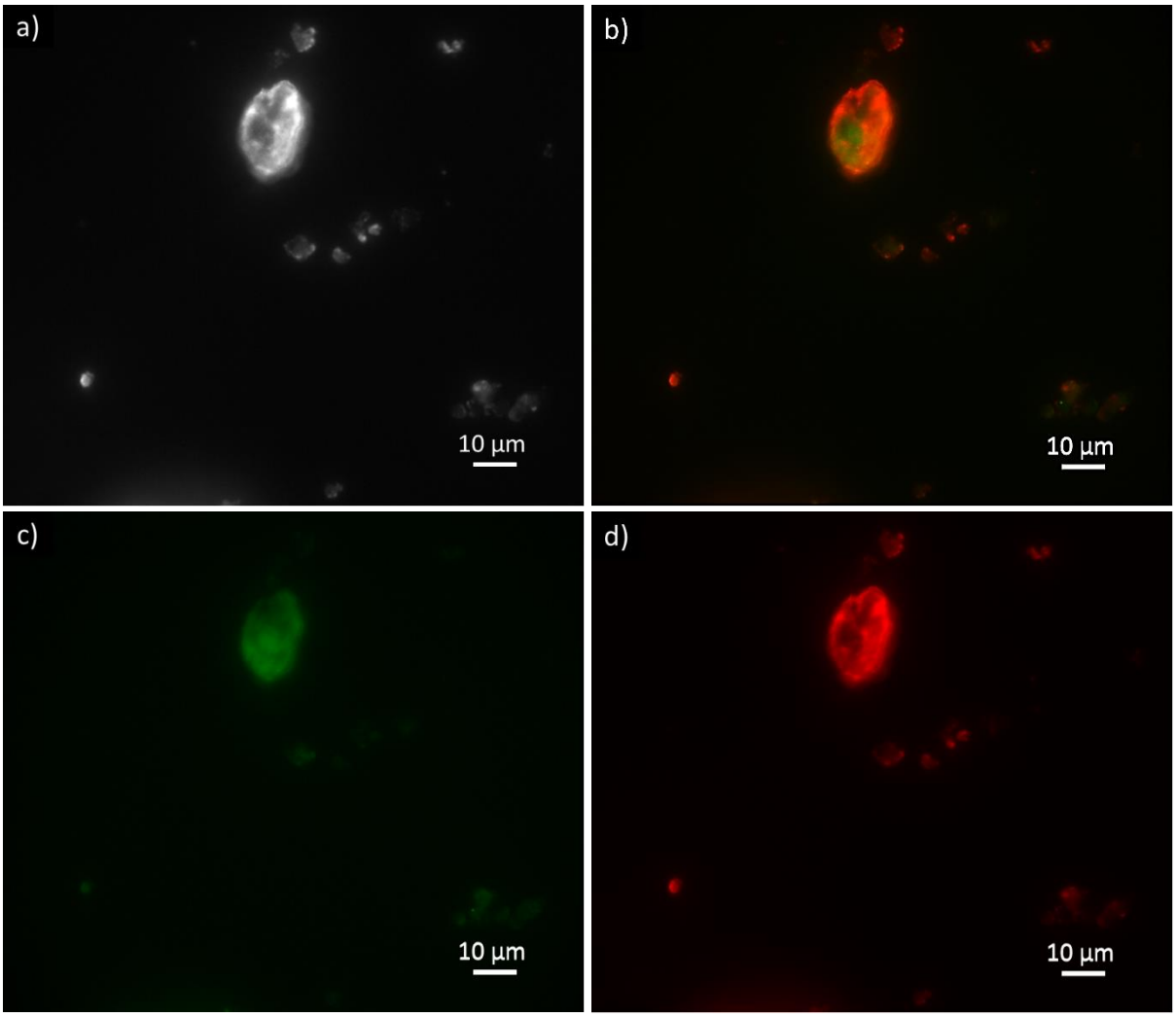

Figure 4.14 Fluorescence imaging of FDH (green channel) and GlyDH (red channel) co-immobilized over B-Clino: brightfield (a), red/green multiple channel overlay (b), green-labelled FDH (c) and red-labelled GlyDH (d).

From Figure 4.14 it is clearly visible that the enzymes appear to be not equally distributed over the zeolite particle, which has the dimensions of approximately 20 µm. In particular, the signal related to ATTO 488 (green) seems to be more uniformly spread, while the one by ATTO 550 (red) is more likely confined to the edges. This can be attributable to the different attitude of the two enzymes to enter inside the pores, like FDH, or to stay outside, like GlyDH, due to the bigger dimensions of this latter.

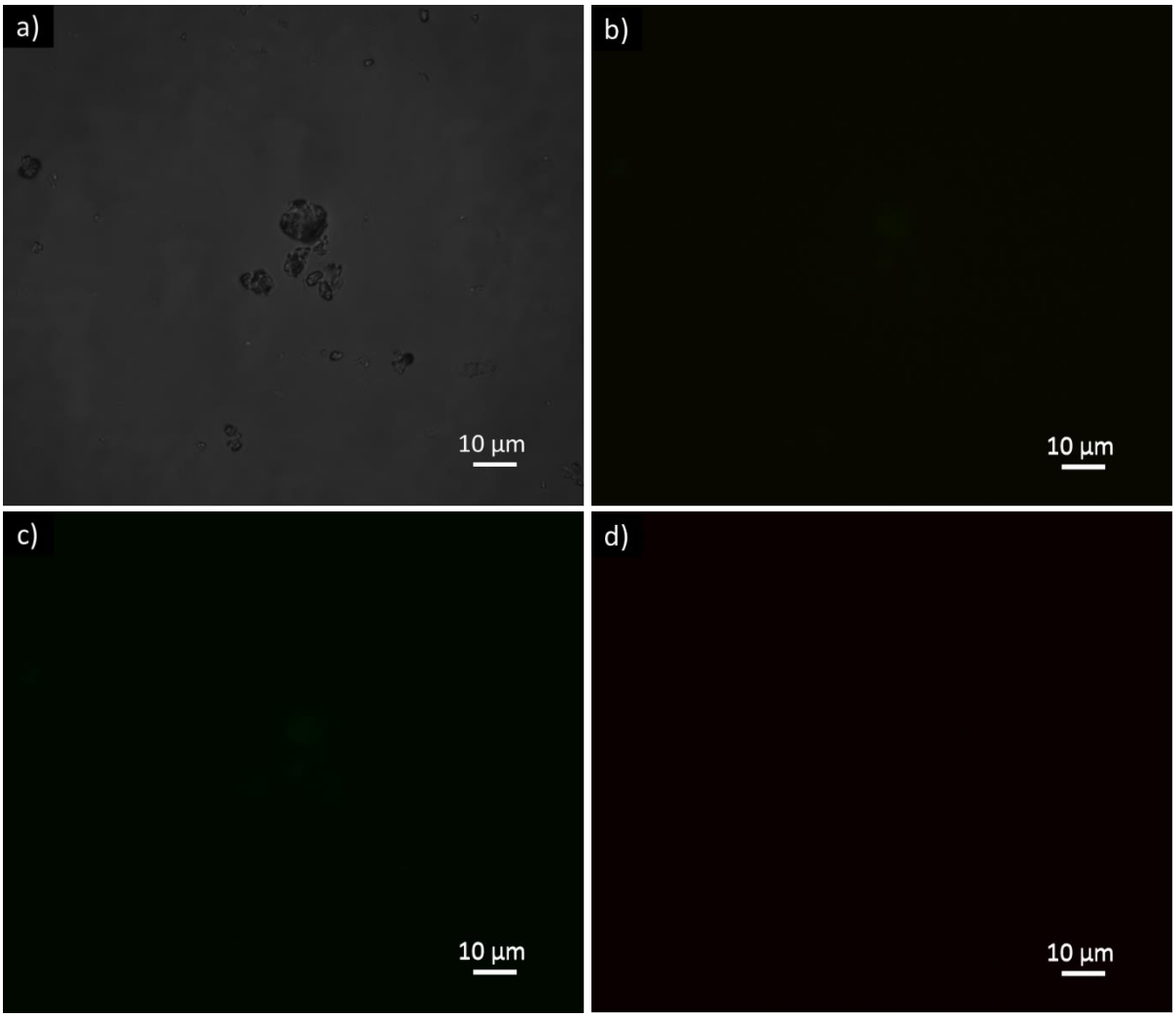

Figure 4.15 Fluorescence imaging of unloaded B-Clino in brightfield (a), multiple channel (b), green channel (c) and red channel (d).

Figure 4.15 was necessary to evidence that the emission of the unloaded support was negligible compared to the coloured enzymes. Instead, all the other supports (B-ZSM5, H-Clino and H-Na-Clino) showed strong emission in quite every channel, invalidating the whole test.

4.4 Production of formic acid

For the different reactions, the concentration of formic acid produced was assessed with HPLC and the values were collected in the following figures. Figure 4.16 is referred to the reaction of FDH immobilized alone over H-Clino, with the addition of cofactor NADH. Figure 4.17, instead, shows the variation of formic acid during the chain-reaction of GlyDH and FDH co-immobilized over H-Clino, with the addition of cofactor NAD^+.

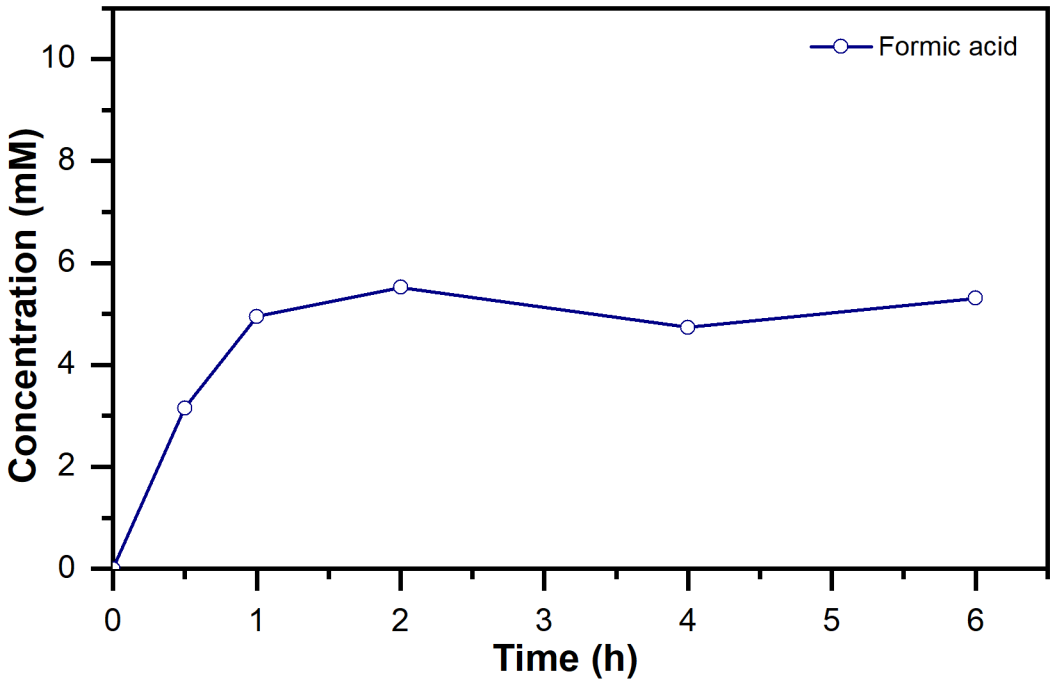

Figure 4.16 Reaction of reduction of CO_2 by FDH: variation of concentration of formic acid.

In Figure 4.16, we can clearly see the successful proceeding of the reaction of reduction of carbon dioxide by FDH with the production of formic acid. The graph shows a maximum value of concentration of formic acid, around 5.5 mM, at 2 hours of reaction, corresponding to 55% of conversion. This can be compared with the performances of FDH over natural zeolite, as reported by Pietricola *et al.* [40], which was around 4.5 mM after 30 minutes. The slight decrease after this maximum value is due to dynamic equilibrium: when NAD^+ and formic acid concentration increased, FDH tended to carry on the reverse reaction, reconverting them back to the original reagents, namely carbon dioxide and NADH. At the end, after 6 hours of reaction, the equilibrium concentration of formic acid settled to its stationary value around 5.3 mM.

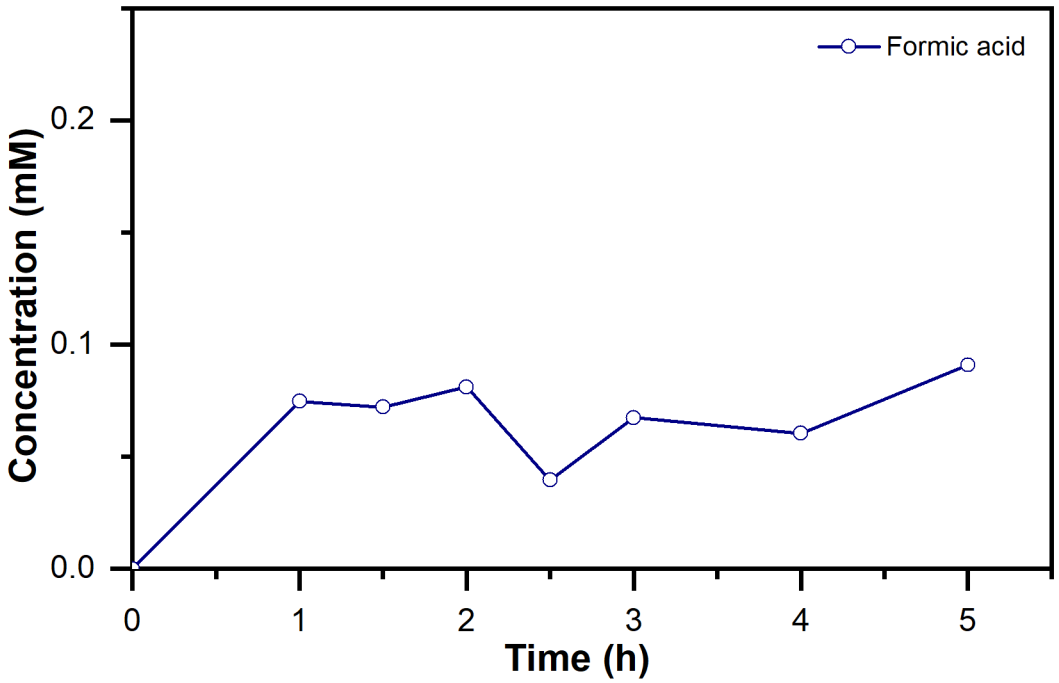

Figure 4.17 Chain-reaction of reduction of CO_2 by FDH and GlyDH (1:1 ratio): variation of concentration of formic acid.

The concentration of formic acid produced from the chain-reaction of FDH and GlyDH over hetero-functionalized H-Clino happened to be negligible with respect to the values obtained from the single direct reaction, with a maximum value around 100 μM.

These performances may be caused by the fact that GlyDH, which is the first element of the chain-reaction, is slower (0.98 IU/g_{sup}) than FDH (2.39 IU/g_{sup}), producing a "bottleneck" phenomenon. In the light of this, in order to improve the production of formic acid, the loading ratio of the two enzymes (FDH/GlyDH) was raised from 1:1 to 1:4, in order to have 2 mg of FDH and 8 mg of GlyDH per gram of support. The results of this attempt are reported in Figure 4.18.

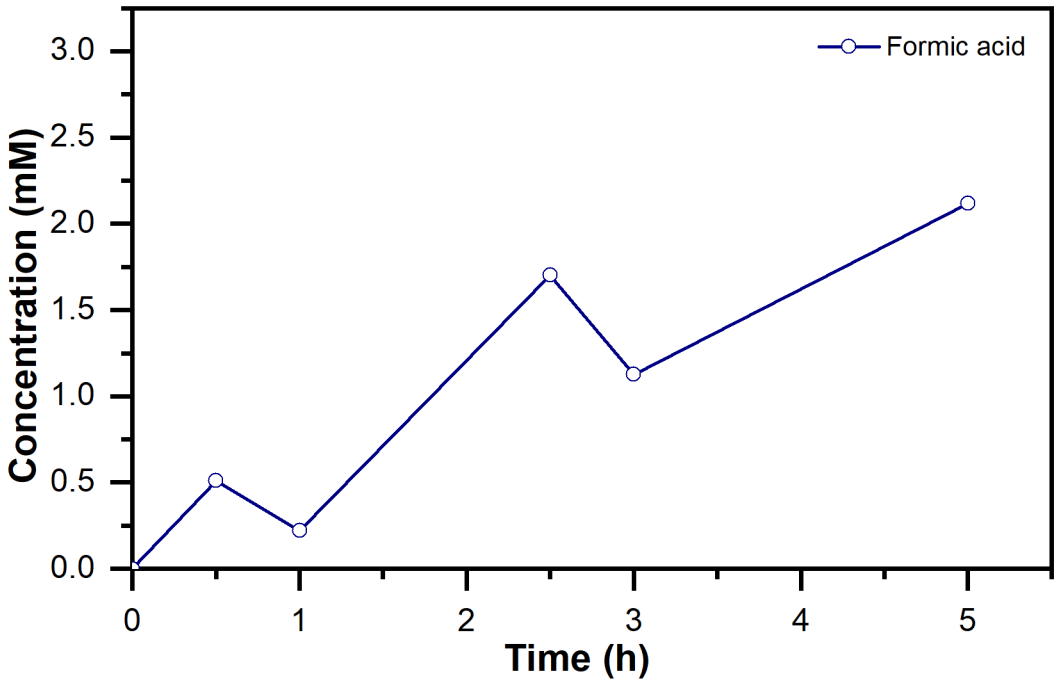

Figure 4.18 Chain-reaction of reduction of CO_2 by 2 mg of FDH and 8 mg of GlyDH per gram of H-Clino (1:4 ratio).

Raising the quantity of GlyDH immobilized over the support, with respect to FDH, allowed to carry out the chain-reaction properly, reaching a maximum value of formic acid concentration of 2.1 mM. In this way, GlyDH immediately started to convert cofactor NAD^+ into NADH, which was instantly utilized by FDH to reduce carbon dioxide into formic acid. After 1 hour of reaction, it is probable that GlyDH started to produce its maximum amount of NADH, so that FDH rapidly produced the peak that was observed at 2.5 hours; nevertheless, since the batch configuration does not involve their removal from the reaction solution, high concentration of products (formic acid, DHA) may have caused the simultaneous proceeding of reverse reactions, namely oxidation of formic acid into CO_2, producing NADH, and reduction of DHA into glycerol, reaching the equilibrium concentration.

Another important effect of the immobilization over H-Clino that can be observed is the alteration of product inhibition effect. As previously reported by Rocha-Martin *et al.* [42], the maximal inhibitory concentration of DHA for soluble GlyDH by *G. stearothermophilus* was 0.42 mM, due to non-competitive mechanism. Since the moles of formic acid produced by FDH have to be equal to the moles of NADH consumed, and these latter are surely lower or equal to the moles of NAD^+ consumed by GlyDH, the concentration of DHA in the reaction mixture reached at least 2.1 mM or higher. Hence, the covalent immobilization over H-Clino reduced the product inhibition, and this may be caused by the shape of the support and the heterofunctionalization, both contributing to the orientation of the protein [42].

5. Conclusions and future developments

In this thesis, the implementation of practical ways to solve two main issues related to enzymatic reduction of carbon dioxide were examined, namely regeneration of pyridine cofactors and immobilization on inorganic supports. In particular, a second enzyme was chosen to restore NADH, i.e. glycerol dehydrogenase, characterized by different dimension and activity features with respect to formate dehydrogenase. These aspects justified the choice of developing aluminosilicate materials with peculiar structure, namely hierarchical zeolites.

Hierarchization process through alkaline desilication was successfully performed over natural clinoptilolite and synthetic ZSM-5. All hierarchical samples increased considerably their surface area, to the same extent as what was reported in the papers taken as reference [36, 37]. They also exhibited both mesopores and macropores, maintaining, however, the original shape of the granules and pores, characteristic of the starting zeolite. In particular, H-Clino and H-Na-Clino maintained the flaky structure of B-Clino, actually showing an enlargement of the slits-like pores between neighbouring scales; similarly, round-shaped granules of H-ZSM5 were essentially unchanged with respect to B-ZSM5's ones. Meanwhile, at nanoscopic level, an increase in roughness with the formation of small ledges can be observed on the surface of hierarchical clinoptilolite. Besides, as recommended, the loss of framework crystallinity of the zeolite was avoided by modulating the Si/Al ratio and by carrying out the alkaline wash in mild conditions [20, 36].

For what hetero-functionalization of the supports is concerned, unexpectedly, no significant correlation was highlighted between the available surface area of the material and the number of moles of aldehydic groups produced on it. In fact, 200-300 μmol/g of glyoxyl groups were formed on each sample, although the surface area ranged from 40 to over 600 m^2/g. A slight increase was observed for hierarchical clinoptilolite samples with respect to B-Clino; however, when it comes to ZSM-5, the behaviour was exactly opposite, with a modest decrease. One reasonable explanation for these contradictory results may be that APTES had higher affinity with the support, hence it gave a sort of saturation effect towards the reactive sites; on the other hand, GPTMS is quite a big molecule, besides it is also bigger than APTES, thus it may have been affected by the natural attitude of zeolites to act as molecular sieves, and could not reach the entire surface, even if some pores were enlarged.

Immobilization of single enzymes, namely FDH only or GlyDH only, proceeded satisfactorily. In particular, yields close to 100% for the first step at neutral pH depict the great affinity of the two enzymes to the immobilization techniques that involves amino groups, and no limitations linked to the diffusion of enzymes were evidenced. By contrast, the change of buffer towards alkaline pH promoted leaching phenomena, reducing the yields up to 60%. Considering that GlyDH from *G. stearothermophilus* is highly sensible to alkaline pH, and consequently returned the worst performances, future developments for this process could take into account the employment of this enzyme extracted from different microorganisms. Some examples are GlyDH from *Cellulomonas sp*. or from *Citrobacter braakii*, which do not suffer from the same sensibility [42]. Another practicable way to overcome the issue is to carry out the immobilization over homo-functionalized supports with only amino groups, which requires to operate only at pH 7 with the addition of glutaraldehyde [18, 40].

Assessing the successful co-immobilization of FDH and GlyDH was obviously not feasible in a quantitative way with Bradford method, since it was not possible to discern the relative amounts of different proteins in solution. In the light of this, a qualitative but pioneering approach was used to directly observe the enzymes at the microscope, with the deployment of fluorescent dyes. This technique was realizable only on base clinoptilolite, whereas all the other supports manifested non negligible fluorescence emission in the channels of interest. However, adequate co-immobilization of the two enzymes was qualitatively proven over B-Clino through fluorescence imaging, since the corresponding two coloured labels were clearly distinguishable in different regions of the carrier particle. Specifically, FDH (labelled in green) was mainly visible in the central area of the granule, while GlyDH (in red) was predominantly confined along the border.

In accordance with the activity results, hierarchical clinoptilolite (H-Clino) turned out to be the best performing material, therefore it was further examined. The effect of native cations into the framework had likewise beneficial effect on enzymatic activity, given that the ion-exchanged zeolite (H-Na-Clino) ensured lower efficiency. By contrast, H-ZSM-5 offered an inappropriate surrounding for the enzymes, resulting in unprofitable residual activity values. In general, from this outcome can be deduced the importance of obtaining a real hierarchical "branched" structure, since the only mesoporosity is not sufficient to achieve higher enzymatic activity [47]. Also, for synthetic zeolite, alternative methods of hierarchization are reported in the literature, that were not implemented in the context of this thesis in order to compare the outcomes of the same procedure in the two different cases of natural and synthetic zeolites. For instance, involving templating compounds, such as cetil-trimetil-amonium bromide (CTAB), in conjunction with alkaline desilication, may be a proper way to generate controlled cylindrical mesopores in the framework of ZSM-5 [20].

Enhanced stability and the good response relative to optimal pH and temperature values of immobilized biocatalysts, with respect to free enzymes, were reflected in satisfying reaction performances. Reduction of CO_2 by FDH over H-Clino, by directly feeding cofactor NADH, achieved a peak of 5.5 mM of formic acid after 2 hours of reaction, reaching the equilibrium value around 5.3 mM after 6 hours. Besides, the chain-reaction involving GlyDH as cofactor converter was successful as well, producing around 2.1 mM of formic acid. This latter result is particularly remarkable since it is, in all probability, owing to different effects: 1) the reduction of the DHA inhibition on GlyDH, and 2) the adjustment of the optimal conditions of the two enzymes over hierarchical zeolite around the operative pH of the reaction, which was between 6.5 and 7.5. In fact, optimal pH of free FDH was 7.5, while it was 10 for GlyDH. Alongside, GlyDH by *G. stearothermophylus* showed complete loss of activity after 1 hour at alkaline pH [42]. Immobilizing the two enzymes over H-Clino shifted the optimal pH of GlyDH towards 8, allowing to enhance the synergistic effect between the biocatalysts.

In sum, the results suggest the potential of macro-mesoporous hierarchical zeolites as enzyme carriers, mainly related to stabilization and mass-transfer enhancement. Despite some clear limitations affecting this work, it could be an initial step towards the improvement of enzymatic processes, making them more sustainable and worthwhile. Future studies should be addressed to finding immobilization procedures that would be more suitable in particular for

GlyDH, not implying alkaline pH. Nevertheless, this strategy can be applied to several further fields of biocatalysis, in which one or more enzymes, with different features, are involved.

List of Symbols

A	Enzymatic activity [IU]
A_0	Initial activity [IU]
A_{FE}	Activity of the free enzyme [IU/mg_{enz}]
A_{IE}	Activity of the immobilized enzyme [IU/g_{sup}]
A_t	Activity at a determined time t [IU]
Abs	Absorbance value at fixed wavelength [abs]
$\Delta Abs/\Delta t$	Time-course absorbance [abs/min]
α	Residual activity [-]
C_e	Concentration of enzyme in solution [mg/mL]
C_f	Concentration of formic acid [mM]
$C_{IO_4^-}$	Concentration of periodate [mmol/mL]
d_{avg}	t-plot average pores diameter [nm]
ε	Molar extinction coefficient [abs L/µmol]
F_S	Stability factor [-]
I	Integral of the peak obtained at the HPLC analysis [-]
k	Thermal decay constant [h^{-1}]
m_{enz}	Mass of enzyme into the solution [mg]
m_{sup}	Mass of support [g]
mol_{gly}	Quantity of glyoxyl groups formed on the surface of the support [µmol]
MW_p	Total structure weight of the protein [Da]
q_E	Enzymatic load on the support [mg_{enz}/g_{sup}]
R^2	Coefficient of determination [-]
R_{act}	Retained activity of the immobilized enzyme [%]
R_{min}	Minimum radius of the protein [nm]
S_{BET}	BET surface area [m^2/g]
S_{Lang}	Langmuir surface area [m^2/g]
V	Volume of the solution into the cuvette [L]
$V_{IO_4^-}$	Volume of periodate solution involved in the reaction [mL]

V_{micro}	t-plot Micropores volume [cm^3/g]
V_p	Cumulative desorption BJH pore volume [cm^3/g]
Y_I	Yield of immobilization [%]
t	Time [h]
$t_{1/2}$	Half-life of the enzyme [h]

References

[1] Bhatia S. K., Bhatia R. K., Jeon J. M., Kumar G., Yang, Y. H., **2019**. "Carbon dioxide capture and bioenergy production using biological system – A review" *Renewable and Sustainable Energy Reviews*, vol. 110, pp. 143-158.

[2] "Trends in Atmospheric Carbon Dioxide, Global Monthly Mean CO_2", *National Oceanic and Atmospheric Administration (NOAA) Earth System Research Laboratories (ESRL)*, https://www.esrl.noaa.gov/gmd/ccgg/trends/global.html, (accessed Nov. 21, 2020).

[3] Subramanian M., **2019**, "Anthropocene now: influential panel votes to recognize Earth's new epoch", *Nature* (doi:10.1038/d41586-019-01641-5)

[4] Yaashikaa P.R., Senthil Kumar P., Varjani S.J., Saravanan A., **2019**, "A review on photochemical, biochemical and electrochemical transformation of CO_2 into value-added products", *Journal of CO_2 Utilization*, vol. 33, pp. 131-147

[5] Long N.V.D., Lee, J., Koo, K.-K., Luis, P., Lee, M., **2017**, "Recent Progress and Novel Applications in Enzymatic Conversion of Carbon Dioxide", *Energies*, vol. 10, no. 4, pp. 473-471.

[6] Shi J., Jiang Y., Jiang Z., Wang X., Wang X., Zhang S., Han P., Yan C., **2015**, "Enzymatic conversion of carbon dioxide", *Chemical Society Reviews*, vol. 44, pp. 5981–6000.

[7] Pellis A., Cantone S., Ebert C., Gardossi L., **2018**, "Evolving biocatalysis to meet bioeconomy challenges and opportunities", *New Biotechnology*, vol. 40, part A, pp. 154-169.

[8] Aggarwal M., Chua T.K., Pinard M.A., Szebenyi D.M., McKenna R., **2015**, "Capturing Carbon Dioxide in beta Carbonic Anhydrase", *RCSB Protein Data Bank,* doi: 10.2210/pdb5BQ1/pdb

[9] Jeoung J.H., Dobbek H., **2007**, "Carbon dioxide activation at the Ni,Fe-cluster of anaerobic carbon monoxide dehydrogenase", *RCSB Protein Data Bank,* doi: 10.2210/pdb3B52/pdb

[10] Goeppert A., Czaun M., Jones J.P., Prakash G.K.S., Olah G.A., **2014**, "Recycling of carbon dioxide to methanol and derived products – closing the loop" *Chemical Society Reviews*, vol. 43, pp. 7995-8048

[11] Din I. U., Shaharun M.S., Alotaibi M.A., Alharthi A.I., Naeem A., **2019**, "Recent developments on heterogeneous catalytic CO2 reduction to methanol", *Journal of CO2 Utilization*, vol. 34, pp. 20-33

[12] Kuwabata S., Tsuda R., Yoneyama H., **1994**, "Electrochemical Conversion of Carbon Dioxide to Methanol with the Assistance of Formate Dehydrogenase and Methanol

Dehydrogenase as Biocatalysts", *Journal of American Chemical Society*, vol. 116, pp. 5437-5443

[13] Obert R., Dave B., **1999**, "Enzymatic Conversion of Carbon Dioxide to Methanol: Enhanced Methanol Production in Silica Sol – Gel Matrices", *Journal of American Chemical Society*, vol.121, pp. 12192-12193.

[14] Guo Q., Gakhar L., Wickersham K., Francis K., Vardi-Kilshtain A., Major D.T., Cheatum C.M., Kohen A., **2016**, "Structural and Kinetic Studies of Formate Dehydrogenase from Candida boidinii", *RCSB Protein Data Bank*, doi: 10.2210/pdb5DN9/pdb

[15] Tanaka N., Kusakabe Y., Ito K., Yoshimoto T., Nakamura K.T., **2002**, "Crystal Structure of Formaldehyde Dehydrogenase from Pseudomonas putida: the Structural Origin of the Tightly Bound Cofactor in Nicotinoprotein Dehydrogenases", *RCSB Protein Data Bank*, doi: 10.2210/pdb1KOL/pdb

[16] Raj S.B., Ramaswamy S., Plapp B.V., **2014**, "Yeast alcohol dehydrogenase structure and catalysis", *RCSB Protein Data Bank*, doi: 10.2210/pdb4W6Z/pdb

[17] *Bioraffineria SATURNO*, https://saturnobioeconomia.it, (accessed Jan. 15, 2021).

[18] Camelin E., Romero O., Piumetti M., Ottone C., Illanes A., Fino D., **2021**, "Mechanisms of interaction among enzymes and supports", in *Nanomaterials for Bio-Catalysis* (Castro G., Nadda A., Nguyen T.A., Qi X., Yasin G.), Chap. 4, Elsevier

[19] Luo J., Meyer A.S., Matieu R.V., Pinelo M., **2015**, "Cascade catalysis in membranes with enzyme immobilization for multi-enzymatic conversion of CO_2 to methanol", *New Biotechnology*, vol. 32, no. 3, pp. 319-327

[20] Koohsaryan E., Anbia M., **2016**, "Nanosized and hierarchical zeolites: A short review", *Chinese Journal of Catalysis*, vol. 37, pp. 447-467

[21] Wu H., Tian C., Song X., Liu C., Yang D., Jiang Z., **2013**, "Methods for the regeneration of nicotinamide coenzymes", *Green Chemistry*, vol. 15, pp. 1773-1789

[22] El-Zahab B., Donnelly D., Wang P., **2007**, "Particle-Tethered NADH for Production of Methanol from CO_2 Catalyzed by Coimmobilized Enzymes", *Biotechnology and Bioengineering*, vol. 99, no. 3, pp. 508-514

[23] Bhuiya M.W., Sakuraba H., Ohshima T., Imagawa T., Katunuma N., Tsuge H., **2004**, "L-glutamate dehydrogenase from Pyrobaculum islandicum complexed with NAD", *RCSB Protein Data Bank,* doi: 10.2210/pdb1V9L/pdb

[24] Vrtis J.M., White A.K., Metcalf W.W., van der Donk W.A., **2002**, "Phosphite Dehydrogenase: A Versatile Cofactor-Regeneration Enzyme", *Angewandte Chemie International Edition*, vol. 41, no. 17, pp. 3257-3259

[25] Cazelles R., Drone J., Fajula F., Ersen., Moldovan S., Galameau A., **2013**, "Reduction of CO_2 to methanol by a polyenzymatic system encapsulated in phospholipids–silica nanocapsules", *New Journal of Chemistry*, vol. 37, pp. 3721-3730

[26] Kumar G.S., Wee Y, Lee I, Sun H.J., Zhao X., Xia S., Kim S., Lee J., Wang P., Kim J., **2015**, "Stabilized glycerol dehydrogenase for the conversion of glycerol to dihydroxyacetone", *Chemical Engineering Journal*, vol. 276, pp. 283-288

[27] Ruzheinikov S.N., Burke J., Sedelnikova S., Baker P.J., Taylor R., Bullough P.A., Muir N.M., Gore M.G., Rice D.W., **2001**, "Crystal Structure of Bacillus Stearothermophilus Glycerol Dehydrogenase", *RCSB Protein Data Bank*, doi: 10.2210/pdb1JPU/pdb

[28] Gao H., Tiwari M.K., Kang Y.C., Lee J.K., **2012**, "Characterization of H_2O-forming NADH oxidase from Streptococcus pyogenes and its application in L-rare sugar production", Bioorganic & Medicinal Chemistry Letters, vol. 22, pp. 1931-1935

[29] Schlager S., Dumitru L.M., Haberbauer M., Fuchsbauer A., Neugebauer H., Hiemetsberger D., Wagner A., Portenkirchner E., Sariciftci N., **2016**, "Electrochemical Reduction of Carbon Dioxide to Methanol by Direct Injection of Electrons into Immobilized Enzymes on a Modified Electrode", *ChemSusChem*, vol. 9, pp 631-635

[30] Hwang I.Y., Lee S.H., Choi Y.S., Park S.J., Na J.G., Chang I.S., Kim C., Kim H.C., Kim Y.H., Lee J.W., Lee E.Y., **2014**, "Biocatalytic Conversion of Methane to Methanol as a Key Step for Development of Methane-Based Biorefineries", *Journal of Microbiology and Biotechnology*, vol. 24, no. 12, pp. 1597-1605

[31] Seefeldt L.C., Yang Z.Y., Lukoyanov D.A., Harris D.F., Dean D.R., Raugei S., Hoffman B.M., **2020**, "Reduction of Substrates by Nitrogenases", *ACS Chemical Reviews*, vol. 120, no. 12, pp. 5082-5106

[32] Kang W., Lee C.C., Jasniewski A.J., Ribbe M.W., Hu Y., **2020**, "Structural evidence for a dynamic metallocofactor during N_2 reduction by Mo-nitrogenase", *RCSB Protein Data Bank,* doi: 10.2210/pdb6VXT/pdb

[33] Smith S.M., Rawat S., Telser J., Hoffman B.M., Stemmler T.L., Rosenzweig A.C., **2011**, "Crystal Structure and Characterization of Particulate Methane Monooxygenase from Methylocystis species Strain M.", *RCSB Protein Data Bank,* doi: 10.2210/pdb3RGB/pdb

[34] Khadka N., Dean D.R., Smith D., Hoffman B.M., Raugei S., Seefeldt L.C., **2016**, "CO_2 Reduction Catalyzed by Nitrogenases: Pathways to Formate, Carbon Monoxide and Methane", *ACS Inorganic Chemistry*, vol. 55, pp. 8321-8330

[35] Yang Z.Y., Moure V.R., Dean D.R., Seefeldt L.C., **2012**, "Carbon dioxide reduction to methane and coupling with acetylene to form propylene catalysed by remodeled nitrogenase", *Proceedings of the National Academy of Sciences of the USA*, vol. 109, no. 48, pp. 19644-19648

[36] Moradi M., Karimzadeh R., Sadat Moosavi E., **2018**, "Modified and ion exchanged clinoptilolite for the adsorptive removal of sulfur compounds in a model fuel: New adsorbents for desulfurization", *Fuel*, vol. 217, pp. 467-477

[37] Mitchell S., Perèz-Ramìrez J., **2011**, "Mesoporous zeolites as enzyme carriers: Synthesis, characterization, and application in biocatalysis", *Catalysis Today*, vol. 168, pp. 28-37

[38] Dosa M., Piumetti M., Bensaid S., Russo N., Baglieri O., Miglietta F., Fino D., **2018**, "Properties of the Clinoptilolite: Characterization and Adsorption Tests with Methylene Blue", *Journal of Advanced Catalysis Science and Technology*, vol. 5, pp. 1-10

[39] Bernal C., Sierra L., Mesa M., **2012**, "Improvement of thermal stability of β-galactosidase from Bacillus circulans by multipoint covalent immobilization in hierarchical macro-mesoporous silica", *Journal of Molecular Catalysis B: Enzymatic*, vol. 84, pp. 166-172

[40] Pietricola G., Ottone C., Fino D., Tommasi T., **2020**, "Enzymatic reduction of CO_2 to formic acid using FDH immobilized on natural zeolite", *Journal of CO2 Utilization*, vol. 42

[41] Lopez-Gallego F., Fernandez-Lorente G., Rocha-Martin J., Bolivar J.M., Mateo C., Guisan J.M., **2020**, "Multi-Point Covalent Immobilization of Enzymes on Glyoxyl Agarose with Minimal Physico-Chemical Modification: Stabilization of Industrial Enzymes", in *Immobilization of Enzymes and Cells: Methods and Protocols* (Guisan J.M., Bolivar J.M., Lopez-Gallego F., Rocha-Martin J.), Fourth Edition, Chap. 5, Methods in Molecular Biology, Springer Protocols

[42] Rocha-Martin J., Acosta A., Berenguer J., Guisan J.M., Lopez-Gallego F., **2014**, "Selective oxidation of glycerol to 1,3-dihydroxyacetone by covalently immobilized glycerol dehydrogenases with higher stability and lower product inhibition", *Bioresource Technology*, vol. 170, pp. 445-453

[43] Tavernini L., Ottone C., Illanes A., Wilson L., **2020**, "Entrapment of enzyme aggregates in chitosan beads for aroma release in white wines", *International Journal of Biological Macromolecules*, vol. 154, pp. 1082–1090

[44] "Fluorescent Labels", *ATTO-TEC GmbH*, https://www.atto-tec.com/?cat=c1_Fluoreszenzlabel-Fluoreszenzlabel.html, (accessed May. 23, 2021).

[45] Thommes M., Kaneko K., Neimark A.V., Olivier J.P., Rodriguez-Reinoso F., Rouquerol J., Sing K.S.W., 2015, "Physisorption of gases, with special reference to the evaluation of surface area and pore size distribution (IUPAC Technical Report)", Pure and Applied Chemistry, vol. 87, pp. 1051-1069

[46] van Koningsveld H., Jansen J.C., van Bekkum H., **1990**, "The monoclinic framework structure of zeolite H-ZSM-5. Comparison with the orthorhombic framework of as-synthesized ZSM-5", *Zeolites*, vol. 10, iss. 4, pp. 235-242

[47] Pietricola G., Tommasi T., Dosa M., Camelin E., Berruto E., Ottone C., Fino D., Cauda V., Piumetti M., **2021**, "Synthesis and characterization of ordered mesoporous silicas for the immobilization of formate dehydrogenase (FDH)", *International Journal of Biological Macromolecules*, vol. 177, pp. 261-270

A mia madre, per avermi presa per mano ogni volta che stavo per cadere, regalandomi uno dei suoi sorrisi più belli e dandomi la forza di sfidare i miei limiti senza esitazione.

A mio padre, il mio *sensei*, per avermi spronata a dare il massimo in ogni sfida, insegnandomi che il detto "più sono grosse, e più fanno rumore quando cadono" non vale solo nel judo.

Ad Albi, per aver sempre creduto in me, anche quando non ci credevo nemmeno io, per il supporto nelle giornate di studio in preparazione di un esame e in quelle di distrazione e relax.

A Eli, perché non sapevo cosa volesse dire avere una sorella, ma adesso, forse, un po' di più.

A Leo, fedele compagno di studio, per sempre con me.

A tutte le persone che hanno reso questo percorso meno solitario e sicuramente più bello.

A Lollo, grazie per la sciarpa, e per tutto ciò che ne è conseguito.

Al mio cuginone Walter e alla cara zia Luisa, per avermi sostenuta e incoraggiata, costantemente, con tutto l'affetto del mondo.

A Caterina, per aver portato un po' di sole, caffè e risate nelle fredde aule del Poli.

A Marco e Martina, i migliori compagni di studio, progetti e aperitivi che potessi chiedere.

A Giulia, Francesca, Mattia e Federico, per le serate spensierate e un po' patriottiche, e per quel profumo di "notti magiche" che mi rimarrà per sempre nel cuore.

A Camilla, alla sua dolcezza infinita, che nonostante la distanza e gli impegni che ci separano, si è fatta sentire più vicina che mai.

Ma anche alle persone che mi hanno remato contro, a chi ha cercato di farmi cadere.

Alle avversità che si sono poste sul mio cammino.

Agli scioperi, all'ansia, alla frustrazione, alla pandemia.

Grazie infinite.